

Macrophage activation and desensitization pathways in inflammatory processes

Dissertation
zur Erlangung des Grades
des Doktors der Naturwissenschaften
der Naturwissenschaftlich-Technischen Fakultät
der Universität des Saarlandes

von
Anna Dembek

Saarbrücken
Mai 2019

Tag des Kolloquiums: 19.09.19
Dekan: Prof. Dr. G. Kickelbick
1. Berichterstatter: Prof. Dr. A. K. Kiemer
2. Berichterstatter: Prof. Dr. M. Schneider
Vorsitz: Prof. Dr. U. Müller
Akad. Mitarbeiter: Dr. A. Kany

"Am Ende wird alles gut.
Wenn es nicht gut ist,
ist es nicht das Ende."

- Fernando Sabino -

Contents

Abbreviations	7
Abstract	10
Zusammenfassung	11
1. Background	12
1.1 Macrophage origin and tissue distribution.....	12
1.2 Macrophage polarization and related functions.....	13
1.3 Macrophage polarization in disease.....	16
1.4 Aim of the present work	19
2. Chapter I Toll-like receptor 2 release by macrophages	20
2.1 Introduction.....	21
2.2 Results.....	23
2.2.1 Previously generated unpublished data	23
2.2.2 TLR2 is detectable in AM supernatant.....	24
2.2.3 Characterization of THP-1-derived ECV	26
2.2.4 Functional analyzes of THP-1 vesicles	34
2.3 Discussion.....	37
3. Chapter II Investigation of human lung tumor-associated macrophages (TAMs) and establishment of a TAM-like macrophage model	40
3.1 Introduction.....	41
3.2 Results.....	44
3.2.1 Human primary AM/TAM mRNA profile and nanoparticle uptake capacity.....	44
3.2.2 Establishment of a TAM-like model for lung macrophages	48
3.2.3 Lipid profile is strongly altered in tumor compared to surrounding lung	55
3.3 Discussion	58

4. Chapter III Hepatic interleukin-6 production is maintained during endotoxin-tolerance and facilitates lipid accumulation	61
4.1 Abstract	62
4.2 Introduction	63
4.3 Results	65
4.3.1 Total lipids and distinct lipid classes are elevated in livers of endotoxin-tolerant animals	65
4.3.2 Regulation of lipogenic genes in the endotoxin tolerance model	66
4.3.3 Kupffer cell depletion by clodronate liposomes and its impact on hepatic lipid composition	66
4.3.4 Crosslink between Kupffer cell-derived cytokines and lipogenesis in endotoxin-tolerance	68
4.4 Discussion	71
4.5 Supplement	75
5. Material and Methods	76
5.1 Material	76
5.1.1 General Material	76
5.1.2 General buffers	76
5.2 Mice	76
5.3 Human lung and lung-tumor tissue	77
5.4 Cell culture	77
5.4.1 Human alveolar macrophages (AMs) and tumor-associated macrophages (TAMs)	77
5.4.2 Human monocyte-derived macrophages (MDM)	78
5.4.3 Human umbilical vein endothelial cells (HUVECs)	80
5.4.4 Cell lines (THP-1, A549, HepG2, HEK-Dual TM hTLR2)	80
5.5 Extracellular vesicle (EV) isolation	81
5.5.1 Nanoparticle tracking analysis (NTA)	82
5.6 RNA isolation and reverse transcription	82
5.7 Quantitative RT-PCR	84

5.8 mRNA sequencing	85
5.9 Determination of protein concentration	86
5.10 Western Blot	86
5.11 Proteomic analysis of EV	87
5.12 cryo-TEM.....	88
5.13 Flow cytometry	89
5.13.1 EV analysis.....	89
5.13.2 Nanoparticle uptake.....	90
5.13.3 Expression of intracellular marker CD68.....	90
5.14 EV uptake experiments	90
5.14.1 EV uptake by primary HUVECs	90
5.14.2 EV uptake by HEK-Dual reporter cells.....	91
5.15 Lipid analysis	91
5.15.1 Lipidomic analysis in human tissue samples	91
5.15.2 Quantification of total lipids (SPV assay) and distinct lipid classes (TLC) in murine liver samples.....	92
5.16 Caspase-3-like activity assay	92
5.17 Histology.....	93
5.18 Enzyme-linked immunosorbent assay (ELISA)	93
5.19 TNF bioassay	93
5.20 Statistics	94
6. References.....	95
Appendix	113
I) Table of selected upregulated DEGs	113
II) Table of selected downregulated DEGs	114
Acknowledgement / Danksagung	115

Abbreviations

ADAM	a disintegrin and metalloprotease
ADAMTS	ADAM with thrombospondin motifs
AM	alveolar macrophage
AP-1	activator protein 1
APMA	4-aminophenylmercuric acetate
ARRD1	arrestin domain-containing protein 1
ARV	acyl-CoA acyltransferase-related enzyme 2 required for viability
AT2B4	plasma membrane calcium-transporting ATPase 4
BSA	bovine serum albumin
CAPZB	F-actin-capping protein subunit beta
CBPM	carboxypeptidase
CCL	CC chemokine ligand
CCR	CC chemokine receptor
CD	cluster of differentiation
CDH	cadherin
CE	cholesteryl ester
CEACAM	carcinoembryonic antigen-related cell adhesion molecule
Cer	ceramide
Co	control
CXCL	C-X-C motif ligand
CYP27A	cytochrome P450 family 27 subfamily A member
CYP51A	cytochrome P450 family 51 subfamily A member
Da	Dalton
Dex	Dexamethasone
DEG	differentially expressed gene
DG	diacylglycerol
DHCR	dehydrocholesterol reductase
EBP	emopamil binding protein
ET	endotoxin tolerance
EV	extracellular vesicle
FC	free cholesterol
FCS	fetal calf serum
FBRL	rRNA 2'-O-methyltransferase fibrillar
FDPS	farnesyl diphosphate synthase
FGF	fibroblast growth factor
Fig.	figure
FLNB	filamin B
GDIR1	Rho GDP-dissociation inhibitor 1
GILZ	glucocorticoid-induced leucine zipper
GR	glucocorticoid receptor
GO	gene ontology
h	hour
HDGF	hepatoma-derived growth factor

HexCer	hexosylceramide
HIF1A	hypoxia-inducible factor 1-alpha
HMGCR	HMG-CoA reductase
HMGCS	HMG-CoA synthase
HNRPL	heterogeneous nuclear ribonucleoprotein L
HSD17B	17-beta hydroxysteroid dehydrogenase
HUVEC	human umbilical vein endothelial cells
ICAM	intercellular adhesion molecule 1
IDHP	isocitrate dehydrogenase
IDI	isopentenyl-diphosphate delta isomerase
IGF	insulin-like growth factor
INSIG	insulin-induced gene
IRF	interferon regulatory factor
ITGA	integrin alpha
k	kilo
KC	Kupffer cell
KLF	Krüppel-like factor
LDLR	low density lipoprotein receptor
LPC	lyso-PC
LPC O	lyso-phosphatidylcholine ether
LPS	lipopolysaccharide
MDM	monocyte-derived macrophage
MFGM	milk fat globule membrane (lactadherin)
MFI	mean fluorescence intensity
min	minute
MMP	matrix metalloproteinase
MSMO	methylsterol monooxygenase
MVK	mevalonate kinase
NSDHL	NAD(P)H steroid dehydrogenase-like
NTA	nanoparticle tracking analysis
OXLA	L-amino-acid oxidase
p	pico
PANTHER	protein annotation through evolutionary relationship
Pam	Pam ₃ CSK ₄ ; TLR2 ligand
PBS	phosphate buffered saline
PC	phosphatidylcholine
PCA	principal component analysis
PC O	PC ether
PDGF	platelet-derived growth factor
PE	phosphatidylethanolamine
PE P	PE-based plasmalogens
PE O	PE ether
PG	phosphatidylglycerol
PGBM	basement membrane-specific heparan sulfate proteoglycan core protein
PI	phosphatidylinositol

PPAR	peroxisome proliferator-activated receptor
PS	phosphatidylserine
PSB	proteasome subunit beta
RL1D1	ribosomal L1 domain-containing protein 1
RLU	relative light units
RNO	reactive nitrogen species
ROS	reactive oxygen species
S1PR	sphingosine-1-phosphate receptor
sec	second
SELE	E-selectin
SM	sphingomyelin
SPV	sulfo-phospho-vanillin assay
SQLE	squalene epoxidase
SREBF	sterol regulatory element-binding protein
TAM	tumor-associated macrophage
TEM	transmission electron microscopy
TG	triacylglycerol
TGFB	transforming growth factor beta
TIE	tyrosine kinase with immunoglobulin-like and EGF-like domains
TLC	thin layer chromatography
TLR	Toll-like receptor
TME	tumor microenvironment
TNF	tumor necrosis factor
UC	ultracentrifugation
VCAM	vascular cell adhesion molecule 1
VEGF	vascular endothelial growth factor

Abstract

Macrophages can adjust their phenotype and functions to the individual microenvironment. Aim of this work was to investigate the polarization of lung and liver macrophages under different pathophysiologically relevant conditions.

Chronic exposure of human alveolar macrophages to bacterial endotoxin and/or a synthetic glucocorticoid induced the expression of the innate immune receptor TLR2. Despite its high abundance, though, the receptor was not functional. Instead, it was released in two different forms: a short and a full-length form. Full-length TLR2 was associated with extracellular vesicles and may contribute to immunosuppression by acting as a decoy receptor.

Macrophages within the tumor microenvironment, i.e., tumor-associated macrophages (TAMs), usually exhibit tumor-promoting functions. An RNA sequencing approach revealed a multitude of significantly downregulated cholesterol metabolism-associated genes in TAMs from human lung tumors when compared with normal lung macrophages (alveolar macrophages). Moreover, TAMs adopted a mixed M1/M2 phenotype, as defined with the help of an *in vitro* model.

In an endotoxin-tolerant state, macrophages fail to produce pro-inflammatory mediators. In the murine liver, though, the pro-inflammatory IL-6 was not subjected to a tolerance response but drove hepatic lipid accumulation, potentially causing steatosis. Kupffer cells, the tissue-resident macrophages of the liver, were identified as the main source of IL-6 by selective depletion.

Zusammenfassung

Makrophagen können Phänotyp und Funktionen an das jeweilige Mikromilieu anpassen. Ziel dieser Arbeit war die Untersuchung der Polarisierung von Lungen- und Lebermakrophagen unter diversen pathophysiologisch relevanten Bedingungen.

Behandlung von humanen Alveolarmakrophagen mit bakteriellem Endotoxin und/oder einem synthetischen Glukokortikoid führte zu einer erhöhten Expression des Immunrezeptors TLR2. Dieser war jedoch funktionsunfähig und wurde in zwei verschiedenen Formen sezerniert: in einer verkürzten und einer langen Variante. Die längere Form war mit extrazellulären Vesikeln assoziiert und zeigte immunsuppressive Funktionen, die durch das Abfangen von TLR2 Liganden zustande zu kommen scheint.

Makrophagen im Tumormikromilieu, d.h. tumorassoziierte Makrophagen (TAMs), sind meist tumorfördernd. RNA-Sequenzierungen zeigten, dass eine Vielzahl von Cholesterinmetabolismus-assoziierten Genen in TAMs im Vergleich zu normalen Lungenmakrophagen (Alveolarmakrophagen) herabreguliert wird. Zudem zeigten TAMs einen gemischten M1/M2-Phänotyp, der mit Hilfe eines *in vitro*-Modells definiert wurde.

Endotoxin-tolerante Makrophagen produzieren keine pro-inflammatorischen Faktoren. In murinen Lebern unterlag das pro-inflammatorische Zytokin IL-6 jedoch keiner Toleranzreaktion, sondern trieb die hepatische Lipidakkumulation voran, was zu Steatose führen kann. Kupffer-Zellen, die Gewebe-Makrophagen der Leber, wurden durch selektive Depletion als Hauptquelle von IL-6 identifiziert.

1. Background

1.1 Macrophage origin and tissue distribution

At the end of the 19th century, Elie Metchnikoff was the first to describe *macrophages*, derived from the Greek words *makros* and *phagein*, literally meaning ‘big eater’ (Atri, Guerfali and Laouini, 2018; Remmerie and Scott, 2018).

For many years, it was hypothesized that macrophages originate from bone marrow-derived monocytes that circulate in the bloodstream. Recent studies provided evidence that most adult tissue-resident macrophages derive from the yolk sac and/or fetal liver during embryonic development and have self-renewal capacity (Epelman, Lavine and Randolph, 2014; Sheng, Ruedl and Karjalainen, 2015; Ginhoux and Guilliams, 2016). To what extent monocyte-derived macrophages contribute to the tissue-resident macrophage pool in steady state is still an open question (Hashimoto *et al.*, 2013; Hume, Irvine and Pridans, 2018; Shapouri-Moghaddam *et al.*, 2018).

In general, the functions of macrophages are similar in all tissues. They maintain tissue homeostasis by engulfing apoptotic or senescent cells, debris, and foreign material, they orchestrate the immune response to pathogens by generating and resolving the inflammatory reaction, and they contribute to tissue development and repair (Italiani and Boraschi, 2014; Remmerie and Scott, 2018; Shapouri-Moghaddam *et al.*, 2018).

Beside that, tissue-resident macrophages are heterogeneous and versatile cells found in virtually all tissues of adult mammals and exhibit accessory functions in dependence of their tissue of residence and the prevailing microenvironment, as reflected by their transcriptional profile (Italiani *et al.*, 2014; Lavin *et al.*, 2014; Okabe and Medzhitov, 2016; Remmerie and Scott, 2018). For example, macrophages in the bone, termed osteoclasts, are specialized in bone resorption, red-pulp macrophages in the spleen are aligned to iron recycling, alveolar macrophages (AMs) in the lung contribute to surfactant clearance, and Kupffer cells in the liver possess an enhanced lipid metabolism (Gordon, Plüddemann and Martinez Estrada, 2014; Gordon and Plüddemann, 2017).

While the precise contribution of origin to tissue-resident macrophage function is another open-ended question, there is considerable evidence that origin may not be the deciding factor in the determination of phenotype and function. For lung AMs, a study demonstrated that yolk sac macrophages as well as fetal and adult monocytes can differentiate into functional and self-maintaining AMs with an almost identical transcription profile when transferred into the empty alveolar niche (van de Laar *et al.*, 2016). Similarly, in the liver, the functionality and gene expression profile of monocyte-derived KCs were highly homologous to those from embryo-derived adult KCs (Scott *et al.*, 2016). Thus, it seems that the local environment into which the progenitor

enters rather than ontogeny dictates the phenotype, fate, and functions of a differentiated macrophage (Gautier *et al.*, 2012; Murray, 2017; Remmerie and Scott, 2018).

1.2 Macrophage polarization and related functions

An essential feature of macrophages is their high plasticity, which allows them to adopt diverse phenotypes in response to equally diverse microenvironmental conditions. Moreover, plasticity is required due to the broad functional spectrum of macrophages ranging from inflammation, host defense, tissue remodeling, and even metabolism (Biswas *et al.*, 2012; Geeraerts *et al.*, 2017). In case of bacterial infection or injury, tissue-resident macrophages and monocytes, recruited from the blood and differentiated into macrophages, induce a protective inflammatory response. It can be divided into different phases, which merge fluently into each other: from pathogen destruction and removal of cellular debris to repairing tissues repair and maintenance of homeostasis (Italiani and Boraschi, 2014; Sica *et al.*, 2015; Ginhoux *et al.*, 2016; Atri, Guerfali and Laouini, 2018). These phases are accompanied by different macrophage activation states induced by the respective cues, such as microbial components, cytokines, or fatty acids. This phenomenon of versatile phenotype adoption is termed “macrophage polarization” and is a complex spatiotemporal process (Mantovani *et al.*, 2004; Sica *et al.*, 2015; Atri, Guerfali and Laouini, 2018; Shapouri-Moghaddam *et al.*, 2018). Based on cell surface markers, production of specific factors, and biological activities, several subtypes of macrophages have been described in mice and humans (Shapouri-Moghaddam *et al.*, 2018). For the purpose of simplification, however, two major polarization programs have been suggested, mirroring the Th1/Th2 polarization scheme of T helper cells: classically activated macrophages or M1 and alternatively activated macrophages or M2, schematically depicted in figure 1-1 (Mantovani *et al.*, 2002, 2004; Biswas and Mantovani, 2012; Sica *et al.*, 2015; Murray, 2017). Originally, the concept of macrophage polarization was defined *in vitro* using transcriptional profiling and conventional approaches. However, such polarization states can also be observed under physiological (ontogenesis, pregnancy) and pathological (allergic and chronic inflammation, cancer) conditions *in vivo* (Sica *et al.*, 2015; Shapouri-Moghaddam *et al.*, 2018).

In an inflammatory environment, microbial stimuli, such as lipopolysaccharide (LPS) alone or in concert with Th1-related cytokines like interferon-gamma (IFN- γ), induce classically activated M1 macrophages *via* activation of diverse transcription factors (e.g., signal transducer and activator of transcription 1 (STAT1), interferon regulatory factor 3 (IRF3), IRF5, or activator protein 1 (AP-1) (Biswas *et al.*, 2012; Sica *et al.*, 2015; Sica and Mantovani, 2012; Wang *et al.*, 2014).

M1 macrophages are characterized by their bactericidal activity and their ability to guide acute inflammatory responses. Therefore, they produce pro-inflammatory cytokines, such as interleukin-1 beta (IL-1 β), IL-6, IL-18, tumor necrosis factor alpha (TNF- α), and type I IFN as well as reactive nitrogen species (RNS) and oxygen species (ROS). Furthermore, they promote cytotoxic adaptive immunity by upregulating MHC class II together with costimulatory molecules cluster of differentiation 40 (CD40), CD80, and CD86. Additionally, M1 macrophages express cytokines like IL-12, IL-23, and IL-27, which can polarize Th1 and Th17 cells, and chemokines like C-X-C motif ligand 9 (CXCL9), CXCL10, CXCL11, CC-chemokine ligand 2 (CCL2), CCL3, and CCL5, necessary for Th1 recruitment (Mantovani *et al.*, 2004; Biswas *et al.*, 2012; Jackaman *et al.*, 2017; Atri, Guerfali and Laouini, 2018; Shapouri-Moghaddam *et al.*, 2018).

With regard to their metabolism, M1 macrophages shift from oxidative metabolism towards the anaerobic glycolytic pathway once activated. Since activation by IFN- γ and LPS is often associated with acute infection and demands a quick and robust anti-microbial response in the hypoxic microenvironment, an anaerobic process such as glycolysis is the best pathway when energy is required (Fraternale, Brundu and Magnani, 2015; Shapouri-Moghaddam *et al.*, 2018). Furthermore, mitochondrial activity in M1 macrophages is reduced leading to the accumulation of citrate and succinate. As a result, citrate is used for the generation of nitric oxide, fatty acids, and ROS, while the accumulation of succinate leads to stabilization of hypoxia-inducible factor 1 alpha (HIF-1 α) and expression of pro-inflammatory and glycolytic factors. Thus, M1 metabolism is also characterized by enhanced fatty acid synthesis (Geeraerts *et al.*, 2017; Shapouri-Moghaddam *et al.*, 2018). Iron metabolism in M1 macrophages is rather intended for retention, what may support their bacteriostatic effect, since iron is essential for bacterial growth (Qiu *et al.*, 2011; Fraternal, Brundu and Magnani, 2015; Shapouri-Moghaddam *et al.*, 2018).

If the acute inflammatory phase continues, M1-activated macrophages and their reactive products can cause severe tissue damage. Therefore, macrophages undergo an M1 to M2 phenotype switch caused by exogenous and endogenous stimuli, gradually acquiring an anti-inflammatory phenotype and initiating a resolution phase associated with the inhibition of inflammation, scavenging of debris, angiogenesis, and tissue repair (Sica *et al.*, 2015; Atri, Guerfali and Laouini, 2018; Shapouri-Moghaddam *et al.*, 2018).

Alternatively activated M2 macrophages exhibit a high phagocytic function supported by enhanced expression of scavenger receptors like CD204, and CD163 (Takeya and Komohara, 2016). Phagocytosis of cell debris and dead or apoptotic cells inhibits the production of pro-inflammatory cytokines, such as TNF- α , IL-1 β , IL-6, and IL-8 through a mechanism involving the autocrine or paracrine secretion of transforming growth factor- β (TGF- β) which subsequently inhibits

further recruitment of monocytes and macrophages. Furthermore, phagocytosis of apoptotic cells inhibits the production of IL-12, IL-23, and IL-27 and stimulates the enhanced production of anti-inflammatory IL-10 (Mantovani *et al.*, 2004; Sica *et al.*, 2015; Shapouri-Moghaddam *et al.*, 2018).

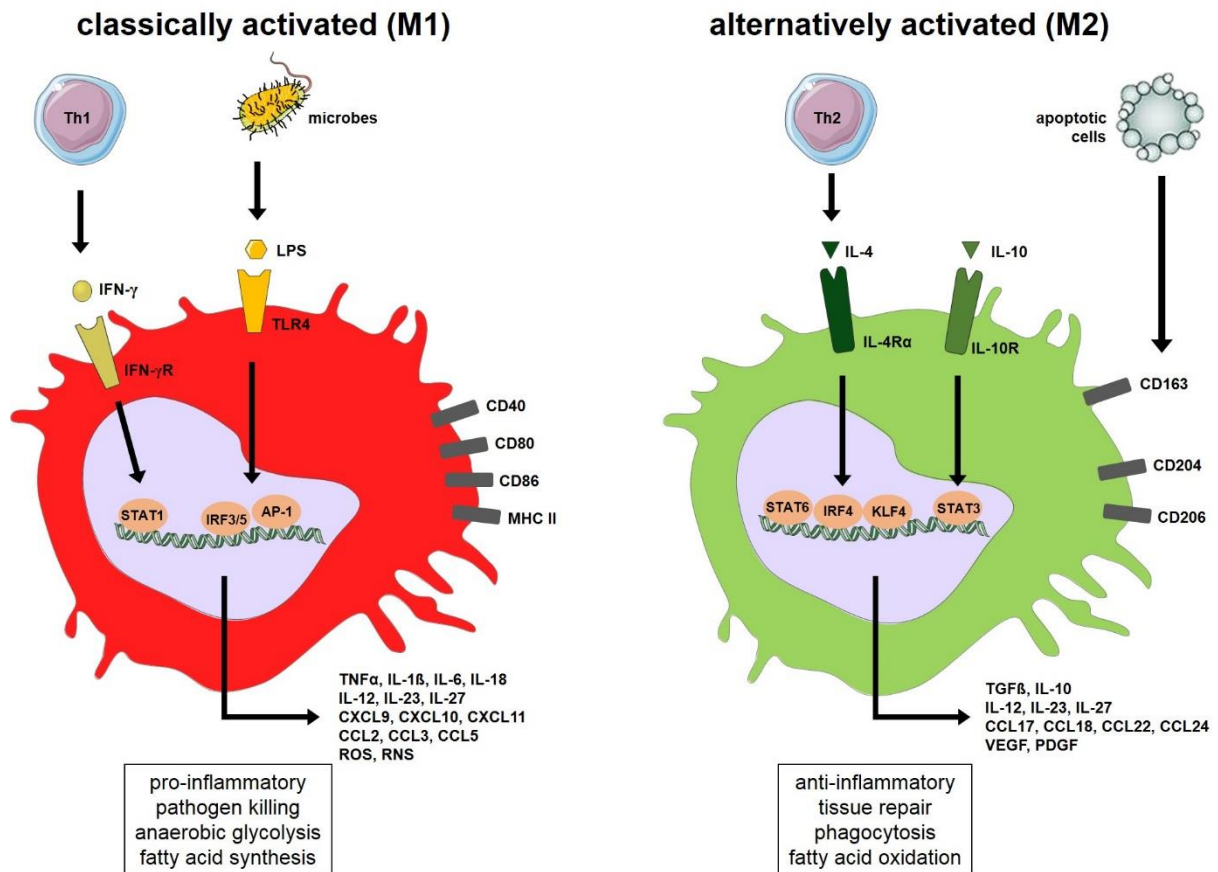


Figure 1-1: Schematic representation of M1- and M2-polarized macrophages. The polarizing signals, related receptors, enhanced surface markers (grey), released cytokines and chemokines, as well as activated transcription factors (light orange) are depicted. Specific functions and metabolic features are indicated in boxes. See text for further information. Illustration was obtained and modified from Servier Medical Art by Servier, <https://smart.servier.com/>, licensed under Creative Commons Attribution 3.0 Unported License, <http://creativecommons.org/licenses/by/3.0/>.

M2 macrophages also express high levels of numerous growth factors such as platelet-derived growth factor (PDGF), and vascular endothelial growth factor (VEGF) and endocytic receptors, including c-type lectins receptor CD206 (also known as mannose receptor) (Wynn and Vannella, 2016; Shapouri-Moghaddam *et al.*, 2018; Suzuki *et al.*, 2018). Additionally, they are critical effectors in Th2 responses, since they are able to recruit Th2, regulatory T cells, eosinophils, and basophils by secretion of chemokines, such as CCL17, CCL18, CCL22, CCL24 (Mantovani *et al.*, 2004; Sica *et al.*, 2015; Shapouri-Moghaddam *et al.*, 2018).

However, depending on the *in vitro* anti-inflammatory stimuli used to generate M2 macrophages, these cells can be subdivided into IL-4/IL-13-activated or IL-10-activated, among others, and may show subtle phenotypic and functional variations (Mantovani *et al.*, 2004; Ginhoux *et al.*, 2016). The canonical M2 stimuli IL-4 or IL-13 are known to activate STAT6, peroxisome proliferator-activated receptors gamma (PPAR γ), Krüppel-like factor 4 (KLF4), and IRF4 through the IL-4 receptor alpha (IL-4 α), whereas IL-10 acting through its receptor IL-10R activates STAT3 (Biswas *et al.*, 2012; Sica and Mantovani, 2012; Wang, Liang and Zen, 2014).

M2 macrophage functions, such as wound healing and tissue repair, require a sustained supply of energy. This request is achieved by oxidative glucose metabolism. Furthermore, M2 metabolism is characterized by high mitochondrial activity, fueled by fatty acid oxidation as well as glutamine metabolism, and coupled to oxidative phosphorylation (Fraternale, Brundu and Magnani, 2015; Geeraerts *et al.*, 2017; Shapouri-Moghaddam *et al.*, 2018). In contrast to M1, M2 macrophages favor iron export that is necessary for tissue repair and proliferation but also promotes tumor growth and metastasis (Biswas and Mantovani, 2012; Biswas *et al.*, 2012; Fraternale, Brundu and Magnani, 2015; Shapouri-Moghaddam *et al.*, 2018).

Of note, in addition to cytokines and signaling through transcription factors, regulation of the transition between M1 and M2 also involves epigenetic modifications as well as diverse microRNAs and hypoxia (Biswas *et al.*, 2012; Sica and Mantovani, 2012; Wang, Liang and Zen, 2014).

1.3 Macrophage polarization in disease

Inflammation is a normal and essential process of infection and wound healing, which usually takes place under strict spatiotemporal orchestration. When it is prolonged or even unresolved, it can result in severe tissue damage and become chronic. Continuous exposure to different factors, such as smoking, excess weight, stress, and bacterial or viral infections, increases the risk of chronic inflammation and associated diseases, including chronic obstructive pulmonary disease, asthma, diabetes, atherosclerosis, and cancer. Moreover, chronic inflammatory pathologies are often accompanied by an imbalance of M1 and M2 macrophages (Sica and Mantovani, 2012; Conway *et al.*, 2016; Atri, Guerfali and Laouini, 2018). Several examples of these macrophage imbalance-associated diseases are shown in figure 1-2.

Sepsis, which is one of the most common causes of death in intensive care units worldwide, is one example of dysregulated inflammation (Biswas and Lopez-Collazo, 2009; Biswas *et al.*, 2012). It is a bi-phasic disease caused by microbe infections, including bacteria, fungi, and viruses, and is subdivided into an initial hyper-inflammatory phase (called systemic inflammatory

response syndrome, SIRS) followed by an immunosuppressed or “immunocompromised” phase. SIRS can also occur independently of sepsis, originating from causes like trauma, burn, surgery, or pancreatitis, and is then termed non-infectious SIRS (Biswas and Lopez-Collazo, 2009; Arora *et al.*, 2019). The initial inflammatory phase of sepsis is mainly characterized by monocytes and macrophages with a hyper-inflammatory phenotype producing overt levels of pro-inflammatory cytokines, such as TNF- α and IL-12 (‘cytokine storm’). This can lead to systemic inflammation, vascular damage, and organ failure (Biswas *et al.*, 2012). However, as sepsis progresses, these monocytes and macrophages become unresponsive and refractory to a subsequent endotoxin challenge, a phenomenon known as endotoxin tolerance (ET), and referred to as compensatory anti-inflammatory response syndrome (CARS; Biswas and Lopez-Collazo, 2009; Cavaillon and Adib-Conquy, 2006). Here, these cells fail to express inflammatory cytokines in response to a re-challenge with, e.g., LPS. In contrast, they produce anti-inflammatory cytokines (mainly TGF- β and IL-10) and decrease their antigen presentation ability (by reduction of MHC II), which promotes immunosuppression and unresponsiveness, respectively (Biswas and Lopez-Collazo, 2009; Hotchkiss, Monneret and Payen, 2013).

Although this functional reprogramming represents a protective mechanism to counteract overwhelming inflammation, there is a high risk of developing secondary infections, potentially leading to mortality (Biswas and Lopez-Collazo, 2009; Sica *et al.*, 2015).

Another example of an M1/M2 switch-associated disease is cancer. Numerous cancer risk factors can be linked to chronic inflammation, which is nowadays established as one of the hallmarks of cancer (Hanahan and Weinberg, 2011). The type of inflammation associated with increased cancer risk is often called “smoldering inflammation” because it is low grade without overt clinical consequences. It can be caused by a chronic microbial infection or persistent irritation by, e.g., smoking, stress, and obesity that may induce a sterile inflammation (Mantovani and Sica, 2010; Qian and Pollard, 2010; Zheng *et al.*, 2017). It is now evident that inflammation is involved in all stages of cancerogenesis, from tumor initiation to progression and metastasis of established tumors (Mantovani and Sica, 2010; Conway *et al.*, 2016; Atri, Guerfali and Laouini, 2018). Macrophages are key mediators in the link between inflammation and cancer (Qian and Pollard, 2010; Biswas *et al.*, 2012). In the cancer-initiating phase, tumor-associated macrophages (TAMs) may have an anti-tumoral, immunostimulatory activity (Mantovani and Sica, 2010; Biswas *et al.*, 2012; Sica *et al.*, 2015). However, once the tumor is established, the microenvironment gets enriched with inflammatory mediators, such as IL-4 and IL10, polarizing TAMs into a pro-tumoral, M2-like phenotype (Mantovani *et al.*, 2002; Qian and Pollard, 2010; Noy and Pollard, 2015; Sica *et al.*, 2015). Hence, M2-like macrophages can perform several tumor-promoting

functions, including stimulation of angiogenesis, remodeling of the extracellular matrix, promotion of cancer cell proliferation, invasion, extravasation and metastasis, and immunosuppression (Solinas *et al.*, 2009; Bremnes *et al.*, 2011).

Obesity-related conditions like insulin resistance, cardiovascular and fatty liver disease, metabolic syndrome, and diabetes are also driven by chronic inflammation (Hotamisligil, 2006; Sica *et al.*, 2015; Shapouri-Moghaddam *et al.*, 2018). Adipose tissue macrophages (ATMs) are a significant component of adipose tissue and are essential players in obesity-associated pathology. Similar to other macrophage populations, ATMs also show heterogeneity and functional plasticity (Biswas *et al.*, 2012). An increase in weight is associated with an ATM phenotype switch. In lean individual, ATMs are considered to be rather M2-like, releasing high levels of cytokines, such as IL-10, and playing a role in maintaining adipose tissue homeostasis. In contrast, ATMs in human obesity are described to be polarized towards an M1 phenotype with up-regulation of pro-inflammatory cytokines (e.g., IL-12, IL-1 β , and TNF- α) and are thereby believed to be the major contributors of obesity-induced insulin resistance, leading to type-2 diabetes (Biswas *et al.*, 2012; Geeraerts *et al.*, 2017; Shapouri-Moghaddam *et al.*, 2018). Additionally, increased uptake of oxidized fats by macrophages in the artery wall leads to M1-like polarization and foam cell formation, low-grade chronic inflammation and plaque formation, important steps in the pathogenesis of atherosclerosis (Biswas *et al.*, 2012; Remmerie and Scott, 2018).

In contrast, M2-polarized macrophages are involved in helminth clearance and are suggested to drive allergic disorders and fibrosis (Sica *et al.*, 2015).

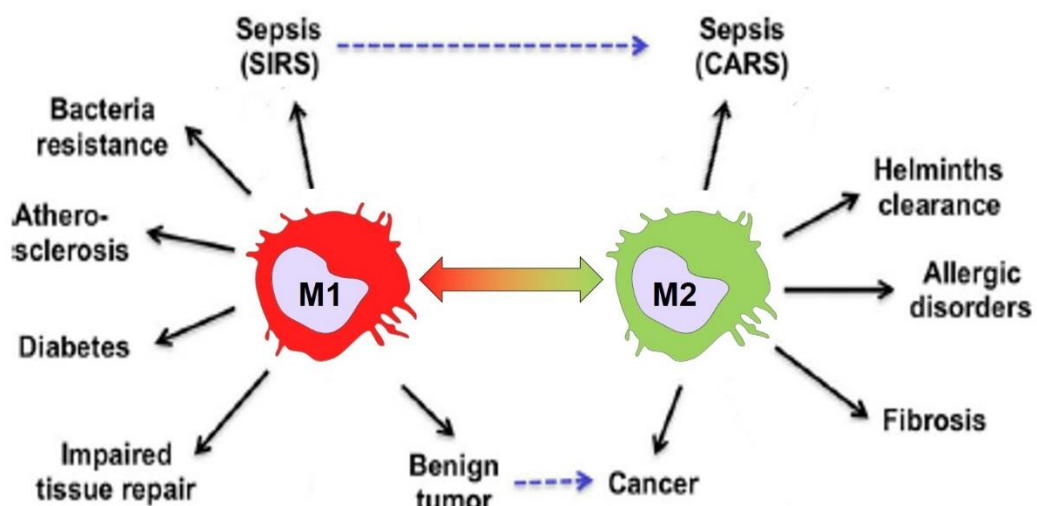


Figure 1-2: M1 and M2 macrophage polarization in disease. Association of M1 and M2 macrophage polarization in distinct diseases. While in defense against bacteria (bacteria resistance), atherosclerosis, diabetes, and impaired tissue repair macrophages rather exhibit an M1 phenotype, in helminths clearance, allergic disorders, and fibrosis they are preferably M2-polarized. During the progression of both, sepsis and cancer, dynamic reprogramming of macrophage polarization occurs. SIRS: systemic inflammatory response syndrome; CARS: compensatory anti-inflammatory response syndrome (CARS); adapted from Sica *et al.* (2015), modified.

1.4 Aim of the present work

Macrophages are key orchestrators of the inflammatory response. Their polarization is influenced by the particular microenvironment and determines their physiological and pathophysiological functions. Understanding the polarization status as well as the polarization process may provide a basis for macrophage-centered therapeutic approaches. Therefore, the aim of this work was to investigate macrophages under different microenvironmental conditions. The three chapters within this thesis address the following questions:

- I)** In what way do chronic inflammation and glucocorticoid-induced immunosuppression influence the expression of TLR2 by primary human alveolar macrophages?
- II)** Which transcriptional phenotype do tumor-associated macrophages from lung tumors exhibit in comparison to alveolar macrophages?
- III)** Is LPS-induced lipid accumulation in murine liver influenced by endotoxin tolerance?

2. Chapter I

Toll-like receptor 2 release by macrophages

A large part of the following chapter has been published as:

“Toll-like receptor 2 release by macrophages: an anti-inflammatory program induced by glucocorticoids and lipopolysaccharide”. Jessica Hoppstädter*, Anna Dembek*, Ahmad Barghash, Claudia Fecher-Trost, Gregor Fuhrmann, Marcus Koch, Annette Kraegeloh, Hanno Huwer, and Alexandra K. Kiemer (under revision) *Frontiers in Immunology*

*Equal contribution

2.1 Introduction

Alveolar macrophages (AMs) are the tissue-resident macrophages in the lung alveolar space. They represent the first line of defense against pathogens in the lower airspace and recognize microbial ligands via pattern recognition receptors (Hoppstädter *et al.*, 2010; Hussell and Bell, 2014). Toll-like receptors (TLRs) are the major pattern recognition receptors of the innate immune system. Virtually every human cell expresses a unique ratio of these receptors, and they sense a wide range of ‘danger’ signals or pathogen-associated molecular patterns (PAMPs) (Medzhitov, 2001; Netea and van der Meer, 2011; Cao, 2016). To date, a total of 10 TLRs have been identified in humans, that can be divided into two main groups: (I) surface-expressed TLRs (i.e., TLR1, 2, 4, 5, 6, and 10) classically known to recognize bacterial, fungal, and parasitic PAMPs; and (II) endosomal TLRs (i.e., TLR 3, 7/8, and 9), which sense viral dsRNA, ssRNA, and unmethylated DNA, respectively (Medzhitov, 2001; Kawasaki and Kawai, 2014; Henrick *et al.*, 2016). After recognition and binding of a specific PAMP, TLRs induce an intracellular signaling cascade that culminates in the activation of the AP-1, NF- κ B, and IRF family of transcription factors (Busillo and Cidlowski, 2013). These signaling cascades result in the secretion of pro-inflammatory factors that ultimately protect the host from microbial infection (Kawasaki and Kawai, 2014; He, Lawlor and Newburg, 2016). Among all TLRs, TLR2 has a special place with its well-characterized sensitivity for a large variety of pathogens, including bacteria, viruses, fungi, mycobacteria, and parasites (Henrick *et al.*, 2012). Unlike other TLRs, TLR2 needs to form heterodimers with either other TLR family members (i.e., TLR1, TLR6 or TLR10) or non-TLR cellular molecules (e.g., CXCR4 or scavenger receptor), to be able to initiate cell activation (Ozinsky *et al.*, 2000; van Bergenhenegouwen *et al.*, 2013). TLR2 comprises a conserved intracellular toll–interleukin-1 receptor homology domain, a single transmembrane domain, and a solenoid ectodomain. The ectodomain of TLRs in vertebrates is composed of 19–21 diverse leucine-rich-repeat modules that function in pathogen recognition (Henrick *et al.*, 2016). Since TLR2 activity plays a prominent role in the pathogenesis of a variety of acute and chronic inflammatory diseases (van Bergenhenegouwen *et al.*, 2013), the regulation of its activation is also crucial (Henrick *et al.*, 2016). A negative regulation of TLR signalling can be accomplished by direct attenuation *via* soluble factors, including soluble TLRs (sTLR) that act as decoy receptors and bind to PAMPs in the extracellular space, preceding their engagement with specific PRRs, thus reducing the TLR signaling efficiency (Liew *et al.*, 2005; fig. 2-A).

LeBouder *et al.* (2003) were the first to describe soluble TLR2 (sTLR2) in breast milk and plasma, followed by its detection in amniotic fluid (Dulay *et al.*, 2009), saliva (Kuroishi *et al.*, 2007) and monocyte supernatant (Kuroishi *et al.*, 2007; Langjahr *et al.*, 2014).

sTLR2 has been found to reduce inflammation by disrupting TLR2 activation without compromising bacterial clearance (Raby *et al.*,

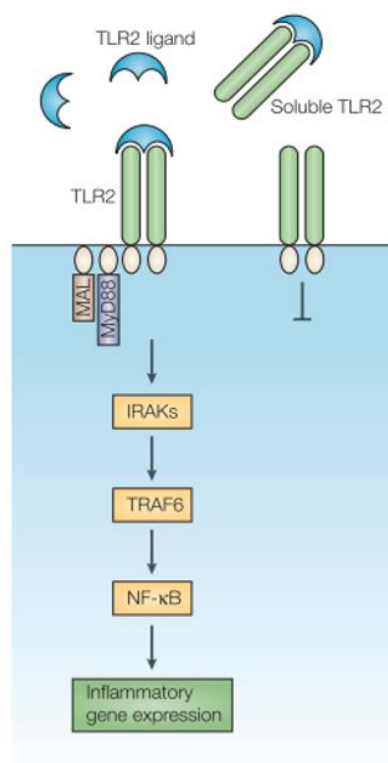


Figure 2-A: Comparison of signal transduction by membrane-bound TLR2 and soluble TLR2 (sTLR2). sTLR2 can compete with TLR2 for microbial ligands and prevent the interaction of TLR2 with ligand and block TLR2 signaling by the decoy mechanism. Figure taken from Liew *et al.*, 2005.

2009), and to be protective against HIV-1 infection (Henrick *et al.*, 2012). For the production of sTLR2, proteolytic cleavage of the TLR2 transmembrane protein has been suggested through a process referred to as ectodomain shedding by disintegrin metalloproteinases (ADAMs) (i.e., ADAM10 and ADAM17) (Langjahr *et al.*, 2014). As only one encoding TLR2 mRNA has been detected, the contribution of alternative splicing can be excluded (LeBouder *et al.*, 2003).

In this part of the work, we aimed to examine TLR2 expression in primary human AMs under inflammatory conditions, as mimicked by prolonged exposure to the bacterial cell wall component lipopolysaccharide (LPS). In addition, we used dexamethasone (Dex), a synthetic glucocorticoid, since glucocorticoids are endogenous anti-inflammatory agents, known to suppress TLR-mediated signaling in general (Chinenov and Rogatsky, 2007; Busillo and Cidlowski, 2013) and remain the mainstays in the treatment of inflammatory and autoimmune pathologies (Cain and Cidlowski, 2017).

2.2 Results

2.2.1 Previously generated unpublished data

In previous unpublished work, Dr. J. Hoppstädter observed an increase of *TLR2* mRNA in primary human AMs after 24 h treatment with LPS, while other investigated TLRs were not affected to a similar extent (fig. 2-1).

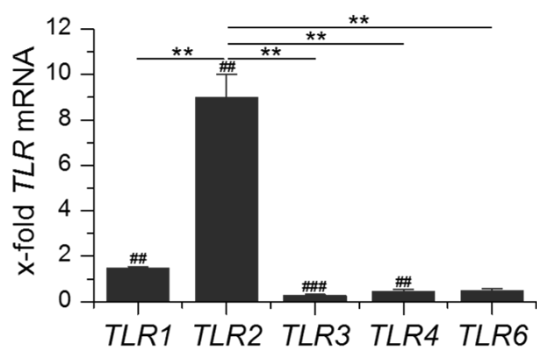


Figure 2-1: Long-Term LPS exposure upregulates *TLR2* in AMs. Primary human AMs were incubated with LPS (100 ng/ml) for 24 h. TLR expression was measured by qPCR. Data from three independent experiments performed in duplicate with cells from different donors are shown and are presented as means + SEM. #*p* < 0.05, ##*p* < 0.01 vs. untreated cells, **p* < 0.05, ***p* < 0.01 as indicated. P-values were generated with ANOVA and Bonferroni's post-hoc test.

On the protein level, TLR2 was highly upregulated after LPS or Dex treatment (fig. 2-2) for up to 24 h as indicated by Western blot analysis (fig. 2-2). The TLR2 induction by Dex was mediated by the glucocorticoid receptor (GR) since it could be abrogated by the GR antagonist RU486 (fig. 2-2, C and D). LPS and Dex treatment had an additive effect (fig. 2-2, C and D).

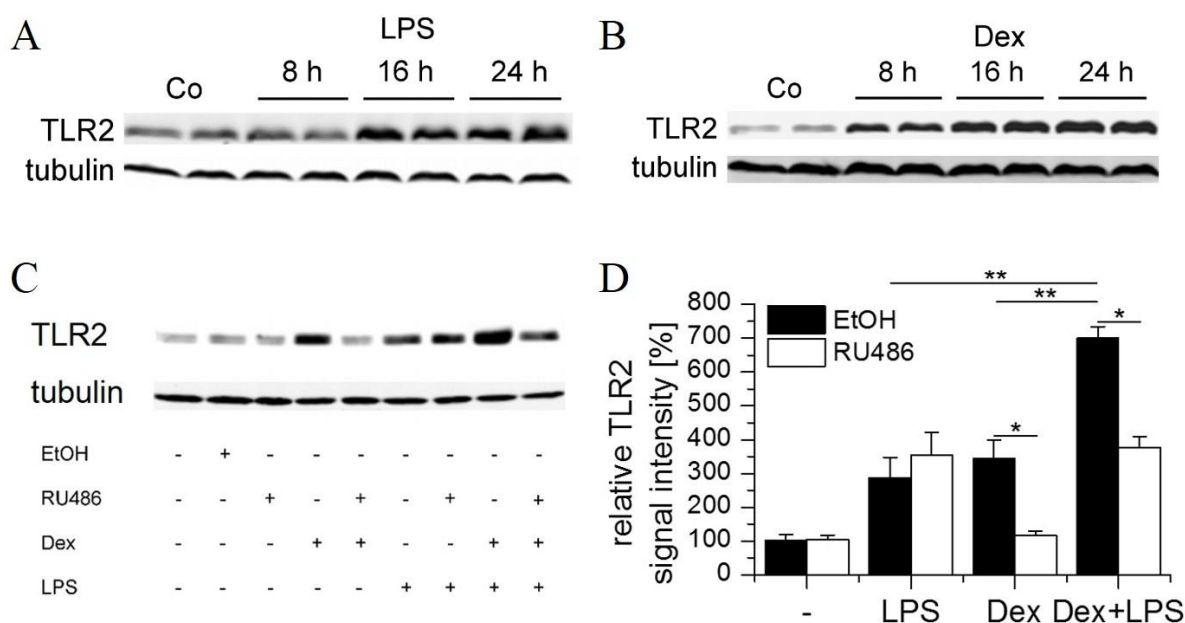


Figure 2-2: Lipopolysaccharide (LPS) and dexamethasone (Dex) upregulate TLR2 in AMs. Primary human AMs were incubated with solvent control (0.1% DMSO, Co), LPS (100 ng/ml; A), or Dex (1 μM; B) for up to 24 h. C and D: AMs were preincubated with the glucocorticoid receptor antagonist RU486 (10 μM) or solvent control (0.1% EtOH) and treated with LPS (100 ng/ml), Dex (1 μM) or both for 24 h. TLR2 expression was measured by Western blot. Data from at least three independent experiments performed in duplicate with cells from different donors are presented as means + SEM. **p* < 0.05, ***p* < 0.01. p-values were generated by ANOVA with Bonferroni's post-hoc test or Mann Whitney U test.

Surprisingly, the TLR2 receptor was not functional since the response towards the TLR2 ligand Pam3CSK4 (Pam) was profoundly impaired as shown by tumor necrosis factor (TNF) bioassay (fig. 2-3). After 4 h of Pam treatment, cells secreted the pro-inflammatory cytokine TNF (fig. 2-3). When preincubated with LPS or Dex for 24 h, Pam-induced TNF secretion was considerably reduced. After preincubation with both LPS and Dex, Pam-induced TNF production was abrogated entirely (fig. 2-3).

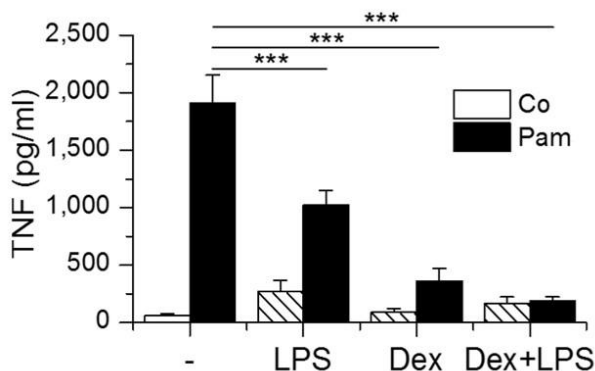


Figure 2-3: Impaired response towards TLR2 ligands in LPS- and/or Dex-pretreated AMs. Cells were preincubated with LPS (100 ng/ml), Dex (1 μ M), or both for 24 h and treated with Pam (1 μ g/ml, 4 h). TNF secretion was assessed by TNF bioassay. Data from at least three independent experiments performed in duplicate with cells from different donors are presented as means + SEM. *** p < 0.001. P-values were generated by ANOVA with Bonferroni's post-hoc test.

2.2.2 TLR2 is detectable in AM supernatant

We speculated that the upregulated, non-functional membrane-bound TLR2 might serve as a precursor for soluble TLR2 (sTLR2), known to antagonize TLR2-dependent cell actions (Raby *et al.*, 2009; Henrick *et al.*, 2016). Supernatants of 24 h LPS+Dex-primed AMs indeed contained the soluble 83 kDa form of TLR2, as indicated by Western blot analysis (fig. 2-4, A). Surprisingly, full-length TLR2 (fTLR2, ~ 102 kDa) could also be detected (fig. 2-4, A). We further hypothesized that this might be due to the production of TLR2-containing extracellular vesicles (EVs), while metalloproteinase (MP) activation may result in enhanced sTLR2 shedding from these vesicles as described by Langjahr *et al.* (2014). Indeed, activation of MPs by 4-aminophenylmercuric acetate (APMA; 10 μ M, 5 h) resulted in a significant increase of the short, soluble TLR2 form compared to the LPS+Dex samples, in which MPs were not activated (fig. 2-4, A and B). In LPS and Dex+APMA supernatants, a slight TLR2 signal could be observed as well (fig. 2-4, A). The absence of tubulin in the Western blot analyzes served as an indicator for cell debris free supernatants (fig. 2-4, A).

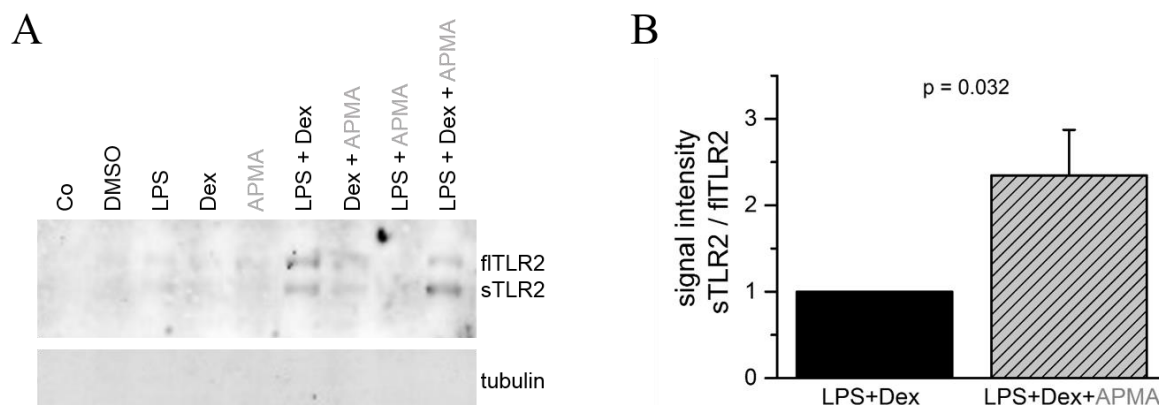


Figure 2-4: TLR2 is detectable as soluble (sTLR2) and full-length (flTLR2) protein in AM supernatant. 0.5×10^6 cells/well were seeded in a 12-well plate and incubated with solvent control (0.1% DMSO), LPS (100 ng/ml), Dex (1 μ M), or LPS+Dex for 24 h in medium without FCS. For the last 5 h of treatment, 10 μ M 4-aminophenylmercuric acetate (APMA) was added to the indicated samples to activate MMPs and therefore induce ectodomain shedding of flTLR2 to sTLR2. TLR2 protein in 10 x concentrated supernatant was detected by Western blot where tubulin served as a control for cell debris (A). Addition of APMA resulted in significantly more sTLR2, expressed as means + SEM of relative sTLR2/TLR2 signal intensities of three independent AM preparations and experiments (B). P-value was generated by student's t-test.

To test our hypothesis about the flTLR2 source, we isolated EVs from AM supernatants by sequential centrifugation, the present gold standard and most common method for vesicle isolation (Momen-Heravi *et al.*, 2013; Markowska *et al.*, 2017; Shao *et al.*, 2018).

After ultracentrifugation at 100.000 x g, we found mostly round vesicles of various sizes (50 – 300 nm) in the supernatant of untreated as well as LPS+Dex treated AMs, as observed by cryo-TEM (fig. 2-5, A). The vesicles were further analyzed by Western blot, and flTLR2 could be detected in the EV fraction of LPS+Dex treated cells (fig. 2-5, B). Additionally, in concentrated supernatants of LPS+Dex treated cells both forms of TLR2 were detectable before ultracentrifugation (UC). In the EV-depleted fraction (after UC), only sTLR2 was detectable in the LPS+Dex supernatant (fig. 2-5, B). In supernatants of untreated (Co) AMs, no TLR2 could be found at all (fig. 2-5, B). These Western blot results were confirmed in three different AM preparations.

Determination of the EV mean size *via* nanoparticle tracking analysis (NTA) revealed for one preparation 222 nm for control vesicle versus 149 nm for LPS+Dex vesicle. In a second preparation, vesicles of similar size were obtained: 170 nm control EV versus 155 nm LPS+Dex EV. NTA could only be performed for two EV preparations due to insufficient amounts of vesicle material.

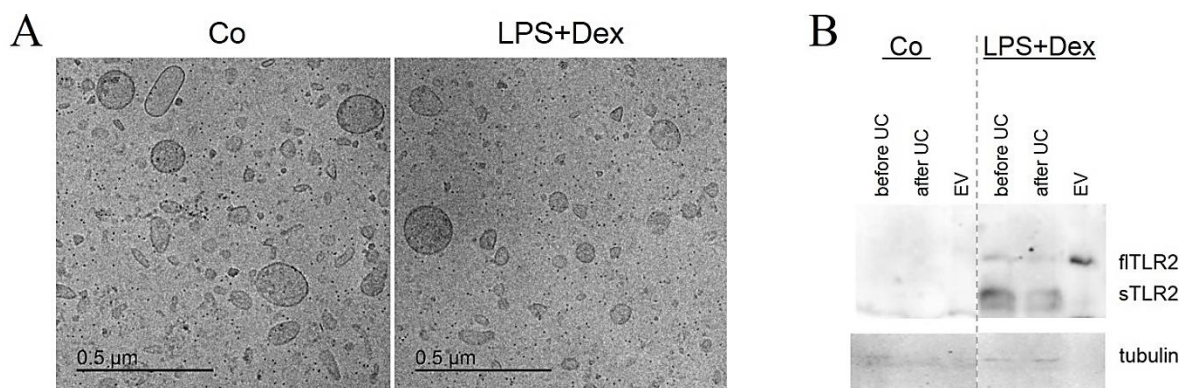


Figure 2-5: Characterization of AM vesicles. Cells were treated with LPS (100 ng/ml) and Dex (1 μ M) for three days before supernatants were harvested and EV were isolated by sequential centrifugation. **A:** Representative cryo-TEM pictures of secreted EV from untreated (Co) and LPS+Dex treated cells. **B:** One representative Western blot result for TLR2 detection in 10 x concentrated AM supernatants before and after ultracentrifugation (UC) and in EV is shown.

In summary, our data show that AMs induce TLR2 under anti-inflammatory conditions. TLR2 is released as the decoy receptor sTLR2 or as full-length TLR2 on EV, which may contribute to immunosuppression.

2.2.3 Characterization of THP-1-derived ECV

Since the yield of primary AMs was too low and variable for extended analyses, we decided to switch to THP-1 cells. For every preparation, 5×10^7 cells were seeded, differentiated with PMA for 48 h and then stimulated for three days in medium without FCS according to the same protocol previously used for AMs. Following EV isolation, NTA was used to determine the EV size and concentration.

Isolated THP-1 vesicles were very consistent in average size (around 220 nm), independent of cell treatment (fig. 2-6, A). However, they differed in their concentration depending on the treatment: After Dex and LPS+Dex treatment, significantly more vesicles could be isolated, approximately 1.5 times more compared to the control in both cases (fig. 2-6, B). After LPS treatment, the vesicle yield was comparable to that of untreated cells (fig. 2-6, B). In addition to NTA, vesicles were analyzed *via* cryo-TEM regarding morphology. All cells produced vesicles that were round in shape and varied in size between 50 and 250 nm (fig. 2-6, C).

To determine whether THP-1 vesicles also contained TLR2, Western blot analyses were performed. EV fractions as well as concentrated supernatants before and after UC were investigated. One representative Western blot result is shown in figure 2-6 (D). As already seen

for AM vesicles, LPS+Dex treated THP-1 secreted EVs containing flTLR2 (fig. 2-6, D). Unexpectedly, flTLR2 was also detected in EV fractions of Dex-treated and untreated cells (fig. 2-6, D), even though the signal in the untreated fraction was very weak. sTLR2 was detectable in every UC fraction, independent of the treatment (fig. 2-6, D).

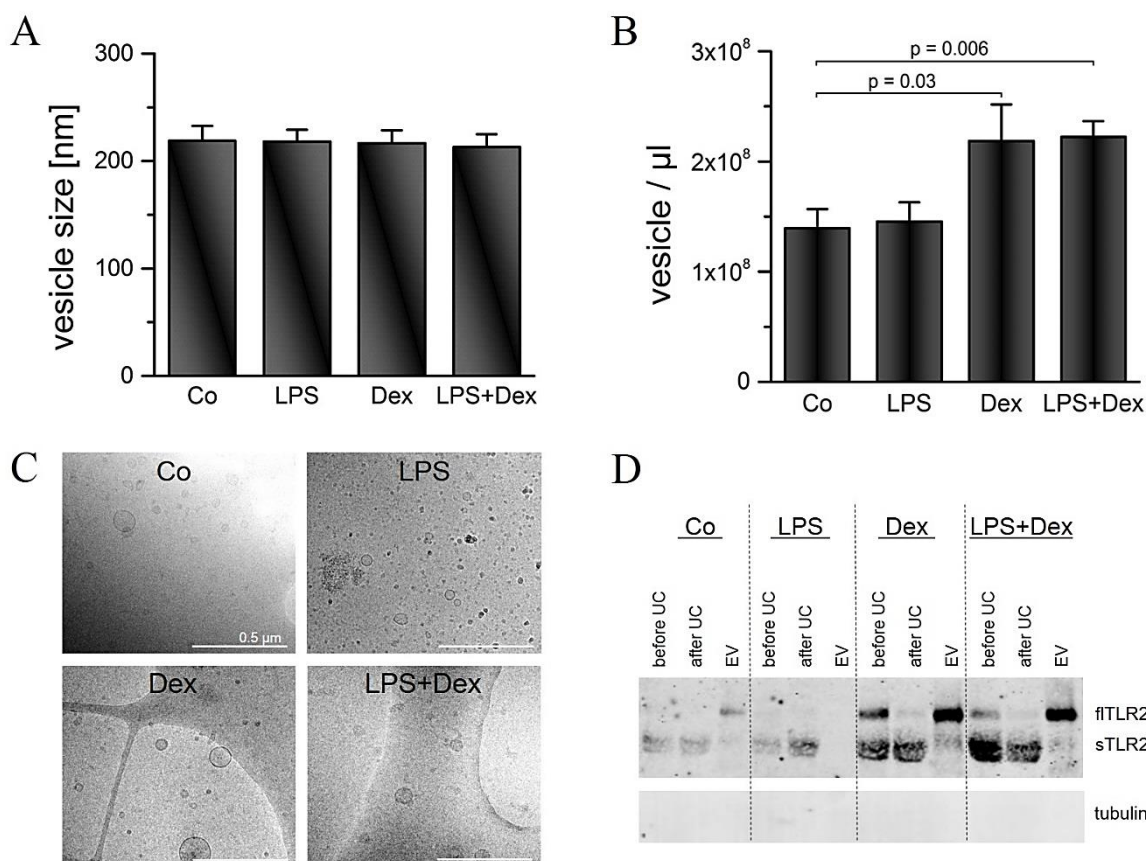


Figure 2-6: Characterization of THP-1 vesicles. Vesicle average size (A) and concentration (B) was determined by nanoparticle tracking analysis. Data are presented as means + SEM (n = 7), and p-values were generated by Mann Whitney U test. C: Morphology of the different EVs is shown in representative cryo-TEM pictures. D: One representative Western blot result out of three for TLR2 detection in 10 x concentrated THP-1 supernatant before and after ultracentrifugation (UC) and in EV fractions. Scale bar = 0.5 μ m

In the vast majority of EV isolations, the vesicle concentration correlated with the protein amount as determined by Pierce BCA assay (fig. 2-7). The slope was significantly different from zero (p = 0.003). Discrepancies might be due to difficulties in preparation since after UC the EV pellet was sometimes hard to dissolve.

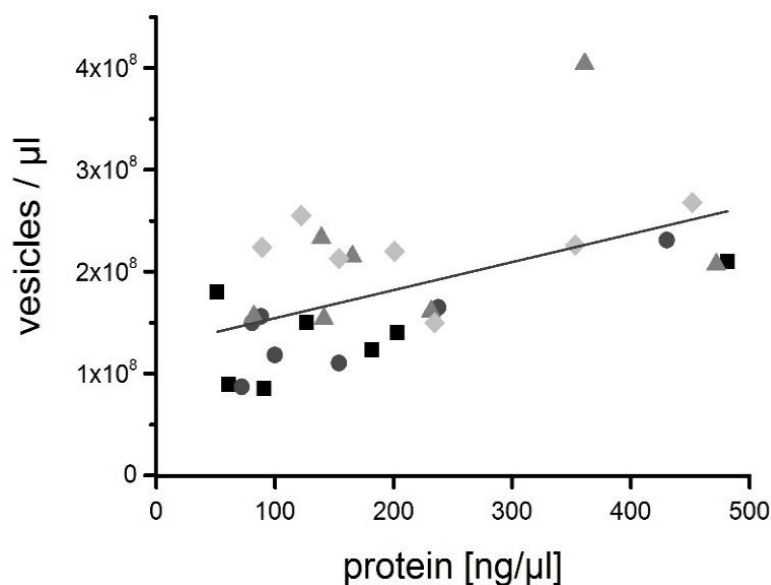


Figure 2-7: Correlation between EV concentration (vesicles/μl) and protein amount. Values for seven individual isolations are given. ■ = Co, ● = LPS, ▲ = Dex and ◆ = LPS+Dex EVs.

Culturing cells without FCS for three days may lead to cell stress causing enhanced apoptosis and thus the generation of apoptotic bodies, which might be isolated in the EV isolation protocol. Therefore, the caspase-3-like assay was performed. Doxorubicin (Doxo) was included as a positive control for apoptosis induction. Apoptosis was not increased under our experimental conditions, neither in THP-1 cells nor in AMs (fig. 2-8).

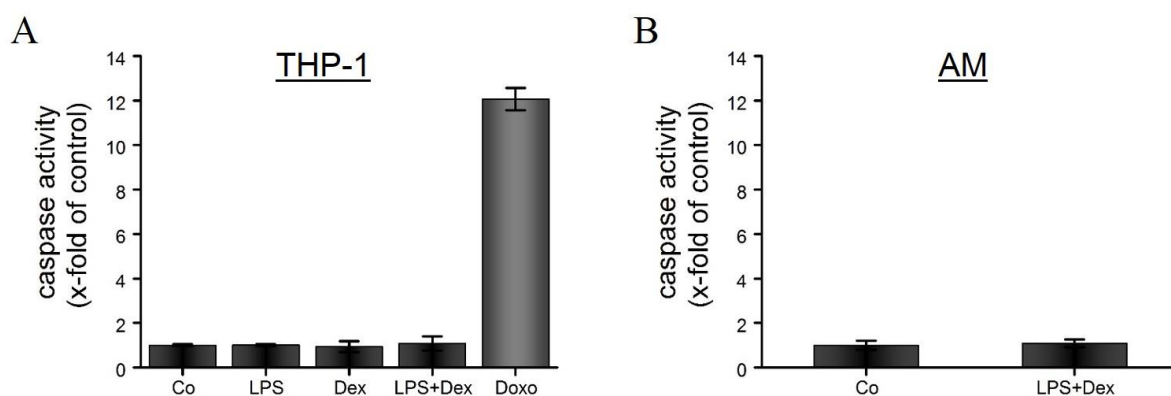


Figure 2-8: Caspase-3-like assay. THP-1 cells (A) and AMs (B) were treated with LPS (100 ng/ml), Dex (1 μM) or both for 3 d. Control cells (Co) were left untreated. THP-1 cells treated with 10 μM Doxorubicin (Doxo) for 24 h served as a positive control. (n = 3, triplicates)

THP-1 EVs were further analyzed by flow cytometry. For this purpose, vesicles were coupled to aldehyde/sulfate latex beads, since the size of EV is under the detection limit of the cytometer (Van Der Pol *et al.*, 2010; Erdbrügger *et al.*, 2014). BSA-saturated beads were used as a control. For direct detection of TLR2 on the EV surface, bead-EV complexes were stained with a fluorochrome-labeled anti-TLR2 antibody. Vesicles from LPS+Dex treated cells ($EV_{LPS+Dex}$) showed a significantly higher mean fluorescence intensity (MFI) compared to beads only but also compared to vesicles from untreated cells (EV_{Co}) (fig. 2-9, A).

In addition, bead-EV complexes were stained with the fluorochrome-labeled TLR2 ligand Pam3CSK4 (Pam). MFI values were highest for $EV_{LPS+Dex}$ samples (fig. 2-9, B). MFI of control vesicles was comparable to the uncoupled beads (fig. 2-9, B).

EVs were additionally characterized by the presence of common markers, tetraspanins CD9 and CD63 (van Niel, D'Angelo and Raposo, 2018), to make sure that both EV types had bound to the beads. Staining with fluorochrome-labeled anti-CD9 and anti-CD63 revealed that bead-coupled EV preparations were positive for both markers. However, the signal intensity for EV_{Co} was about twice as high compared to $EV_{LPS+Dex}$ (fig. 2-9, C and D). This might be either due to a differential bead-binding capacity of both EV types or a distinct expression of tetraspanins on the EV surface. Discrepancies between vesicle amount and protein concentration might also contribute to the overall effect.

To investigate whether the different cell treatments had an impact on vesicle composition, EV preparations were analyzed by high-resolution tandem mass spectrometry (MS/MS).

A total of 709 proteins was detected, and 401 proteins occurred in all four ECV types (fig. 2-10). 41 proteins were found exclusively in vesicles from untreated cells, 31 exclusively after LPS treatment, 23 after Dex, and 48 after LPS+Dex treatment (fig. 2-10). These exclusive proteins were examined for their molecular function according to GO terms using the PANTHER GO classification system (version 11) (fig. 2-10). Most of them were associated with catalytic activity, followed by binding as a molecular function (blue and dark grey, fig. 2-10).

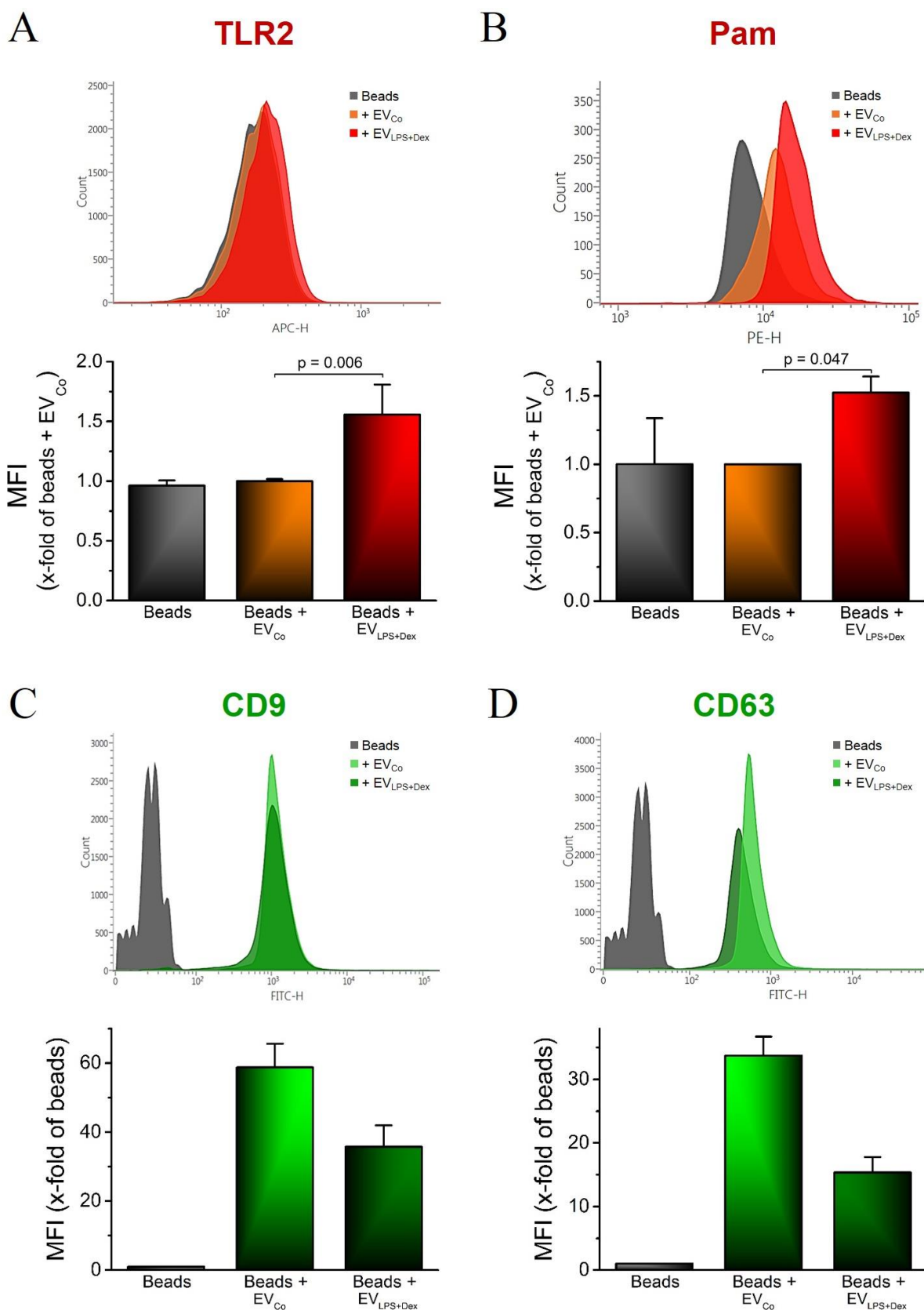


Figure 2-9: Analysis of EV-coated beads by flow cytometry. A-D: In each case, one representative histogram overlay is shown (top) together with the quantification of three independent preparations (mean + SEM, bottom) for anti-TLR2 (A), Pam (B), anti-CD9 (C), and anti-CD63 (D). Quantification data are expressed as mean fluorescence intensity (MFI) x-fold of Beads+EV_{Co} (A and B) or of uncoated beads (C and D), and p-values were generated by Mann Whitney U test (A, C and D) or one sample t-test (B).

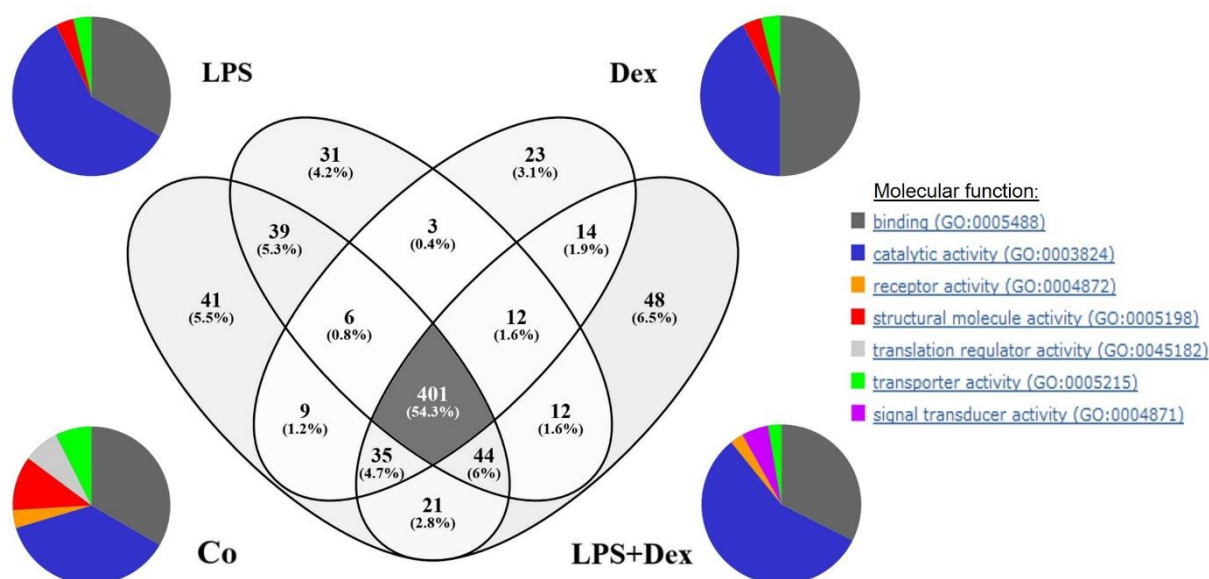


Figure 2-10: Venn diagram representing protein distribution according to proteomics results for THP-1 EV. 709 proteins were found in total. Exclusive proteins were categorized regarding their molecular function according to GO terms using the PANTHER GO classification system (version 11). The Venn diagram was generated with Venny (version 2.1; Oliveros 2007). Data were obtained from three independent vesicle preparations.

Subsequently, the data of the individual three measurements were examined in more detail. TLR2 was detected in every single LPS+Dex sample and in two of three Dex samples, but in none of the controls or LPS samples (fig. 2-11, bottom). However, this finding fits only partially to the Western blot results (fig. 2-6, D), since TLR2 was also detectable in EV secreted from untreated THP-1 cells by this method.

In order to check the reproducibility between the preparations, a whole series of markers were selected and compared. Exclusive, unique spectrum count raw data of the selected EV marker proteins are shown in figure 2-11 for the independent preparations per treatment. A distinction was made between exosome specific (like CD63, ICAM1, and RHOG), overlapping (like CD9, CD81, annexins, or RAB proteins), and microvesicle specific (like fibronectin (FINC), PECAM1, and ARF6) markers, respectively, according to Van Niel et al. (2018). Compared to flow cytometry, where tetraspanins CD9 and CD63 seemed to be more abundant on EV_{Co}, their detection level was almost identical according to mass spectrometry analysis (compare fig. 2-8, C and D, and fig. 2-11).

Overall, the EV-specific protein distribution was quite similar and seemed to be independent of the cell treatment (fig. 2-11). However, expression of two particular proteins was strikingly imbalanced, indicated by a small scale symbol in figure 2-11. The exosome specific MFGM, also known as lactadherin, was highly expressed in EV from Dex and LPS+Dex cells, compared to the low or in parts non-expression in EV from LPS-exposed or untreated cells (fig. 2-11). In

contrast, the microvesicle-specific cluster of differentiation (CD) 82 was present in EV_{Co} and EV_{LPS}, but less abundant in EV_{Dex} and EV_{LPS+Dex} (fig. 2-11).

		Co			LPS			Dex			LPS+Dex			
exosome specific	PKM	71	60	88	76	66	94	67	50	78	65	68	81	⚖️
	ENOA	34	30	38	35	28	31	42	35	33	38	41	37	
	MFGM	10	11	0	12	9	0	46	46	24	45	56	35	
	CD63	8	9	7	8	7	5	8	8	5	7	9	7	
	ICAM1	12	16	10	13	17	12	11	10	5	9	14	6	
	PERE	2	5	0	0	3	0	0	3	0	0	0	0	
	1433Z	14	17	13	17	14	13	22	15	15	17	24	17	
	1433T	10	7	13	5	4	12	12	13	14	9	17	15	
	M4K4	8	10	5	10	13	0	8	4	2	6	2	0	
	RHOG	2	0	3	0	0	0	4	2	0	3	3	3	
overlapping markers	H2A2	6	5	4	4	6	3	5	5	3	5	4	4	
	H2B2	18	21	15	15	28	15	14	25	19	16	24	21	
	H4	36	32	30	30	38	34	32	40	38	31	36	37	
	H3.1	23	15	15	15	16	13	14	23	19	18	19	14	
	HSP90	64	59	60	63	50	56	56	46	56	52	56	65	
	ITAM	55	64	61	64	50	53	55	53	48	58	54	58	
	ITB2	34	50	40	47	35	26	44	43	36	40	57	37	
	ANXA2	29	35	32	31	35	31	37	34	26	38	42	31	
	ANXA4	19	16	14	21	14	14	19	19	12	18	22	16	
	ANXA5	32	32	30	33	32	26	34	29	31	34	40	34	
	ANXA6	28	36	14	25	31	10	28	27	8	22	40	18	
	RHOA	7	11	10	9	7	7	9	8	10	11	10	9	
	CD9	8	9	7	8	6	7	8	8	7	6	7	7	
	CD81	8	8	6	6	7	6	7	8	5	7	7	6	
	RAB1A	8	10	9	9	9	8	6	7	4	8	8	10	
	RAB5C	8	9	5	7	5	6	9	7	6	7	6	7	
	RAB7A	11	11	11	13	11	9	12	12	10	11	11	10	
RAB14	8	6	6	7	6	7	7	4	4	8	6	5		
TSG101	4	7	2	7	7	2	6	8	2	4	2	2		
VPS4B	4	6	3	3	5	3	4	4	4	3	3	4		
microvesicle specific	FINC	152	138	144	161	125	118	227	121	129	224	158	162	⚖️
	PECAM1	13	17	16	18	11	13	11	14	9	18	14	11	
	CD82	10	10	3	10	9	2	7	4	0	3	3	0	
	PLD3	3	3	6	2	0	2	3	2	5	5	6	3	
	RAB11B	9	5	3	4	4	3	8	4	3	5	4	6	
	ROCK1	0	0	4	0	0	0	2	4	4	3	5	3	
	ARF6	2	2	2	2	2	0	2	3	2	3	3	0	
TLR2	0	0	0	0	0	0	8	5	0	10	11	7		

Figure 2-11: TLR2 and EV marker distribution in EVs from differentially treated THP-1 cells. Exclusive unique spectrum count raw data are shown for all three independent preparations per treatment. A distinction was made between exosome specific, overlapping and microvesicle specific markers, respectively, according to Van Niel et al. (2018). Small scale symbols indicate an imbalance in protein abundance between Co and LPS+Dex preparations.

Moreover, EV_{Co} and $EV_{LPS+Dex}$ samples were compared regarding differentially enriched proteins. A volcano plot representing the differential enrichment between the two EV types as well as the most significantly enriched proteins for each of them is shown in figure 2-12 (A). For mathematical reasons, only proteins that appeared under both stimulation conditions could be taken into account.. The following proteins were at least 2-fold enhanced in $EV_{LPS+Dex}$ (p-value < 0.05): lactadherin (MFGM), carboxypeptidase (CBPM), F-actin-capping protein subunit beta (CAPZB), isocitrate dehydrogenase (IDHP), proteasome subunit beta type-1 and -2 (PSB1/2), Rho GDP-dissociation inhibitor 1 (GDIR1), arrestin domain-containing protein 1 (ARRD1), filamin-B (FLNB), and plasma membrane calcium-transporting ATPase 4 (AT2B4).

Cluster of differentiation (CD) 36, heterogeneous nuclear ribonucleoprotein L (HNRPL), L-amino-acid oxidase (OXLA), ribosomal L1 domain-containing protein 1 (RL1D1), basement membrane-specific heparan sulfate proteoglycan core protein (PGBM), and rRNA 2'-O-methyltransferase fibrillar (FBRL) were significantly decreased in $EV_{LPS+Dex}$ compared to EV_{Co} .

For easier comparison of reproducibility between the three individual vesicle preparations, a heatmap based on the ratio $[\log_2(EV_{LPS+Dex}/EV_{Co})]$ was generated for the significantly altered proteins (fig. 2-12, B).

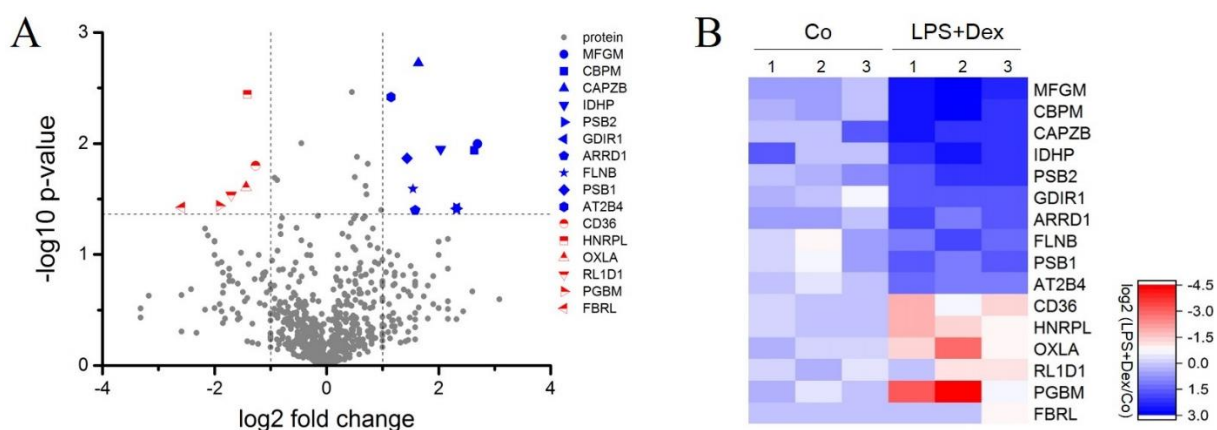


Figure 2-12: Identification of the proteins differentially enriched in EV_{Co} and $EV_{LPS+Dex}$. **A:** Volcano plot representing the differential enrichment between the two EV types as well as the most significantly enriched proteins for each of them. X-axis = $\log_2(EV_{LPS+Dex}/EV_{Co})$. Y-axis = $-\log_{10}$ (adjusted p-value). The horizontal broken line indicates p-value = 0.05, vertical broken lines indicate x-fold of control = 0.5 and 2. **B:** Heatmap based on the ratio $[\log_2(EV_{LPS+Dex}/EV_{Co})]$ of protein quantities in each fraction and three independent preparations (1-3). MFGM: lactadherin; CBPM: carboxypeptidase; CAPZB: F-actin-capping protein subunit beta; IDHP: isocitrate dehydrogenase; PSB2: proteasome subunit beta type-2; GDIR1: Rho GDP-dissociation inhibitor 1; ARRD1: arrestin domain-containing protein 1; FLNB: filamin-B; PSB1: proteasome subunit beta type-1; AT2B4: plasma membrane calcium-transporting ATPase 4; CD36: cluster of differentiation 36; HNRPL: heterogeneous nuclear ribonucleoprotein L; OXLA: L-amino-acid oxidase; RL1D1: ribosomal L1 domain-containing protein 1; PGBM: basement membrane-specific heparan sulfate proteoglycan core protein; FBRL: rRNA 2'-O-methyltransferase fibrillar

2.2.4 Functional analyzes of THP-1 vesicles

To examine the functionality of the isolated EVs, two possibilities were taken into consideration: one inhibitory or decoy scenario and one uptake scenario. Primary human umbilical vein embryonic cells (HUVECs) were used as target cells since they are known to have low TLR2 baseline expression. This allows activation by Pam treatment, which might be either amplified or attenuated by EV addition. Expression of adhesion molecules such as *intercellular adhesion molecule 1* (ICAM), *vascular cell adhesion molecule 1* (VCAM) and *E-selectin* (SELE) was used as readout parameter.

In the first scenario, TLR2 on EVs from LPS+Dex-treated cells would compete with membrane-bound TLR2 for potential ligands, and thus inhibit intracellular TLR2 signaling by a decoy mechanism. To test this assumption, EVs were pre-incubated with the TLR2 ligand Pam (fig. 2-13, A). The EV-Pam mix was then used for HUVEC treatment (fig. 2-13, A).

In the second scenario, vesicles would be taken up by HUVECs and deliver functional TLR2 to the cells, thereby amplifying the response after Pam treatment. For the experimental procedure depicted in figure 2-13 (B), HUVECs were incubated with EV, washed, and stimulated with Pam. Pam-induced gene expression changes were determined *via* qRT-PCR. In addition to the three adhesion molecules *ICAM*, *VCAM*, and *SELE*, the expression of the inflammatory marker *CC-chemokine ligand 2* (*CCL2*) was also determined.

In the decoy experiment, *CCL2* was significantly decreased in HUVECs treated with $EV_{LPS+Dex}$ compared to EV_{Co} (fig. 2-13, C). In addition, the three adhesion molecules showed a decreased expression, although not significantly so (fig. 2-13, C).

On the other hand, delivery of functional TLR2 *via* EV to HUVECs did not occur, since none of the activation markers was increased after preincubation with $EV_{LPS+Dex}$ (fig. 2-13, D).

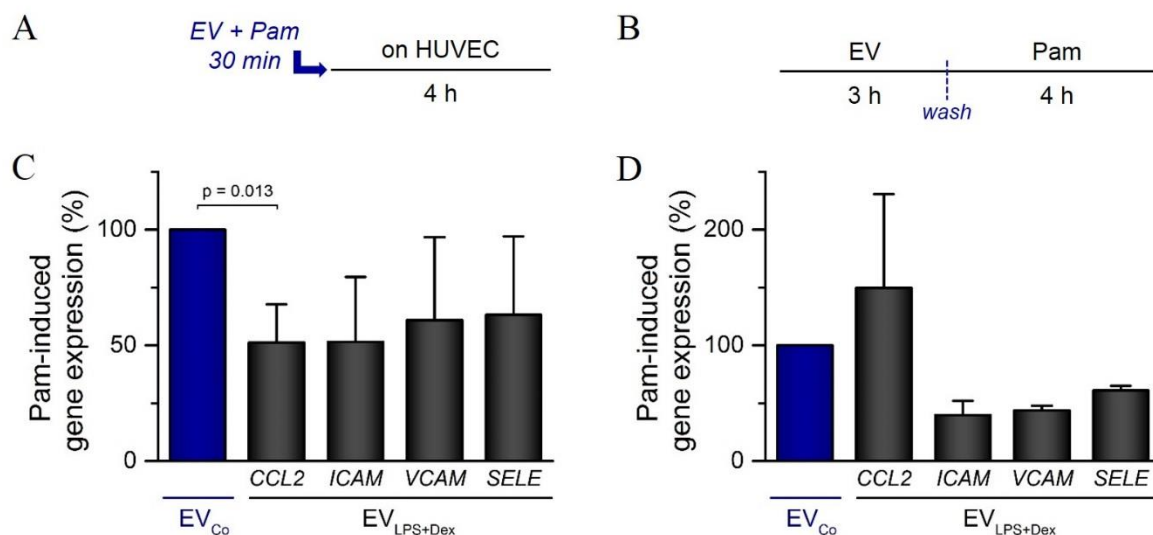


Figure 2-13: EV function. Pam-induced gene expression (in %) was measured by qRT-PCR after vesicle (5×10^9 in total) pre-incubation with $1 \mu\text{g/ml}$ Pam for 30 min prior to stimulation of HUVECs with ECV-Pam mix (A + C). Alternatively, HUVECs were incubated for 3 h prior to washing and 4 h treatment with $1 \mu\text{g/ml}$ Pam (B + D). Data from experiments with three independent THP-1 vesicle preparations and different HUVEC donors are shown as mean + SEM and p-values were generated by one sample t-test.

In addition, a more sensitive model, i.e. HEK-Dual™ hTLR2 (NF/IL8) cells, were used. This commercially available reporter cell line was generated by stable transfection of the human TLR2 (hTLR2) and CD14 genes, according to the supplier. It features a triple knockout of TLR3, TLR5, and the TNF receptor (TNFR), thereby avoiding interferences caused by the activation of other signaling pathways. The cells express a secretable luciferase reporter construct under the control of the endogenous IL-8 promotor. The chemokine IL-8 was shown to be produced in response to TLR2 agonists in an NF- κ B and AP-1 dependent-manner (Roebuck, 1999; Qin, Li and Qiao, 2016). Thus, TLR2 stimulation can be easily monitored by the TLR2 agonist-induced expression of IL-8-dependent luciferase in this cell line.

The TLR2 agonists Pam and FSL-1 were pre-incubated with the EVs for 30 min before addition to the cells (fig. 2-14, A). After 24 h, luciferase activity was measured in the cell supernatant. Compared to EV_{Co}, TLR2-containing EV_{LPS+Dex} decreased luciferase secretion in response to FSL-1 significantly (fig. 2-14, B) but barely in response to Pam (fig. 2-14, C).

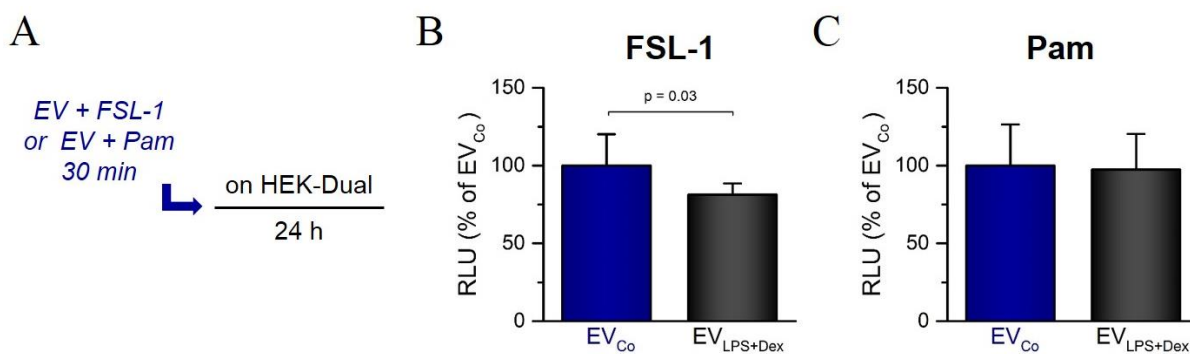


Figure 2-14: Influence of EVs on IL-8 production in HEK-Dual™ hTLR2 (NF/IL8) cells. **A:** Scheme of the experimental procedure. Cells were stimulated with TLR2 agonists FSL-1 (1 ng/ml) (**B**) or Pam (0.1 ng/ml) (**C**). After 24 h, luciferase activity in the supernatant was determined and is shown as percentage of RLU (relative luminescence units) with values for EV_{Co} set as 100%. Data show the means + SEM of three independent experiments performed in duplicates. p-values were calculated by one sample t-test.

In summary, ECV_{LPS+Dex} reduced TLR2-dependent signal transduction rather than increasing it, suggesting an overall inhibitory function for ECV_{LPS+Dex}.

2.3 Discussion

AMs are one of the first lines of defense against the invasion by airborne pathogens. The activation of TLRs triggers the production of pro-inflammatory cytokines, which in turn activate the hypothalamic-pituitary axis to induce the synthesis and secretion of anti-inflammatory glucocorticoids by the adrenal cortex (Hermoso *et al.*, 2004; Chinenov and Rogatsky, 2007).

Almost two decades ago, two studies showed that TLR2, but not TLR4, is induced by TLR4-mediated LPS signaling in adipocytes (Lin *et al.*, 2000) and murine macrophages (Matsuguchi *et al.*, 2000), respectively. Further studies showed an LPS-induced TLR2 up-regulation through TLR4-dependent signaling also in murine lung endothelial cells (Fan, Randall and Asrar, 2003), as well as in murine AMs in the context of antecedent hemorrhagic shock (Fan *et al.*, 2006). These studies correspond to our observations of LPS-mediated TLR2, but not TLR1/4/3/6 up-regulation in human AMs. Paradoxically, there is an emerging amount of work documenting that glucocorticoids also enhance inflammation and innate immunity, for instance by upregulating TLR2 (Busillo and Cidlowski, 2013; Cain and Cidlowski, 2017). The glucocorticoid-mediated induction of TLR2 has been shown in multiple human epithelial cell types (Shuto *et al.*, 2002; Hermoso *et al.*, 2004; Homma *et al.*, 2004) and in human dendritic cells (Rozkova *et al.*, 2006). Furthermore, glucocorticoid-induced TLR2 expression seems to be further enhanced in a synergistic manner by the presence of pro-inflammatory cytokines (e.g., TNF- α) or *Haemophilus influenzae* (Shuto *et al.*, 2002; Hermoso *et al.*, 2004; Homma *et al.*, 2004; Chinenov and Rogatsky, 2007), supporting our findings of an additive effect for LPS and Dex. However, TLR2 was not functional in our experimental setting. This might be due to the fact that its dimerization partners (TLR1 and 6) were not upregulated in LPS-exposed AMs, suggesting a different function for TLR2.

Since there was an emerging number of publications about sTLR2 (recently reviewed by Henrick *et al.*, 2016), we hypothesized that this soluble form was present in AM supernatants and found that sTLR2 was indeed produced, in particular by LPS/Dex-treated macrophages. In addition, we detected an unexpected protein that corresponded to full-length TLR2. The shorter form was enriched after activation of MPs, indicating that ectodomain shedding leads to sTLR2 production (Langjahr *et al.*, 2014). Already in 2014, Langjahr *et al.* observed a full-size TLR2 glycoprotein in human macrophage supernatant and hypothesized that it might correspond to the full-length protein associated with membrane vesicles. This hypothesis is supported by our results showing that flTLR2 is present in isolated EVs.

Under physiological and pathological conditions, almost all cell types release cell-derived phospholipid-based bilayer membrane vesicles equipped with functional surface and membrane proteins and encapsulating diverse cargoes, including proteins, cytokines, lipids, and nucleic acids (Fuhrmann et al., 2015; Yáñez-Mó et al., 2015). EVs have been suggested to significantly contribute to intercellular communication (Colombo, Raposo and Théry, 2014; Zhang *et al.*, 2015; Kalra, Drummen and Mathivanan, 2016; van Niel, D'Angelo and Raposo, 2018). They are categorized as exosomes, microvesicles (MVs), and apoptotic bodies based on their size, pathway of formation, and membrane composition (Yáñez-Mó *et al.*, 2015). Exosomes, which are 30–200 nm in size, derive from the late endosome. MVs are between 100–1,000 nm in diameter and are formed through outward budding of the plasma membrane. Apoptotic bodies are derived from apoptotic cells and are very heterogeneous in size and morphology, therefore being distinctly different from the other two EV subtypes (Fuhrmann, Herrmann and Stevens, 2015; Ohno, Drummen and Kuroda, 2016). Since exosomes and microvesicles display a similar appearance and composition as well as an overlapping size distribution, it is difficult to define their origin once isolated (Smith *et al.*, 2015; van Niel, D'Angelo and Raposo, 2018). Thus, we made no further distinction between vesicle types in this work. However, the appearance of apoptotic bodies could be excluded, because neither AMs nor THP-1 macrophages showed morphological changes nor elevated caspase 3 activity upon treatment.

Flow cytometric analysis with EVs confirmed the presence of TLR2 on the surface of EV_{LPS+Dex} and indicate an intact ligand binding ability. Furthermore, the different cell treatments seemed to have an impact on vesicle composition, since a number of proteins was differentially enriched. It is well established that exogenous stress as well as inflammatory or infectious processes can affect EV properties, such as composition (Fuhrmann, Herrmann and Stevens, 2015; Kalra, Drummen and Mathivanan, 2016). However, the overall EV-specific protein distribution (van Niel, D'Angelo and Raposo, 2018) was independent of the cell treatment.

That AMs can communicate with other cells within the alveolar space *via* EVs has been recently reviewed by Lee et al. (2018). Therefore, we incubated our macrophage-derived EVs with primary endothelial cells and a HEK reporter cell line. EVs can interact with their recipient cells in different ways: (I) direct activation of target cell surface receptors, (II) membrane fusion with the recipient cell or (III) incorporation into the target *via* endocytosis, pinocytosis, or phagocytosis (Jansen *et al.*, 2017; van Niel, D'Angelo and Raposo, 2018). Previous reports showed the uptake of EVs by different endothelial cells (Durak-Kozica *et al.*, 2018). Furthermore, *Mycobacterium tuberculosis*-infected murine macrophages released ECVs inducing VCAM and TLR2 in murine

endothelial cells (Li *et al.*, 2018). In contrast, our study revealed anti-inflammatory properties of macrophage-derived EVs.

The overall inhibitory function for EV_{LPS+Dex} suggests that they may act as a decoy, as previously shown for sTLR2 (Raby *et al.*, 2009; Langjahr *et al.*, 2014).

This decoy activity may involve competition for not only the microbial ligand but also the heterodimerization partners (Raby *et al.*, 2009). On the other hand, flTLR2 associated with EVs may either catch microbial molecules or opsonize the whole bacterium, thereby initiating the uptake by phagocytes. This hypothesis is supported by the high MFGM (also called MFGE8 or lactadherin) content in EV_{LPS+Dex}, as MFGM is known to potentiate phagocytosis (Hanayama *et al.*, 2002; Raymond, Ensslin and Shur, 2009; Buzás *et al.*, 2018).

In summary, we showed that sTLR2 and full-length TLR2 are released by macrophages under anti-inflammatory conditions. Our data suggest that vesicle-bound flTLR2 may have decoy functions, which may contribute to immunosuppression induced by GCs and chronic infections.

3. Chapter II

Investigation of human lung tumor-associated macrophages (TAMs) and establishment of a TAM-like macrophage model

Parts of the following results presented in this chapter have been published in:

“M2 polarization enhances silica nanoparticle uptake by macrophages”. Jessica Hoppstädter, Michelle Seif, Anna Dembek, Christian Cavelius, Hanno H. Huwer, Annette Kraegeloh and Alexandra K. Kiemer (2015) *Frontiers in Pharmacology*; 6:55. doi: 10.3389/fphar.2015.00055.

3.1 Introduction

Lung cancer represents the leading cause of cancer-related mortality worldwide, with an estimated 2.09 million new cases diagnosed and 1.76 million deaths expected from the disease in 2018, according to the World Health Organization (WHO; as at September 12, 2018; <https://www.who.int/en/news-room/fact-sheets/detail/cancer>).

According to its histology (WHO guidelines, Travis et al. 2004) and recently also according to tumor genetics (WHO guidelines, Travis et al. 2015), lung cancer can be divided into two major types: small cell lung cancer (SCLC) representing a minority of about 15% and non-small cell lung cancer (NSCLC) representing about 85% of cases (Molina *et al.*, 2008; Ahmad and Gadgeel, 2016). These two types of cancers grow, spread, and are treated in different ways, so distinguishing between these two types is important (Travis, 2011). NSCLC can be further classified into several subtypes based on their histological characteristics. The most common subtypes are adenocarcinoma (40%), squamous-cell carcinoma (30%), and large-cell carcinoma (15%) (Rivas-Fuentes *et al.*, 2015), and are visualized in figure 3-A. Within this thesis, only adenocarcinomas were investigated, as they represent the majority of lung cancers and are most commonly described in the literature.

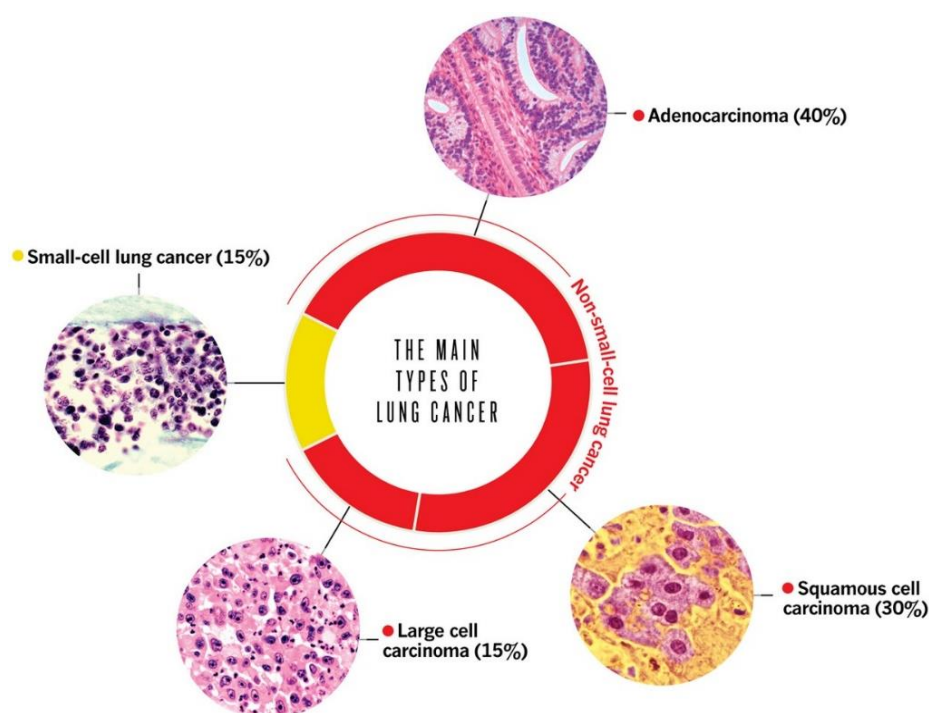


Figure 3-A: The main types of lung cancer with percentage distribution. Based on histology, lung cancer can be divided into the main groups small-cell lung cancer and none small-cell lung cancer (NSCLC). NSCLC can be further classified into the following subtypes: adenocarcinoma, squamous-cell carcinoma and large-cell carcinoma. Graphic modified after Bender (2014).

The best option for cure is surgical resection of the tumor. However, the majority of patients are diagnosed in an advanced or even metastatic state, when surgery is no longer feasible. Further therapy options are radiation and chemotherapy, although in all cases a resistance ultimately develops (Molina *et al.*, 2008; Conway *et al.*, 2016). In recent years, targeted therapy has been

considered promising, especially when mutations in the *epidermal growth factor receptor (EGFR)* and rearrangements in *anaplastic lymphoma kinase (ALK)* are present, but only a very small proportion of adenocarcinoma patients carry these mutations (Travis *et al.*, 2015; Ahmad and Gadgeel, 2016; Cheng *et al.*, 2017). Overall, the 5-year survival rate for NSCLC failed to increase significantly within the last decade and remains at 15-18% (Molina *et al.*, 2008; Conway *et al.*, 2016).

In the past, cancer research focused on the tumor cell itself. In recent years, however, investigations of the tumor microenvironment (TME) and its essential function in supporting malignancy has become more and more important, especially with regard to new immunotherapies (Quail and Joyce, 2013). Among the diverse cell types of the TME, macrophages are the most abundant non-tumor cell type in most cancers (Noy and Pollard, 2015). These tumor-associated macrophages (TAMs) can compose up to 50% of the solid tumor mass (Solinas *et al.*, 2009; Mills, Lenz and Harris, 2016; Parayath, Parikh and Amiji, 2018) and are therefore discussed as new auspicious treatment target in oncology (Conway *et al.*, 2016; Mills, Lenz and Harris, 2016; Mantovani *et al.*, 2017).

In NSCLS, many reports have described a correlation between TAM density or phenotype and clinical outcomes (Quatromoni and Eruslanov, 2012; Conway *et al.*, 2016; Takeya and Komohara, 2016). The vast majority of this reports is based on immunohistochemistry, as reviewed by Conway *et al.* (2016).

TAMs have been suggested to rather represent an M2-like phenotype, driven by the TME (Wang *et al.*, 2011; Italiani and Boraschi, 2014). In general, a high prevalence of TAMs with M2 polarization, especially in tumor stroma correlates with poor prognosis (Ohtaki *et al.*, 2010; Zhang *et al.*, 2011; Gentles *et al.*, 2015; Yuan *et al.*, 2015) since these cells exert several tumor-promoting functions, including stimulation of angiogenesis, remodeling of the extracellular matrix, promotion of cancer cell proliferation, invasion, extravasation and metastasis, and immunosuppression (Solinas *et al.*, 2009; Bremnes *et al.*, 2011). In early stages of NSCLC, however, density of tumor-preventing M1-TAMs in tumor islets is associated with extended survival (Zeni *et al.*, 2007; Ohri *et al.*, 2009; Ma *et al.*, 2010). In contrast, AMs, the predominant tissue-resident macrophages of the lung, are considered to exhibit a rather tumor-preventing, M1-like phenotype (Hopstädter *et al.*, 2010; Almatroodi, McDonald and Pouniotis, 2014), at least in healthy individuals (Hussell and Bell, 2014). AMs were shown to originate from embryonic precursors that populate the lung around birth and can self-maintain in adulthood through local proliferation with minimal contribution of circulating monocytes in the steady-state (Guilliams *et al.*, 2013;

Ginhoux and Guilliams, 2016). In case of inflammation or injury, though, circulating bone marrow-derived monocytes significantly contribute to AM pools (Maus *et al.*, 2006; Epelman, Lavine and Randolph, 2014). This might explain why TAMs are suggested to be also mainly derived from bone marrow monocytes (Franklin and Li, 2016; Lahmar *et al.*, 2016; Bolli *et al.*, 2017) and differentiate into macrophages under the influence of the TME (fig. 3-B).

Due to both, their heterogeneous origin and their different environment, it is conceivable that these two populations (resident AMs vs. monocyte-derived TAMs) play different or even opposing roles in tumor progression. Thus, identifying key features of each population may help to target them therapeutically.

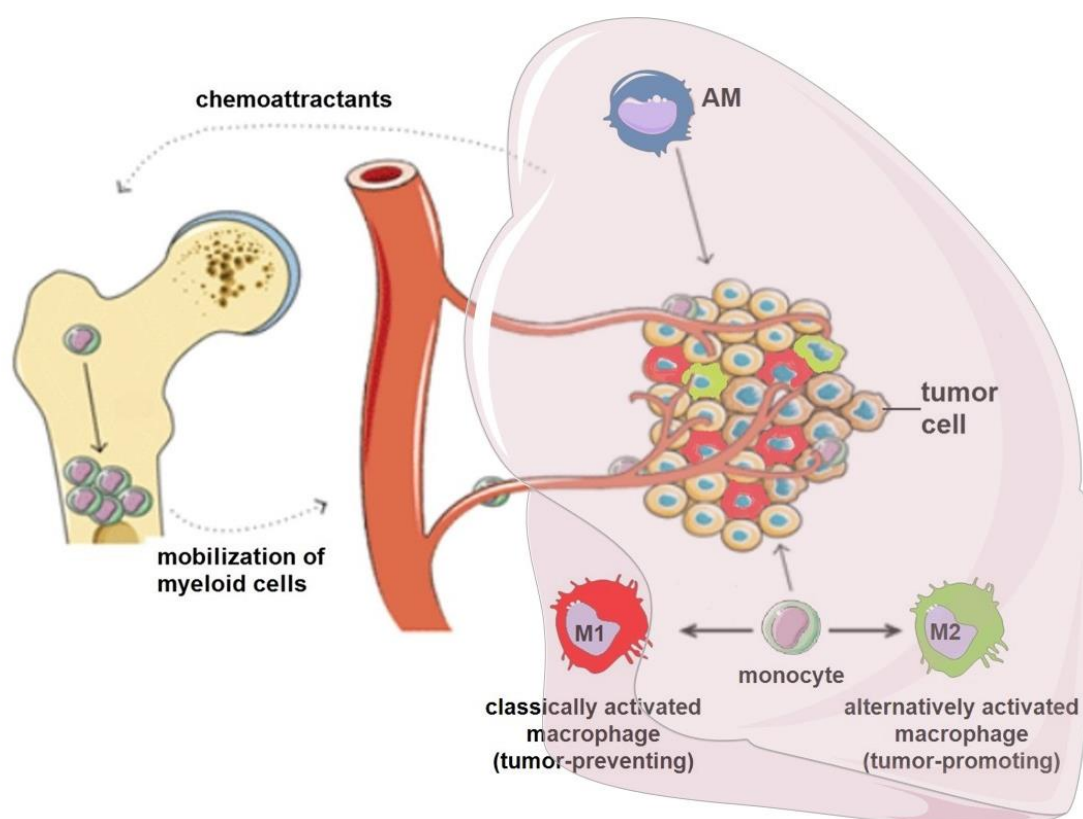


Figure 3-B: Macrophage contribution to the tumor mass. Monocytes are recruited to the tumor site by chemoattractants and differentiate into macrophages. Under the influence of tumor cells and the associated microenvironment, they can be either rather M1- or M2-polarized. Further information can be found in the text. AM: alveolar macrophage. Illustration was obtained and modified from Servier Medical Art by Servier, <https://smart.servier.com/>, licensed under Creative Commons Attribution 3.0 Unported License, <http://creativecommons.org/licenses/by/3.0/>.

3.2 Results

3.2.1 Human primary AM/TAM mRNA profile and nanoparticle uptake capacity

Human primary TAMs were obtained after digestion of adeno- or squamous cell carcinoma tumor tissue from patients undergoing lung resection, whereas AMs were isolated from the surrounding non-tumor lung tissue. AM populations mostly consisted of large, round cells, whereas TAMs were more heterogenous in size and shape (fig. 3-1, A). Intracellular CD68, often used as a marker specific for macrophages (Holness and Simmons, 1993; Hoppstädter et al., 2010), was detected by flow cytometry in over 95% of the cells contained in AM and TAM preparations, thereby identifying them as macrophages (fig. 3-1, B).

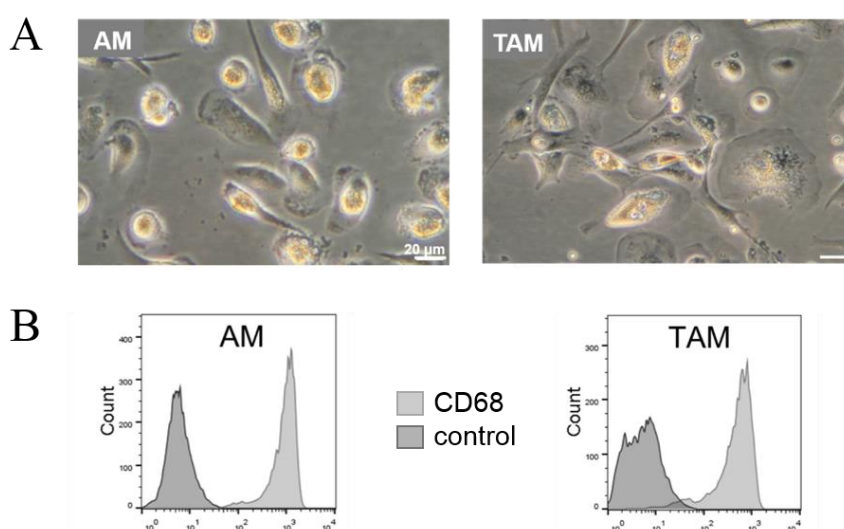


Figure 3-1: AM and TAM morphology and purity. A: Morphology was examined by light microscopy. One representative image is given. Scale bar: 20 μm. B: CD68 expression in AMs and TAMs. Data show one histogram representative of four independent flow cytometry experiments. Light gray: specific staining; dark gray: isotype control.

AMs and TAMs were analyzed and discerned on the transcriptome level using paired-end mRNA sequencing technique from Illumina[®]. Cells were isolated from tumor tissue and autogenic lung tissue from one male and two female adenocarcinoma patients at comparable age and cancer stage. mRNA was prepared from both macrophage types of each individual in technical triplicates and each replicate was sequenced separately.

Principal component analysis (PCA) revealed a prominent discrimination between not only AMs and TAMs (right and left side of the plot, fig. 3-2) but also between all three patients. The matching technical replicates clustered, indicating that the sample and library preparation gave reproducible results. However, one TAM preparation from patient 2 and one AM preparation from patient 3 could not be taken into consideration for analysis due to technical difficulties. For these

two samples, the RNA yield was already low, so that their libraries got too few reads for a sufficient analysis.

The PCA plot further allowed a discrimination between the two female patients at the top (P2 and P3, fig. 3-2) and the male patient (P1, fig. 3-2) in the bottom part. Within each patient, a clear shift to the left from AMs to TAMs could be observed.

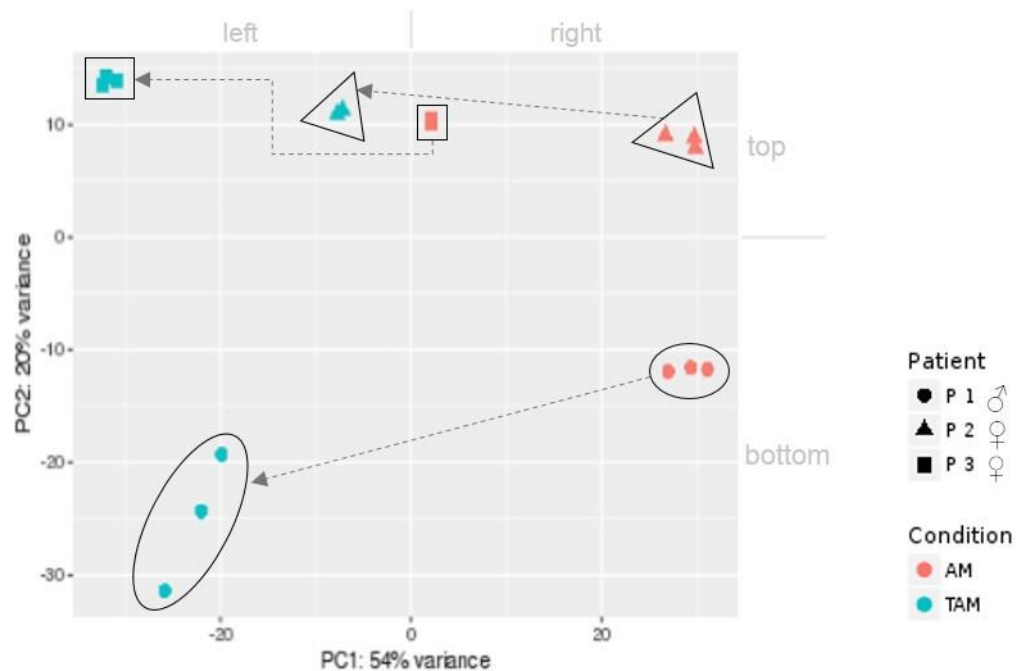


Figure 3-2: Principal component analysis plot of mRNA-Seq results from AMs (red) and TAMs (green) from three different patients (P1 – P3) prepared in technical triplicates. The patients' sex is also indicated. An arrow per patient displays a shift to the left from AMs to TAMs. PC: principal component.

A total of 4,812 genes were differentially expressed in TAMs compared to AMs, with 3,018 upregulated and 1,794 downregulated genes. Figure 3-3 (A) illustrates the differentially expressed genes (DEG) in a volcano plot, i.e. \log_2 fold change was plotted against $-\log_{10}$ p-value. Negative \log_2 fold change values represent downregulated genes, whereas positive values represent upregulated genes. Raw data of the illustrated and additional selected genes are available in the appendix.

As expected, previously described markers of M2-polarization, such as matrix metalloproteinases and angiogenesis related genes (e.g. *VEGFA*, *IGF1*) were upregulated in TAMs (fig. 3-3, B and C) as well as chemokines from the alpha and beta type (fig. 3-3, D) and genes encoding proteins involved in cell adhesion and migration (fig. 3-3, E). Surprisingly, the expression of many cholesterol metabolism-associated genes was significantly decreased, among these: HMG-CoA reductase and synthase (*HMGCR*, *HMGCS*), mevalonate kinase (*MVK*), and sterol regulatory element-binding protein 2 (*SREBF2*; fig. 3-3, F).

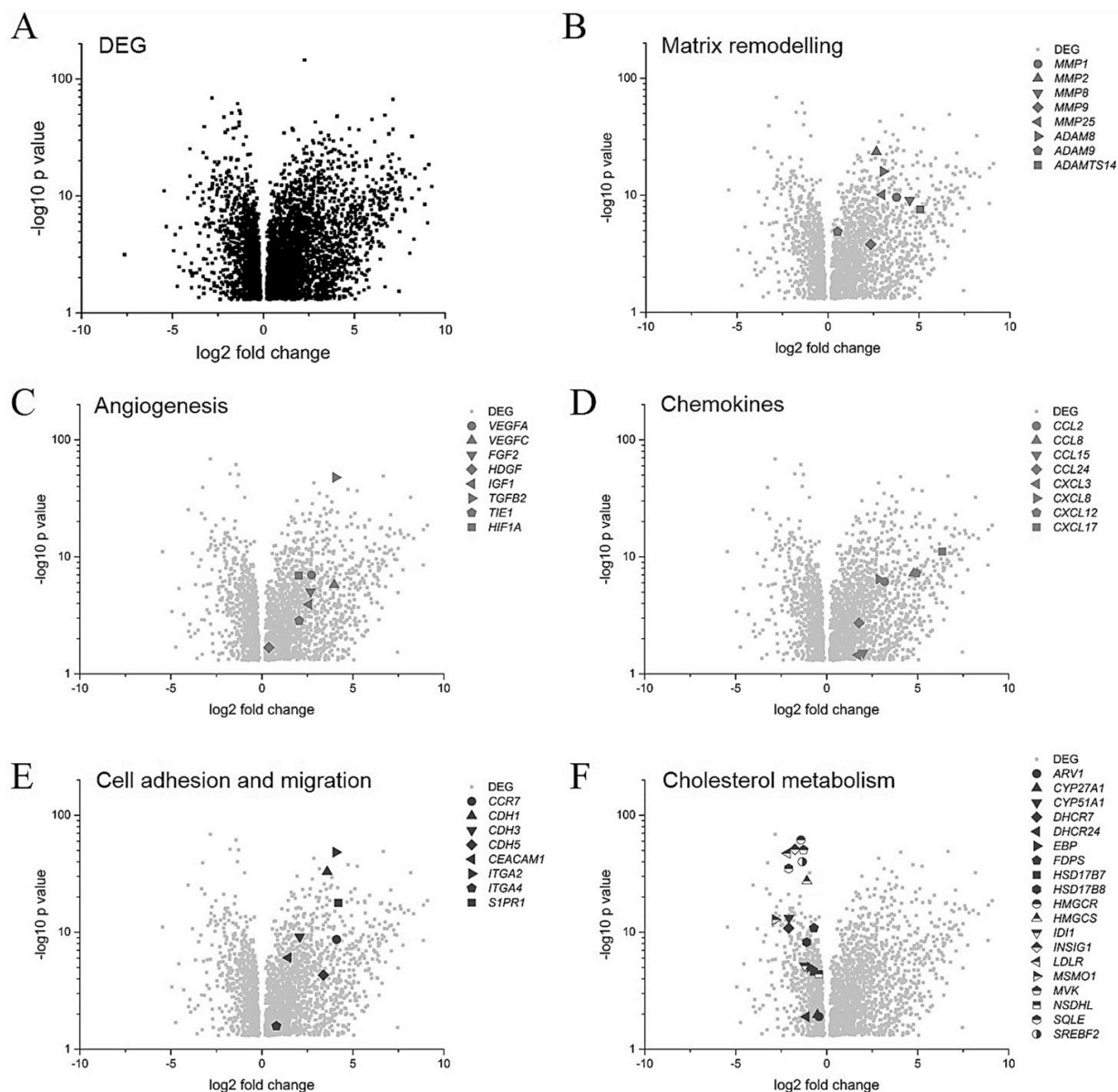


Figure 3-3: Differentially expressed genes (DEG) shown as volcano plots. Log₂ fold change is plotted against –log₁₀ p-value. **A:** All DEGs are shown. Matrix remodelling (**B**) and angiogenesis markers (**C**) are highlighted as well as genes encoding either chemokines (**D**) or proteins involved in cell adhesion/migration (**E**) and cholesterol metabolism (**F**). MMP1/2/8/9/25: matrix metalloproteinases 1/2/8/9/25; ADAM8/9: a disintegrin and metalloprotease 8/9; ADAMTS: ADAM with thrombospondin motifs; VEGFA/C: vascular endothelial growth factor A/C; FGF2: fibroblast growth factor 2; HDGF: hepatoma-derived growth factor; IGF1: insulin-like growth factor 1; TGFB2: transforming growth factor beta 2; TIE1: tyrosine kinase with immunoglobulin-like and EGF-like domains 1; HIF1A: hypoxia-inducible factor 1-alpha; CCL2/8/15/24: CC chemokine ligand 2/8/15/24; CXCL3/8/12/17: C-X-C motif ligand 3/8/12/17; CCR7: CC chemokine receptor 7; CDH1/3/5: cadherin 1/3/5; CEACAM1: Carcinoembryonic antigen-related cell adhesion molecule 1; ITGA2/4: integrin alpha 2/4; S1PR1: sphingosine-1-phosphate receptor 1; ARV1: acyl-CoA acyltransferase-related enzyme 2 required for viability; CYP27A1/51A1: cytochrome P450 family 27/51 subfamily A member 1; DHCR7/24: dehydrocholesterol reductase 7/24; EBP: emopamil binding protein; FDPS: farnesyl diphosphate synthase; HSD17B7/8: 17-beta hydroxysteroid dehydrogenase 7/8; HMGCR/S: HMG-CoA reductase/synthase; IDI1: isopentenyl-diphosphate delta isomerase 1; INSIG1: insulin-induced gene 1; LDLR: low density lipoprotein receptor; MSMO1: methylsterol monooxygenase 1; MVK: mevalonate kinase; NSDHL: NAD(P)H steroid dehydrogenase-like; SQLE: squalene epoxidase; SREBF2: sterol regulatory element-binding protein 2. Volcano plots were generated by Dr. Jessica Hopstädter.

In general, genes that were upregulated in TAMs play a role in signal processing and cell motion as determined by “protein annotation through evolutionary relationship” (PANTHER) Gene Ontology (GO) term classification system, version 11 (Top 15 for biological processes shown in table 3-1, A). The vast majority of downregulated genes belonged to biological processes involving lipid metabolism or biosynthesis (table 3-1, B).

Table 3-1: Top 15 gene ontology (GO) biological processes for upregulated (A) and downregulated (B) genes in TAMs compared to AMs according to false discovery rate of PANTHER classification system (version 11).

A	upregulated GO biological process	fold enrichment	raw P-value	false discovery rate
	response to stimulus (GO:0050896)	1.38	7.22E-50	1.13E-45
	signaling (GO:0023052)	1.5	1.12E-41	4.36E-38
	cell communication (GO:0007154)	1.49	2.65E-41	8.29E-38
	cell migration (GO:0016477)	2.53	1.54E-40	4.01E-37
	positive regulation of cellular process (GO:0048522)	1.49	2.03E-39	3.53E-36
	biological regulation (GO:0065007)	1.22	3.21E-39	5.01E-36
	cell surface receptor signaling pathway (GO:0007166)	1.82	4.83E-39	6.86E-36
	regulation of biological process (GO:0050789)	1.24	6.67E-39	8.68E-36
	signal transduction (GO:0007165)	1.49	1.52E-37	1.70E-34
	developmental process (GO:0032502)	1.45	6.35E-37	5.83E-34
	locomotion (GO:0040011)	2.19	1.28E-36	1.11E-33
	regulation of multicellular organismal process (GO:0051239)	1.71	1.45E-36	1.19E-33
	cell motility (GO:0048870)	2.32	8.82E-36	6.56E-33
	localization of cell (GO:0051674)	2.32	8.82E-36	6.89E-33
	movement of cell or subcellular component (GO:0006928)	2.03	4.32E-34	2.94E-31

B	downregulated GO biological process	fold enrichment	raw P-value	false discoverx rate
	cellular process (GO:0009987)	1.11	1.60E-11	2.50E-07
	small molecule metabolic process (GO:0044281)	1.58	2.11E-10	1.65E-06
	sterol biosynthetic process (GO:0016126)	5.99	1.41E-09	4.40E-06
	detection of chemical stimulus (GO:0009593)	0.16	8.83E-10	4.60E-06
	secondary alcohol biosynthetic process (GO:1902653)	6.36	1.41E-09	5.50E-06
	cellular metabolic process (GO:0044237)	1.18	2.48E-09	6.47E-06
	biological process (GO:0008150)	1.06	4.87E-09	7.61E-06
	cholesterol biosynthetic process (GO:0006695)	6.35	3.57E-09	7.96E-06
	small molecule biosynthetic process (GO:0044283)	2.02	4.48E-09	8.76E-06
	lipid biosynthetic process (GO:0008610)	2.01	9.40E-09	1.22E-05
	lipid metabolic process (GO:0006629)	1.65	1.17E-08	1.31E-05
	fatty acid metabolic process (GO:0006631)	2.45	1.11E-08	1.34E-05
	sensory perception of chemical stimulus (GO:0007606)	0.23	3.14E-08	3.07E-05
	metabolic process (GO:0008152)	1.15	3.91E-08	3.39E-05
	monocarboxylic acid metabolic process (GO:0032787)	2.06	4.16E-08	3.42E-05

TAMs have been suggested to represent M2-like macrophages promoting tumor cell proliferation, angiogenesis, matrix turnover, and repression of adaptive immunity (Solinas *et al.*, 2009). In contrast, AMs are considered to exhibit a more pro-inflammatory, M1-like phenotype

(Hoppstädter *et al.*, 2010). Since M1 and M2 macrophages differ in their uptake capacity for nanoparticles (Hoppstädter *et al.*, 2015), we hypothesized that these differences might also be evident in TAMs and AMs. The uptake of 26 nm fluorescent silica particles was indeed enhanced in TAMs from adenocarcinoma patients when compared with AMs, as assessed by flow cytometry (fig. 3-4).

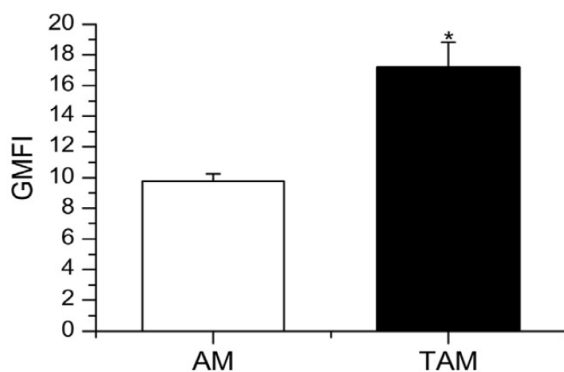


Figure 3-4: Nanoparticle uptake by AMs and TAMs. GMFI mean values + SEM obtained from independent experiments with AMs obtained from two and TAMs obtained from four different donors. P-values were calculated by Student's t-test. * $p < 0.05$ compared with AMs.

3.2.2 Establishment of a TAM-like model for lung macrophages

Due to the limited availability of primary *in vivo* polarized human TAMs, we wanted to establish an *in vitro* TAM-like macrophage model based on a report of Edin *et al.* (2013). In order to mimic the tumor microenvironment, human monocyte-derived macrophages (MDM) were exposed to A549 lung tumor cell supernatant. In addition, MDMs were polarized with either LPS/IFN- γ towards an M1-like phenotype or with IL-10 or IL-4 towards an M2-like phenotype as established models of macrophage polarization (Sica and Mantovani, 2012; Martinez and Gordon, 2014).

M0, M1, M2(IL4), M2(IL10), and TAM-like macrophages were compared on the transcriptomic level by mRNA sequencing. MDMs from three different donors were polarized and analyzed as biological replicates.

M1 as well as M2(IL4) expressed a high number of genes that were differentially expressed when compared with TAM-like cells, indicating that they are highly different from not only TAM-like but also from all the other macrophage types (fig. 3-5). In contrast, there were just a few upregulated and downregulated DEGs in TAM-like versus M0 or M2(IL10), suggesting that TAM-like cells are more similar to these two types (fig. 3-5) and adapt an alternatively activated phenotype when exposed to A549 supernatant.

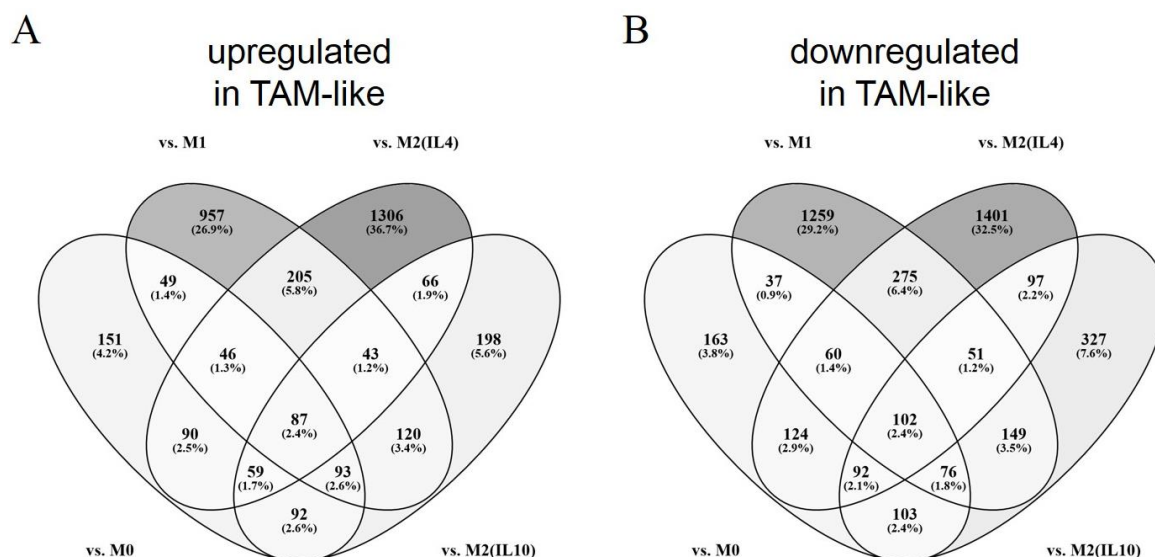


Figure 3-5: Number of differentially expressed genes in TAM-like macrophages versus all other treatments. A: Upregulated genes in TAM-like cells. B: Downregulated genes in TAM-like cells. Venn diagrams were generated with Venny (version 2.1; Oliveros 2007).

Figure 3-6 (A) illustrates the DEGs of TAM-like vs. M0 in a volcano plot, i.e. log₂ fold change was plotted against -log₁₀ p-value. Again, negative log₂ fold change values represent downregulated genes, whereas positive values represent upregulated genes. As already seen in primary TAMs, the expression of many cholesterol metabolism-associated genes was also significantly decreased in TAM-like cells (fig. 3-6, B). In contrast, of the 15 highlighted genes in figure 3-6 (B), only four genes were significantly altered in M1 vs. M0 (*ARV1*, *DHCR24*, *EBP*, *INSIG1*), two in M2(IL4) vs. M0 (*HMGCS*, *LDLR*) and none at all in M2(IL10) vs. M0.

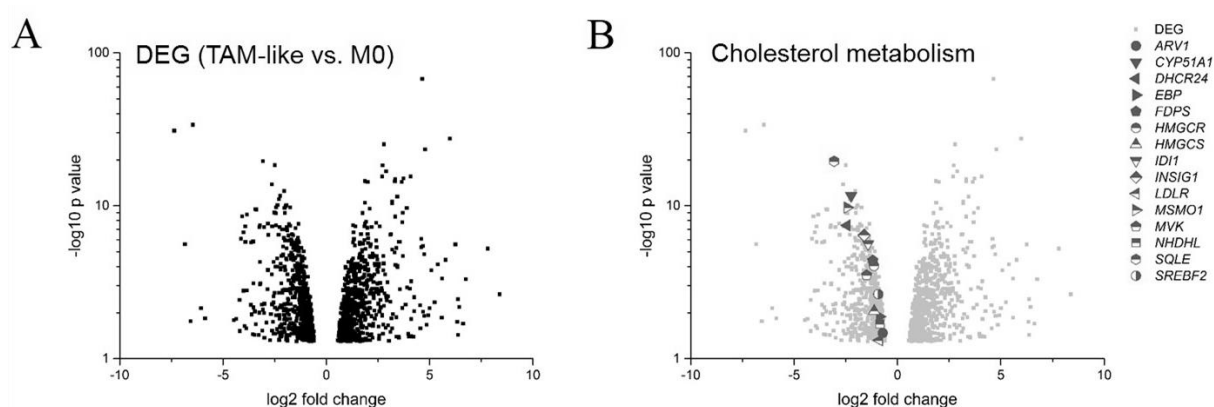


Figure 3-6: DEGs of TAM-like vs. M0 shown as volcano plots. Log₂ fold change is plotted against -log₁₀ p-value. A: All DEGs are shown. B: Genes related to the cholesterol metabolism are highlighted. ARV1: acyl-CoA acyltransferase-related enzyme 2 required for viability; CYP51A1: cytochrome P450 family 51 subfamily A member 1; DHCR24: dehydrocholesterol reductase 24; EBP: emopamil binding protein; FDPS: farnesyl diphosphate synthase; HMGCR/S: HMG-CoA reductase/synthase; IDI1: isopentenyl-diphosphate delta isomerase 1; INSIG1: insulin-induced gene 1; LDLR: low density lipoprotein receptor; MSMO1: methylsterol monooxygenase 1; MVK: mevalonate kinase; NSDHL: NAD(P)H steroid dehydrogenase-like; SQLE: squalene epoxidase; SREBF2: sterol regulatory element-binding protein 2. Volcano plots were generated by Dr. Jessica Hoppstädter.

Furthermore, the differentially expressed genes from both the *in vitro* TAM-like model and primary *ex vivo* AMs/TAMs were compared. Prior to this, AMs/TAMs were contrasted with the generally well-established polarization states M1, M2(IL4) and M2(IL10). Overlapping DEGs in TAMs vs. AMs and polarized MDM vs. M0, each, were classified according to GO terms at the biological process level using the PANTHER GO classification system (version 11). The top 15 biological processes are represented in following figures 3-7 to 3-10, for up- and downregulated DEGs separately.

Common to all enhanced genes was the involvement in *cytokine-mediated signaling pathway* (GO:19221) and in *cell surface receptor signaling pathway* (GO:0007166) (fig. 3-7 to 3-10).

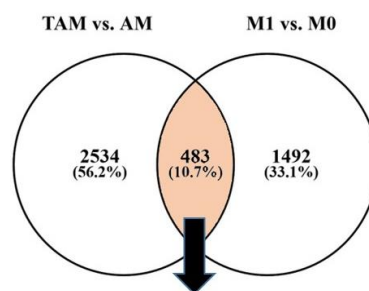
M1 and TAMs shared many genes, 10.7% of the upregulated and 6.7% of the downregulated genes (fig. 3-7), and comprised in biological processes associated with response to stimuli (fig. 3-7, A) or lipogenesis (fig. 3-7, B).

For M2(IL4) it is striking that similar or even identical processes are regulated by up- and downregulated DEGs, i.e. *cell surface receptor signaling pathway* or *regulation of response to stimulus* (fig. 3-8). As the identified processes were rather general, this indicated a somehow activated but undirected/unspecific state after IL-4 treatment. Interestingly, there was no connection to lipogenesis alterations in M2(IL4) cells compared to TAMs.

Common upregulated genes in M2(IL10) vs. M0 and TAMs vs. AMs were mostly related to signaling and its regulation (fig. 3-9, A). No statistically significant biological process could be found within the overlap of downregulated DEGs according to PANTHER GO (figure 3-9, B).

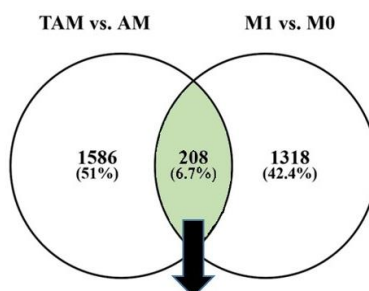
Primary TAMs and TAM-like cells shared 5% of upregulated genes, which were mainly involved in biological processes like signal processing - as already seen in *ex vivo* cells (table 3-1, A) - and angiogenesis, typically connected with cancerogenesis (fig. 3-10, A). Almost all of the top 15 biological processes, which resulted from the 4.2% common downregulated genes, belonged to lipid biogenesis and metabolism or more precisely to the steroid/cholesterol biogenesis part (fig. 3-10, B).

A



upregulated GO biological process	fold enrichment	raw P-value	false discovery rate
cellular response to cytokine stimulus (GO:0071345)	3.81	6.62E-23	5.18E-19
cytokine-mediated signaling pathway (GO:0019221)	4.61	2.45E-22	1.28E-18
defense response (GO:0006952)	3.18	6.10E-21	2.39E-17
response to organic substance (GO:0010033)	2.23	1.14E-19	3.56E-16
immune system process (GO:0002376)	2.28	2.67E-19	6.97E-16
regulation of response to stimulus (GO:0048583)	1.92	5.56E-19	1.24E-15
response to stimulus (GO:0050896)	1.52	1.80E-18	3.53E-15
positive regulation of biological process (GO:0048518)	1.7	2.41E-18	4.19E-15
response to stress (GO:0006950)	2.04	5.94E-18	8.46E-15
cell surface receptor signaling pathway (GO:0007166)	2.32	5.58E-18	8.74E-15
response to external biotic stimulus (GO:0043207)	3.45	7.51E-18	9.04E-15
cellular response to organic substance (GO:0071310)	2.32	4.01E-17	3.92E-14
positive regulation of cellular process (GO:0048522)	1.74	3.86E-17	4.03E-14
inflammatory response (GO:0006954)	4.69	5.28E-17	4.35E-14
negative regulation of biological process (GO:0048519)	1.75	5.20E-17	4.53E-14

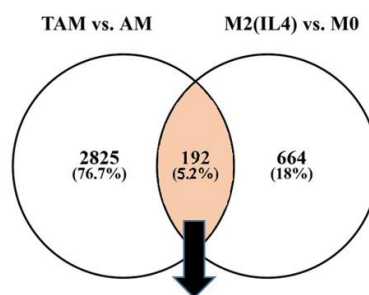
B



downregulated GO biological process	fold enrichment	raw P-value	false discovery rate
small molecule metabolic process (GO:0044281)	3.26	1.83E-15	2.87E-11
oxidation-reduction process (GO:0055114)	3.94	6.60E-12	5.16E-08
cellular respiration (GO:0045333)	9.54	7.36E-10	3.84E-06
fatty acid metabolic process (GO:0006631)	6.15	2.06E-09	6.44E-06
generation of precursor metabolites and energy (GO:0006091)	5.31	2.77E-09	7.22E-06
monocarboxylic acid metabolic process (GO:0032787)	4.71	3.53E-09	7.90E-06
cellular lipid metabolic process (GO:0044255)	3.34	5.61E-09	1.10E-05
monocarboxylic acid catabolic process (GO:0072329)	10.08	3.03E-08	5.28E-05
fatty acid catabolic process (GO:0009062)	11.43	4.39E-08	6.87E-05
organophosphate metabolic process (GO:0019637)	3.08	6.06E-08	8.62E-05
lipid biosynthetic process (GO:0008610)	3.92	8.47E-08	9.47E-05
lipid metabolic process (GO:0006629)	2.85	7.45E-08	9.72E-05
respiratory electron transport chain (GO:0022904)	10.63	8.25E-08	9.93E-05
organic acid metabolic process (GO:0006082)	3.04	1.36E-07	1.25E-04
fatty acid oxidation (GO:0019395)	12.26	1.21E-07	1.27E-04

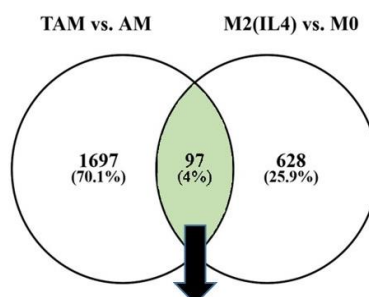
Figure 3-7: Top 15 GO terms that result from the DEG overlap between TAM vs. AM and M1 vs. M0. Up-regulated (A) and downregulated (B) GO biological processes according to false discovery rate of PANTHER classification system (version 11).

A



upregulated GO biological process	fold enrichment	raw P-value	false discovery rate
cell surface receptor signaling pathway (GO:0007166)	2.69	2.21E-12	1.73E-08
response to cytokine (GO:0034097)	3.84	1.16E-11	4.53E-08
cytokine-mediated signaling pathway (GO:0019221)	4.86	2.44E-11	5.45E-08
response to stimulus (GO:0050896)	1.63	1.15E-11	5.98E-08
cellular response to cytokine stimulus (GO:0071345)	3.95	2.43E-11	6.35E-08
regulation of response to stimulus (GO:0048583)	2.08	2.27E-11	7.10E-08
positive regulation of cellular process (GO:0048522)	1.89	8.75E-11	1.52E-07
regulation of cell killing (GO:0031341)	15.36	8.21E-11	1.61E-07
immune response (GO:0006955)	2.82	2.01E-10	3.15E-07
cell migration (GO:0016477)	3.69	1.08E-09	1.54E-06
cell communication (GO:0007154)	1.8	2.13E-09	2.38E-06
regulation of lymphocyte mediated immunity (GO:0002706)	9.91	1.89E-09	2.47E-06
locomotion (GO:0040011)	3.15	2.09E-09	2.51E-06
positive regulation of signal transduction (GO:0009967)	2.83	2.47E-09	2.58E-06
positive regulation of response to stimulus (GO:0048584)	2.42	3.06E-09	2.99E-06

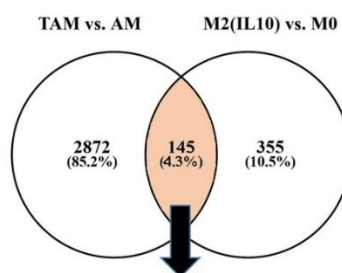
B



downregulated GO biological process	fold enrichment	raw P-value	false discovery rate
cell surface receptor signaling pathway (GO:0007166)	2.82	9.53E-08	1.49E-03
positive regulation of signaling (GO:0023056)	2.95	2.10E-06	1.10E-02
positive regulation of signal transduction (GO:0009967)	3.1	1.72E-06	1.35E-02
positive regulation of intracellular signal transduction (GO:1902533)	3.59	4.76E-06	1.49E-02
signal transduction (GO:0007165)	1.91	7.30E-06	1.63E-02
cell communication (GO:0007154)	1.88	4.19E-06	1.64E-02
positive regulation of cell communication (GO:0010647)	2.84	6.95E-06	1.82E-02
cellular response to stimulus (GO:0051716)	1.72	9.46E-06	1.85E-02
signaling (GO:0023052)	1.83	1.31E-05	2.28E-02
cytokine-mediated signaling pathway (GO:0019221)	4.29	2.57E-05	2.88E-02
regulation of response to stimulus (GO:0048583)	1.97	2.39E-05	2.88E-02
regulation of intracellular signal transduction (GO:1902531)	2.67	1.85E-05	2.89E-02
regulation of JNK cascade (GO:0046328)	8.57	2.25E-05	2.94E-02
immune effector process (GO:0002252)	3.35	2.23E-05	3.18E-02
inflammatory response (GO:0006954)	4.9	4.35E-05	4.54E-02

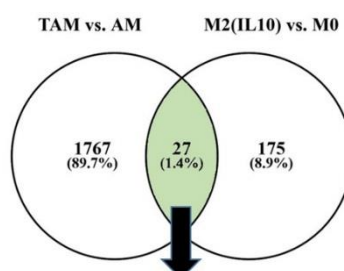
Figure 3-8: Top 15 GO terms that result from the DEG overlap between TAM vs. AM and M2(IL4) vs. M0. Upregulated (A) and downregulated (B) GO biological processes according to false discovery rate of PANTHER classification system (version 11).

A



upregulated GO biological process	fold enrichment	raw P-value	false discovery rate
regulation of response to stimulus (GO:0048583)	2.05	2.29E-08	3.59E-04
signal transduction (GO:0007165)	1.88	1.52E-07	7.94E-04
regulation of cell adhesion (GO:0030155)	4.26	3.15E-07	1.23E-03
cell surface receptor signaling pathway (GO:0007166)	2.39	4.34E-07	1.36E-03
regulation of cell proliferation (GO:0042127)	2.69	1.51E-06	1.58E-03
signaling (GO:0023052)	1.76	1.50E-06	1.68E-03
regulation of signal transduction (GO:0009966)	2.11	1.48E-06	1.79E-03
regulation of cell communication (GO:0010646)	2.06	1.16E-06	1.82E-03
regulation of signaling (GO:0023051)	2.04	1.29E-06	1.83E-03
regulation of immune response (GO:0050776)	3.23	1.43E-06	1.87E-03
response to organic substance (GO:0010033)	2.19	1.10E-06	1.92E-03
cytokine-mediated signaling pathway (GO:0019221)	4.19	8.72E-07	1.95E-03
cellular response to stimulus (GO:0051716)	1.66	1.01E-06	1.98E-03
regulation of immune system process (GO:0002682)	2.7	2.35E-06	2.30E-03
cellular response to organic substance (GO:0071310)	2.31	2.88E-06	2.66E-03

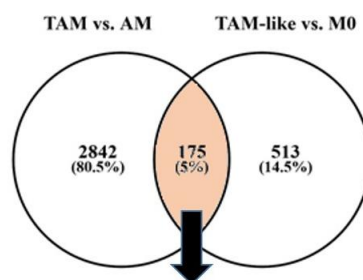
B



No statistically significant results.

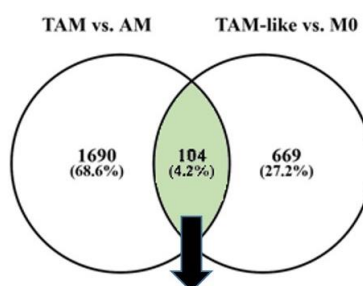
Figure 3-9: Top 15 GO terms that result from the DEG overlap between TAM vs. AM and M2(IL10) vs. M0. **A:** Upregulated GO biological processes according to false discovery rate of PANTHER classification system (version 11). **B:** Within the overlap of downregulated DEGs no statistically significant biological process could be found according to PANTHER GO.

A



upregulated GO biological process	fold enrichment	raw P-value	false discovery rate
cell surface receptor signaling pathway (GO:0007166)	2.74	4.89E-12	7.64E-08
regulation of response to stimulus (GO:0048583)	2.11	2.32E-10	1.81E-06
regulation of multicellular organismal process (GO:0051239)	2.39	4.83E-10	2.52E-06
cellular response to stimulus (GO:0051716)	1.7	1.05E-08	2.74E-05
signal transduction (GO:0007165)	1.87	7.40E-09	2.89E-05
regulation of response to external stimulus (GO:0032101)	3.77	3.50E-08	5.46E-05
signaling (GO:0023052)	1.79	3.15E-08	5.46E-05
cell communication (GO:0007154)	1.77	2.63E-08	5.86E-05
immune system process (GO:0002376)	2.25	6.60E-08	8.59E-05
regulation of cell differentiation (GO:0045595)	2.66	6.44E-08	9.15E-05
response to cytokine (GO:0034097)	3.27	1.34E-07	1.31E-04
cytokine-mediated signaling pathway (GO:0019221)	4.08	1.54E-07	1.42E-04
blood vessel development (GO:0001568)	4.48	4.07E-07	3.53E-04
cell migration (GO:0016477)	3.26	4.65E-07	3.82E-04
vasculature development (GO:0001944)	4.28	7.63E-07	5.96E-04

B



downregulated GO biological process	fold enrichment	raw P-value	false discovery rate
secondary alcohol biosynthetic process (GO:1902653)	73.57	4.40E-24	6.87E-20
sterol biosynthetic process (GO:0016126)	66.07	1.87E-23	1.46E-19
cholesterol biosynthetic process (GO:0006695)	72.26	1.55E-22	8.07E-19
secondary alcohol metabolic process (GO:1902652)	30.6	5.31E-21	2.07E-17
alcohol biosynthetic process (GO:0046165)	35.1	8.66E-21	2.71E-17
sterol metabolic process (GO:0016125)	27.59	2.87E-20	7.47E-17
cholesterol metabolic process (GO:0008203)	30.44	7.63E-20	1.70E-16
steroid biosynthetic process (GO:0006694)	24.9	1.82E-17	3.55E-14
regulation of cholesterol metabolic process (GO:0090181)	44.96	4.12E-16	6.43E-13
alcohol metabolic process (GO:0006066)	13.17	8.56E-16	1.22E-12
steroid metabolic process (GO:0008202)	14.34	1.31E-15	1.70E-12
small molecule biosynthetic process (GO:0044283)	8.19	2.43E-15	2.72E-12
organic hydroxy compound metabolic process (GO:1901615)	9.37	6.39E-14	6.24E-11
lipid biosynthetic process (GO:0008610)	7.2	1.84E-12	1.37E-09
lipid metabolic process (GO:0006629)	4.62	7.62E-12	5.17E-09

Figure 3-10: Top 15 GO terms that result from the DEG overlap between TAM vs. AM and TAM-like vs. M0. Upregulated (A) and downregulated (B) GO biological processes according to false discovery rate of PAN-THER classification system (version 11).

Although the overlap of DEGs between M1 and TAMs is quite big at first glance, much bigger than between TAM-like and TAMs, the proportion of overlapping genes is almost similar (figure 3-7 vs. 3-10). This is due to the fact that many more DEGs in total could be detected in M1 vs. M0 compared with TAM-like vs. M0. Looking at the upregulated DEGs, M1 vs. M0 shared 24.4% and TAM-like vs. M0 25.4% of their genes with primary TAMs vs. AMs. For the down-regulated genes, the proportion is even more similar: 13.6% (M1) compared with 13.4% (TAM-like) overlapping genes with TAMs vs. AMs.

All the results taken together indicate that stimuli from the tumor microenvironment as well as from A549 supernatants altered signal processing and lipid metabolism of the investigated TAMs and TAM-like macrophages in a similar manner, although primary TAM cells share similarities with M1 cells, too.

3.2.3 Lipid profile is strongly altered in tumor compared to surrounding lung

It is well described in the literature that tumors have an altered lipid profile compared to the adjacent tissue (Baenke *et al.*, 2013; Marien *et al.*, 2015; Eggers *et al.*, 2017)

The investigated primary TAMs and in vitro TAM-like macrophages both had a multitude of downregulated genes associated with lipid synthesis. Some of these genes have been previously reported to be downregulated by a lipid-rich microenvironment. Thus, the lipid composition in adenocarcinoma and non-tumor was examined by lipidomic analyses of 29 adenocarcinoma and 22 non-tumor lung tissues.

Most of the investigated lipids (~ 70%) were strongly upregulated in tumor compared with normal lung tissue: the glycerophospholipids phosphatidylethanolamine (PE), PE-based plasmalogens (PE P), PE ether (PE O), phosphatidylinositol (PI), phosphatidylcholine (PC), lyso-PC (LPC) and PC ether (PC O) (fig. 3-11, A); the glycerolipid triacylglycerol (TG) (fig. 3-11, B); the sphingolipids ceramide (Cer) and hexosylceramide (HexCer) (fig. 3-11, C); the sterol lipids cholesteryl ester (CE) and free cholesterol (FC) (fig. 3-11, D). Only phosphatidylglycerol (PG), a typical lung surfactant component, exhibited a lower abundance in tumor when compared to lung tissue (fig. 3-11, A). In four of the 17 analyzed lipid classes, no significant difference could be detected between tumor and lung: The glycerophospholipids phosphatidylserine (PS) and lyso-phosphatidylcholine ether (LPC O) (fig. 3-12, A); the glycerolipid diacylglycerol (DG) (fig. 3-12, B); the sphingolipid sphingomyelin (SM) (fig. 3-12, C).

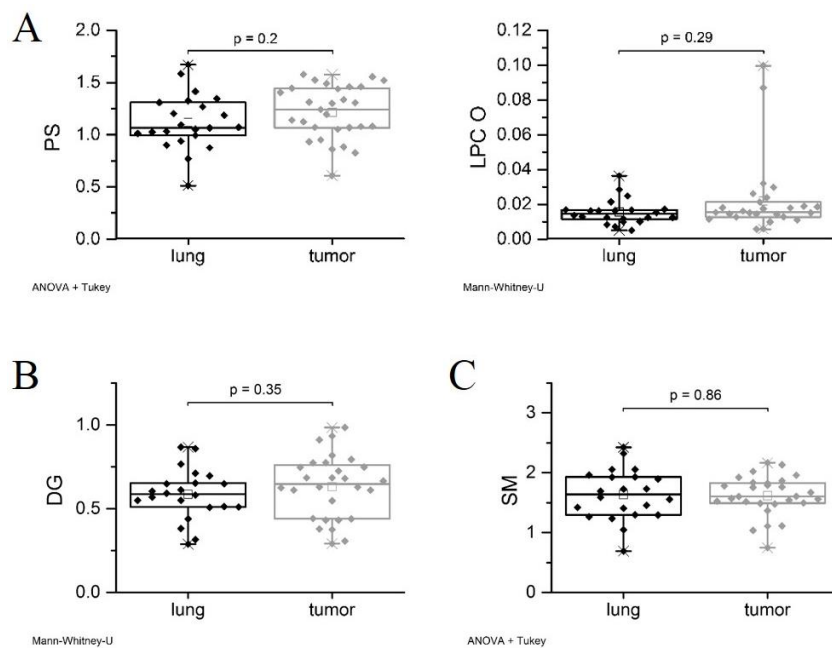


Figure 3-12: Non-altered lipid classes in lung tumor compared to non-tumor lung tissue. **A:** The glycerophospholipids phosphatidylserine (PS) and lyso-phosphatidylcholine ether (LPC O). **B:** The glycerolipid diacylglycerol (DG). **C:** The sphingolipid sphingomyelin (SM). Tumor tissues = 29, lung tissues = 22. P-values were determined for each lipid class by ANOVA with post-hoc Tukey test or Mann Whitney U test as indicated in the figure and were Benjamini-Hochberg-corrected with a false discovery rate of 5%.

3.3 Discussion

TAMs are key orchestrators of cancer-related inflammation in NSCLC and other cancer types, and cancer cells actively guide monocyte recruitment from blood into tumor tissues to their own advantage (Solinas *et al.*, 2009; Burg, Heusinkveld and Burg, 2011). To target TAMs therapeutically is a big challenge in present immunotherapy development, especially because contribution of tissue-resident macrophages to tumor progression, such as AMs in lung tumor progression in the context of the present study, is barely investigated so far (Solinas *et al.*, 2009; Almatroodi, McDonald and Pouniotis, 2014). We isolated TAMs and autogenic AMs from patient tissue and discerned them on the transcriptome level using mRNA sequencing technique. The prominent discrepancies revealed via PCA indicated fundamental differences between the TAM and the AM transcriptome in general. Additionally, one sample set was clearly separated from the other two. This separation could be based on the fact that the patient had a tumor with minimal regional lymph node involvement, in contrast to the other two patients with no lymph node infestation (Goldstraw *et al.*, 2016). It is more likely though, that the transcriptomic differences compared to the other two preparations was due the patient being male, whereas the other two were female. A gender-dependent outcome of immune therapy, as well as an enrichment of immune-related genes in NSCLC in women compared to men, is described in the literature (Araujo *et al.*, 2016; Pinto *et al.*, 2018).

The genes we found to be differentially expressed in TAMs vs. AMs corresponded to well-established TAM properties, which assists tumor development by driving angiogenesis through related cytokines and receptors, remodeling of extracellular matrix, and facilitating cell migration (Martinez *et al.*, 2008; Rivas-Fuentes *et al.*, 2015; Conway *et al.*, 2016). In contrast, the multitude of downregulated, cholesterol metabolism-associated genes in TAMs was unexpected at first, but recent immunometabolism studies have shown that macrophage activation state and function is related to alterations in their metabolic profile (reviewed by Geeraerts *et al.*, 2017). The generally decreased cholesterol metabolism suggests an excesses of cellular cholesterol, possibly due to the lipid-enriched environment (DiMarco and Fernandez, 2015). In accordance with the latest results from Eggers and colleagues (2017), the vast majority of investigated lipid classes in whole-tumor tissues was clearly enhanced compared with healthy lung tissue. Therefore, an excessive uptake of cholesterol, by efferocytosis of apoptotic cells for instance, may lead to downregulation of not only cholesterol and fatty acid synthesis but also pro-inflammatory gene expression (Spann *et al.*, 2012; Viaud *et al.*, 2018), supporting an M2 phenotype. Furthermore, the pro-inflammatory stimulus IFN has been recently shown to suppress cholesterol biosynthesis

pathways (Robertson *et al.*, 2016), which is a possible indication of why primary TAMs are more similar to M1 than to M2 in the *in vitro* model.

However, downregulation of SREBP2, a master regulator of lipid homeostasis, supports an anti-inflammatory TAM bias (Guo *et al.*, 2018). In contrast, decreased levels of the nuclear receptor peroxisome proliferator-activated receptor gamma (PPAR γ) seems to rather support a pro-inflammatory TAM phenotype, since PPAR γ primes alternative macrophage activation and anti-inflammatory properties in men and mice (Bouhlef *et al.*, 2007; Odegaard *et al.*, 2007; Schneider *et al.*, 2014). However, PPAR γ has an established role in lipid metabolism and is highly expressed in lung AMs (Remmerie and Scott, 2018). It is required for AM differentiation *via* GM-CSF (Schneider *et al.*, 2014), but also for the exercise of AM's accessory function compared to other macrophages, catabolizing surfactant (Kopf, Schneider and Nobs, 2015; Remmerie and Scott, 2018), which is why they possess a strong lipid metabolism signature within their core genes in general (Gautier *et al.*, 2012; Poczobutt *et al.*, 2016; Misharin *et al.*, 2017). Therefore, it is possible, that *PPARG* (PPAR γ) was not downregulated in TAMs due to any related pro-inflammatory phenotype or functions, but compared to the physiologically high level in AMs. AMs in healthy individuals do not neatly fit into either a strict M1 or M2 classification. An increase in M2 characteristics in AMs seems to be a feature of many inflammatory lung diseases, e.g. COPD, or exposure to cigarette smoke (Almatroodi, McDonald and Pouniotis, 2014; Hussell and Bell, 2014). The fact that we have no information on the patients' health status (COPD, Asthma) or smoking behavior makes it difficult to interpret the inflammation status and phenotype, also in comparison with TAMs.

Furthermore, a comparison of our data to results from other groups is even more difficult, since a majority of studies do not differentiate between NSCLC subtypes and staging (Zhang *et al.*, 2011) or do not take smoking, COPD, age or gender into consideration for interpretation (Almatroodi *et al.*, 2016). A large current study by Lavin and colleagues (2017) for example identified tumor-driven immune changes in early lung adenocarcinoma by comparing patient's blood monocytes, healthy lung and tumor CD45 positive cells. They detected a distinct transcriptional signature in TAMs, which indicated an immunosuppressive phenotype, using large antibody panels and mass cytometry, followed by single cell sequencing. For our investigations, 'bulk' mRNA sequencing technique was used. This allows a look at the cross-section of the TAM transcriptome instead of an isolated cell and could explain the discrepancies why only half of the altered genes described in TAMs by Lavin *et al.* agree with our results.

In addition, the classification of M1/M2 markers in the literature might be misleading, at least in case of AMs/TAMs. Looking at the abundance of currently used markers, our TAM transcription

profile suggests an M1-like phenotype, since for instance *CD163*, *MSR-1* (CD204), and *PPARG* (PPAR γ) are downregulated, while *CD14*, *CCL5*, *STAT4*, *HIF1A* (HIF-1), and *TLR2* are upregulated (Mantovani *et al.*, 2004; Foey, 2012; Murray *et al.*, 2014; Takeya and Komohara, 2016; Zheng *et al.*, 2017). For normal human AMs, a high expression of CD163 and CD206 is described, though (Schneider *et al.*, 2014; Joshi, Walter and Misharin, 2018) and they also express the often used macrophage marker CD68. In different studies, a combination of CD68 and either CD163 or CD206 was often used to define M2-like TAMs in NSCLC (Ohri *et al.*, 2009; Ma *et al.*, 2010; Zhang *et al.*, 2011; Chung *et al.*, 2012; Conway *et al.*, 2016), what could have led to confusing conclusions regarding the TAM phenotype.

In summary, besides the increased phagocytosis capacity (Lang *et al.*, 2002), the downregulation of cholesterol metabolism-associated genes represents the most striking difference of TAMs compared to AMs. This was also reflected in our TAM-like *in vitro* model, i.e., MDMs treated with A549 supernatant. On the other hand, our primary TAMs do not show many similarities to either M2(IL4) or M2(IL10), but rather to M1 cells.

Nowadays, the strict classification of TAM populations within dichotomous M1 and M2 subtypes is more and more regarded as oversimplified, and sometimes overinterpreted, as macrophages have been described as highly plastic cells that can demonstrate a variety of phenotypes (Edin *et al.*, 2013; Martinez and Gordon, 2014; Almatroodi *et al.*, 2016; Mantovani *et al.*, 2017). Although markers of M1 and M2 phenotypes are still used to describe and categorize the phenotype and function of macrophages, it is meanwhile established for TAMs to have a mixed phenotype driven by the individual TME (Qian and Pollard, 2010; Sica and Mantovani, 2012; Edin *et al.*, 2013; Noy and Pollard, 2015).

Furthermore, the generally decreased cholesterol metabolism suggests an excess of cellular cholesterol, possibly due to a lipid-enriched environment (DiMarco and Fernandez, 2015). In accordance with the latest results from Eggers and colleagues (2017), the vast majority of investigated lipid classes in whole-tumor tissues was clearly enhanced compared with healthy lung tissue.

For further TAM studies in NSCLC, a more detailed analysis of TME components might allow more precise interpretations. Individual factors, such as smoking and sex, but also cancer stage and location of TAMs within the tumor, should also be taken into account

4. Chapter III

Hepatic interleukin-6 production is maintained during endotoxin-tolerance and facilitates lipid accumulation

The following chapter has already been published as:

“Hepatic interleukin-6 production is maintained during endotoxin-tolerance and facilitates lipid accumulation”. Anna Dembek*, Stephan Laggai*, Sonja M. Kessler, Beate Czepukojc, Yvette Simon, Alexandra K. Kiemer and Jessica Hoppstädter (2017) *Immunobiology*; 222, pp. 786-796. doi: 10.1016/j.imbio.2017.01.003.

*Equal contribution

4.1 Abstract

Gut-derived bacterial endotoxins, such as lipopolysaccharide (LPS), contribute to the pathogenesis of steatosis and steatohepatitis by activating Kupffer cells, the resident liver macrophages. Exposure of macrophages to low doses of LPS causes hyporesponsiveness upon subsequent endotoxin challenge, a phenomenon termed endotoxin or LPS tolerance. In the present study, we aimed to examine whether LPS-induced lipid accumulation is affected by endotoxin tolerance.

LPS pretreatment reduced the expression of pro-inflammatory mediators upon subsequent high-dose LPS treatment in murine livers. Total lipid and lipid class analysis indicated that LPS-induced lipid accumulation was not affected by endotoxin tolerance, although it was dependent on the presence of Kupffer cells. Analysis of the expression of lipogenic genes revealed that sterol regulatory element binding transcription factor 1 (*Srebf1*) and its target elongation of very long chain fatty acids-6 (*Elovl6*) were upregulated upon LPS administration in livers from LPS-tolerant and non-tolerant mice, whereas the expression of peroxisome proliferator-activated receptor- α (*Ppara*), a key inducer of lipid degradation, was decreased. Neither Interleukin (IL)-6 expression nor the activation of its downstream effector signal transducer and activator of transcription (STAT) 3 were suppressed in liver tissues of LPS-tolerized mice. *In vitro* experiments confirmed that recombinant or macrophage-derived IL-6 was a potent activator of the lipogenic factor STAT3 in hepatocytes. Accordingly, IL-6 treatment led to increased lipid levels in this cell type.

In summary, our data show that endotoxin tolerance does not influence LPS-induced hepatic lipid accumulation and suggest that IL-6 drives hepatic lipid storage.

4.2 Introduction

Over the last decades, a lifestyle shift in Western societies has led to massively increased obesity rates (Swinburn *et al.*, 2011). Obesity and diabetes mellitus are the key features of the metabolic syndrome, which strongly correlates with the development of non-alcoholic fatty liver disease (NAFLD) (Browning *et al.*, 2004; Adams, Angulo and Lindor, 2005; de Alwis and Day, 2008; Bellentani *et al.*, 2010).

With an estimated prevalence of 20-35% in the adult population in Western countries, NAFLD has been predicted to become the most common cause for liver transplantations by the year 2030 (Byrne and Targher, 2015; Sayiner *et al.*, 2016). The pathogenesis of NAFLD is widely believed to start with simple steatosis, which is characterized by excessive hepatic lipid accumulation (Angulo, 2002; Adams, Angulo and Lindor, 2005). The progression from steatosis to advanced inflammatory states, such as alcoholic steatohepatitis (ASH) or non-alcoholic steatohepatitis (NASH), is mediated by the release of inflammatory cytokines (Day, 2010). Both ASH and NASH can further progress to hepatic cirrhosis and may finally result in the development of hepatocellular carcinoma (HCC) (Adams *et al.*, 2009; Ascha *et al.*, 2010; Fabbrini, Sullivan and Klein, 2010).

Chronic alcohol consumption associated with ASH as well as high-caloric food intake resulting in NASH have been reported to increase the permeability of the intestinal barrier for bacteria and microbial products, such as lipopolysaccharides (LPS), an effect referred to as the leaky gut syndrome (Bode, Kugler and Bode, 1987; Nanji *et al.*, 1993; Enomoto *et al.*, 1998; Bode and Bode, 2003; Amar *et al.*, 2008). LPS exposure elicits strong immune responses by activation of Toll-like receptor 4 (TLR4). Interestingly, TLR4 knockout animals were protected from steatohepatitis in a methionin cholin-deficient (MCD) or high-fat diet (HFD) mouse model, two common models that exhibit signs of liver injury similar to human NASH (Rivera *et al.*, 2007; Csak *et al.*, 2011; Li *et al.*, 2011). TLR4 has also been suggested to play a role in the pathogenesis of ASH (Uesugi *et al.*, 2001), and a recently published report demonstrated that progression from steatohepatitis to HCC was linked to TLR4 expression in macrophages (Miura *et al.*, 2016).

Kupffer cells are the resident liver macrophages, the main source of TLR4 in the liver (Fisher *et al.*, 2013), and have been implicated in the regulation of the hepatic lipid content and composition in a NASH mouse model (Kessler *et al.*, 2014). In chronic or acute liver diseases, Kupffer cells can be activated either *via* pathogen-associated or damage-associated molecular patterns (PAMPs / DAMPs). Upon stimulation, they secrete pro-inflammatory mediators, such as interleukin (IL)-6, IL-1 β , and tumor necrosis factor (TNF)- α (Park *et al.*, 2010; Ganz and Szabo,

2013). Permanent exposure of monocytes and macrophages to even low doses of endotoxins, such as LPS, leads to a state of hyporesponsiveness, a phenomenon termed LPS or endotoxin tolerance. LPS-tolerant macrophages are characterized by the lack of pro-inflammatory mediator production after re-stimulation with LPS. In contrast, the production of anti-inflammatory mediators, such as IL-10 or glucocorticoid-induced leucine zipper (GILZ), can even be enhanced (Biswas and Lopez-Collazo, 2009; Pena *et al.*, 2011; Bohannon *et al.*, 2013; Hoppstädter and Kiemer, 2015; Hoppstädter, Kessler, *et al.*, 2015).

Since macrophages are the central mediators of inflammation and have also been suggested to play a vital role in lipid homeostasis, we aimed to examine whether endotoxin tolerance influences hepatic lipid accumulation.

4.3 Results

4.3.1 Total lipids and distinct lipid classes are elevated in livers of endotoxin-tolerant animals

To study the impact of endotoxin tolerance on hepatic metabolism, we analyzed the total lipid content in liver tissues from endotoxin-tolerant animals and compared them to non-tolerant livers. Interestingly, the total hepatic lipid content was elevated in the non-tolerant as well as in the tolerant group after high dose LPS administration (fig. 4-1, A). Analysis of the lipid composition revealed an increase of all lipid classes that were detectable in these tissues, except for cholesteryl esters (fig. 4-1, B-G). When we determined the phosphatidylcholine/phosphatidylethanolamine (PC/PE) ratio (fig. 4-1, H), which has been shown to decline during the progression from simple steatosis to steatohepatitis (Li *et al.*, 2006), we observed a reduction in livers of both non-tolerant and tolerant LPS-treated animals.

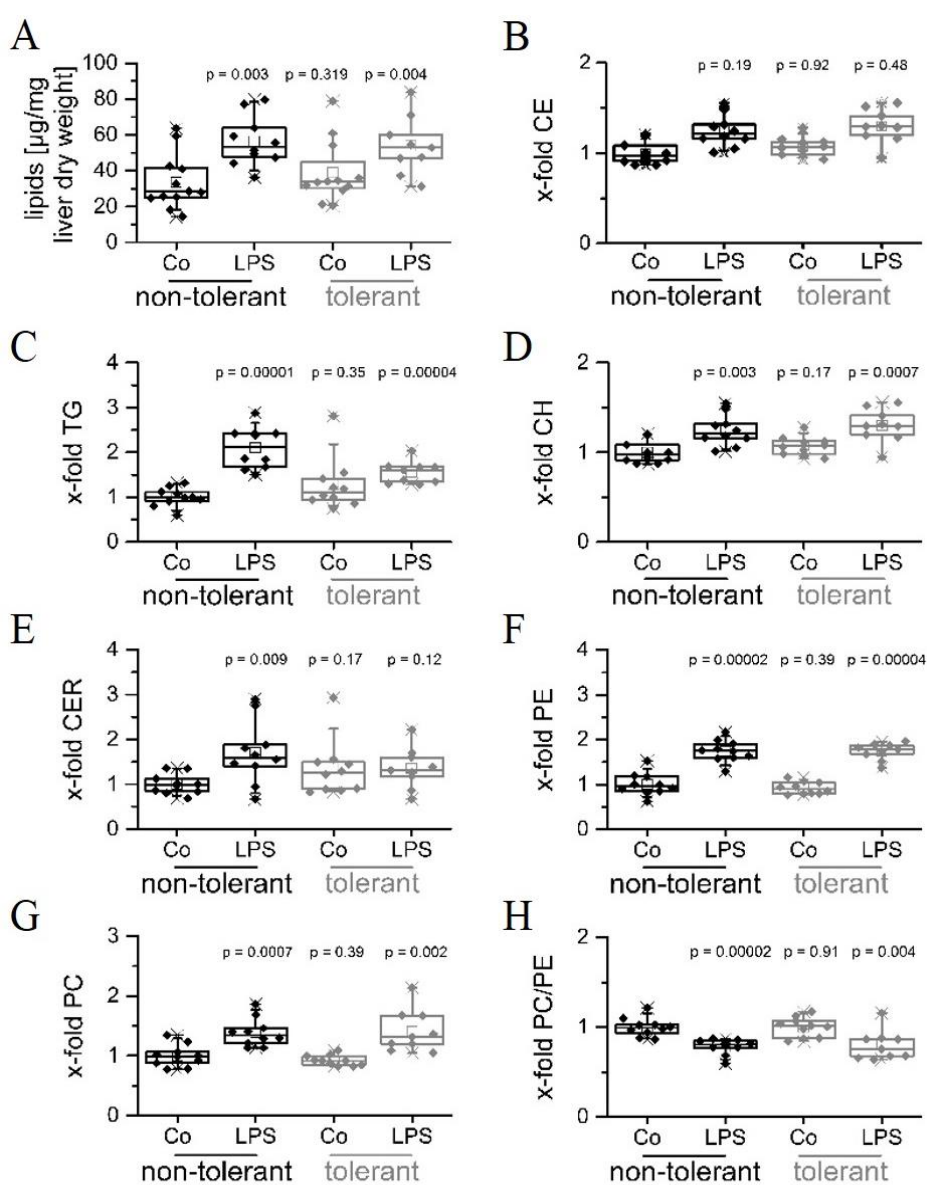


Figure 4-1: Total lipids and distinct lipid classes are elevated in livers of endotoxin tolerant animals. Lipid analysis of non-tolerant or tolerant animals treated with high-dose LPS (LPS) or vehicle alone (Co) ($n = 10-12$). P-values were calculated in comparison with non-tolerant Co (Mann Whitney U test). **A:** Quantification of total lipids by SPV assay. **B-G** Analysis of distinct lipid classes by TLC. Cholesteryl ester (**B**), triglycerides (**C**), cholesterol (**D**), ceramides (**E**), phosphatidylethanolamine (PE) (**F**), and phosphatidylcholine (PC) (**G**) levels were analyzed and shown as x-fold of non-tolerant Co. **H:** PC/PE ratio calculated from TLC values and shown as x-fold of non-tolerant Co.

4.3.2 Regulation of lipogenic genes in the endotoxin tolerance model

Lipogenesis is mainly orchestrated by two major regulatory transcription factors for lipid synthesis, i.e. sterol regulatory element-binding transcription factor 1 (SREBF-1; sterol-dependent) and MLX-interacting protein-like (MLXIPL, also known as carbohydrate-responsive element-binding protein; carbohydrate-dependent) (Musso, Gambino and Cassader, 2009). On the other hand, peroxisome proliferator-activated receptor (PPAR)- α represents a key inducer of lipid degradation (Lefebvre *et al.*, 2006). *Srebfl* and elongation of very long chain fatty acids-6 (*Elovl6*), the direct target of SREBF-1 (Kumadaki *et al.*, 2008), were upregulated in the livers of endotoxin-tolerant mice as well as in non-tolerant livers after LPS treatment (fig. 4-2, A and B). Hepatic *Ppara* mRNA expression was downregulated in LPS-treated non-tolerant as well as tolerant mice (fig. 4-2, C), whereas *Mlxipl* mRNA levels were not modified by LPS administration (fig. 4-2, D). These data suggest that LPS affects lipid homeostasis by modulating the expression of lipogenic and lipid degrading enzymes.

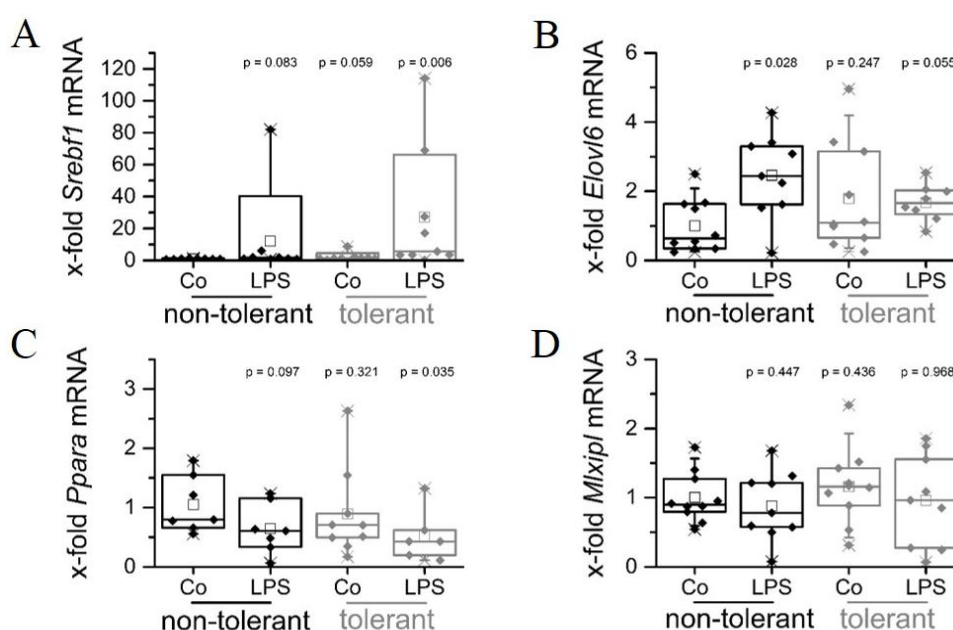


Figure 4-2 - Hepatic expression of lipogenic genes in the endotoxin tolerance model. A-D: Real-time RT-PCR analysis of *Srebfl* (A), *Elovl6* (B), *Ppara* (C) and *Mlxipl* (D) in livers of non-tolerant or tolerant animals treated with high-dose LPS or vehicle. mRNA expression levels were normalized to non-tolerant Co (n = 10). P-values were calculated in comparison with non-tolerant Co (Mann Whitney U test).

4.3.3 Kupffer cell depletion by clodronate liposomes and its impact on hepatic lipid composition

Kupffer cell-derived pro-inflammatory mediators, such as IL-6, IL-1 β and TNF- α , can promote the development of steatosis and steatohepatitis (Park *et al.*, 2010; Ganz and Szabo, 2013; Tilg, Moschen and Szabo, 2016). Thus, we hypothesized that the lipogenic effect of LPS might depend

on the presence of Kupffer cells. To test this assumption, we injected mice with clodronate liposomes, which specifically and potently deplete liver macrophages (Van Rooijen and Sanders, 1996).

Macrophage depletion was confirmed by the diminished expression of the murine macrophage marker F4/80 (*Emr1*) in livers of clodronate liposome-treated animals (fig. 4-3, A and B). Lipid class analysis showed that three out of six lipid classes, namely cholesterol, ceramides, and phosphatidylcholine, were significantly decreased in the livers of Kupffer cell-depleted LPS-treated animals when compared with LPS-injected controls (fig. 4-3, C). Triglycerides and phosphatidylethanolamine also tended to be downregulated, whereas the cholesteryl ester content seemed unchanged (fig. 4-3, C).

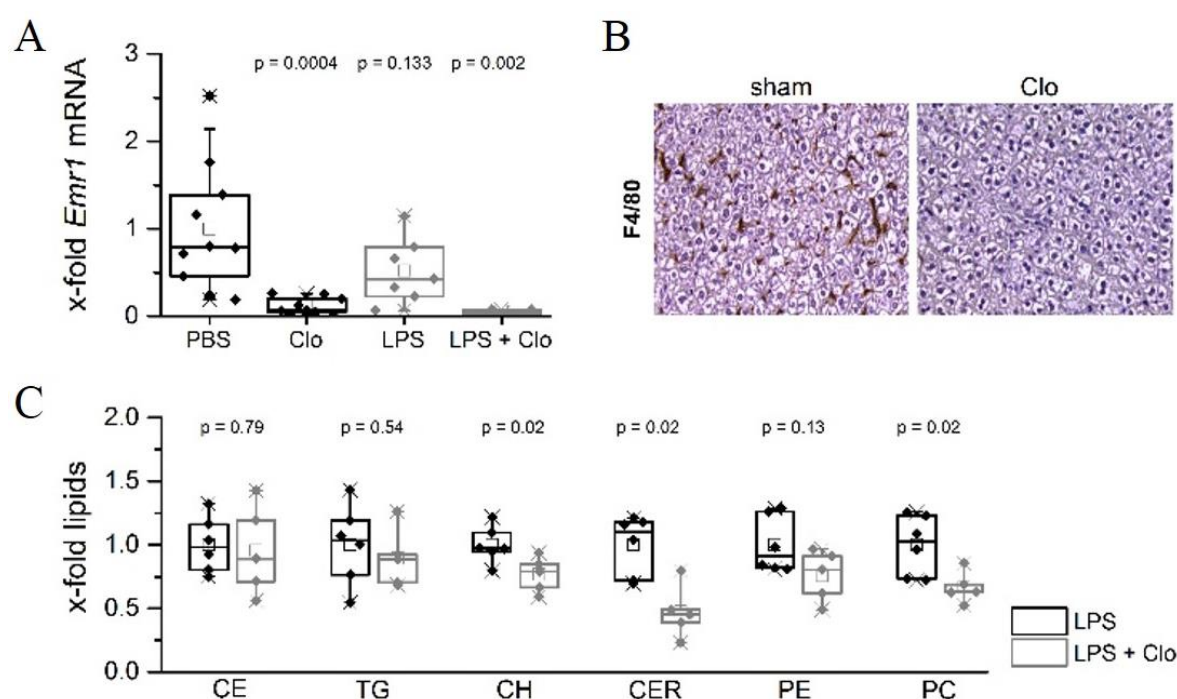


Figure 4-3: Kupffer cell depletion by clodronate liposomes and its impact on lipid composition. **A, B:** Confirmation of Kupffer cell depletion by clodronate liposomes (Clo) compared with PBS liposomes (PBS) ($n = 9-10$). **A:** Real-time RT-PCR analysis of *Emr1* (F4/80) mRNA expression. Data are presented as x-fold PBS controls, and p-values were generated in comparison with PBS controls (Mann Whitney U test). **B:** Immunohistochemical staining against Kupffer cell marker F4/80 in liver tissues of animals treated with sham or Clo liposomes (original magnification 200x). **C:** Mice were either treated with Clo liposomes or sham, followed by LPS ($n = 5-6$), and TLC analysis of distinct lipid classes present in liver tissue was performed. Data are presented as x-fold levels of naïve animals, and p-values were calculated compared with non-depleted controls (t-test). CE: cholesteryl ester, TG: triglycerides, CH: cholesterol, CER: ceramides, PE: phosphatidylethanolamine, PC: phosphatidylcholine.

Since clodronate treatment also efficiently abrogated the LPS-induced hepatic expression of *Tnf*, *Il1b*, and *Il6* mRNA (fig. 4-4, A-C), an involvement of Kupffer cell-derived cytokines in the lipogenic effect of LPS was suggested.

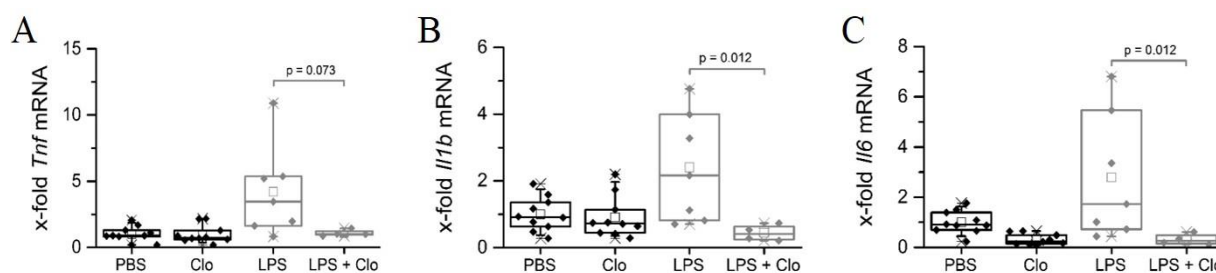


Figure 4-4: The impact of Kupffer cell depletion on the expression of inflammatory cytokines. Real-time RT-PCR analysis of *Tnf* (A), *Il1b* (B), and *Il6* (C) mRNA expression in livers of animals treated with PBS (PBS) or clodronate (Clo) liposomes, followed by LPS administration (n = 5-10). P-values were calculated in comparison with PBS controls (Mann Whitney U test).

4.3.4 Crosslink between Kupffer cell-derived cytokines and lipogenesis in endotoxin tolerance

Next, we wondered whether the changes in total lipid content and lipid composition in the endotoxin tolerance model might depend on lipogenic cytokines secreted by Kupffer cells. Hepatic *Il6* mRNA levels were increased when animals were treated with high dose LPS (fig. 4-5, A). Interestingly, LPS-induced *Il6* mRNA upregulation was also observed in the livers of LPS-tolerized mice (fig. 4-5, A and B).

In contrast, the pro-inflammatory factors *Tnf*, *Il1b*, *Cxcl10*, *Il12b*, and *Nos2* showed a lower expression in liver tissues of LPS-treated endotoxin-tolerant mice when compared with their non-tolerant littermates, whereas the induction of the anti-inflammatory marker genes *Arg1* and *Il10* was not repressed (fig. 4-5, B and data not shown) (Hoppstädter, Kessler, *et al.*, 2015). Moreover, TNF- α serum levels were reduced in tolerized animals, whereas IL-6 levels were not (fig. 4-5, C). In line with these findings, signal transducer and activator of transcription 3 (STAT3), a direct target of IL-6, was equally activated in livers of LPS-treated tolerant and non-tolerant animals, as shown by Western blot analysis (fig. 4-5, D and E).

To test the hypothesis that IL-6 facilitates the cross-talk between Kupffer cells and hepatocytes, HepG2 cells were incubated with recombinant IL-6 for up to 60 minutes. IL-6 treatment efficiently activated STAT3 in hepatocytes, whereas LPS did not (fig. 4-6, A and B). Next, we employed macrophage-conditioned medium (MCM) of non-tolerant and tolerant human monocyte-derived macrophages. LPS tolerance in macrophages was confirmed by qPCR analysis. The expression of *TNF* and *CXCL10* mRNA upon LPS exposure was strongly reduced in LPS-tolerant macrophages, whereas no difference between naïve and tolerant cells regarding *IL6* mRNA levels could be detected (fig. 4-6, C).

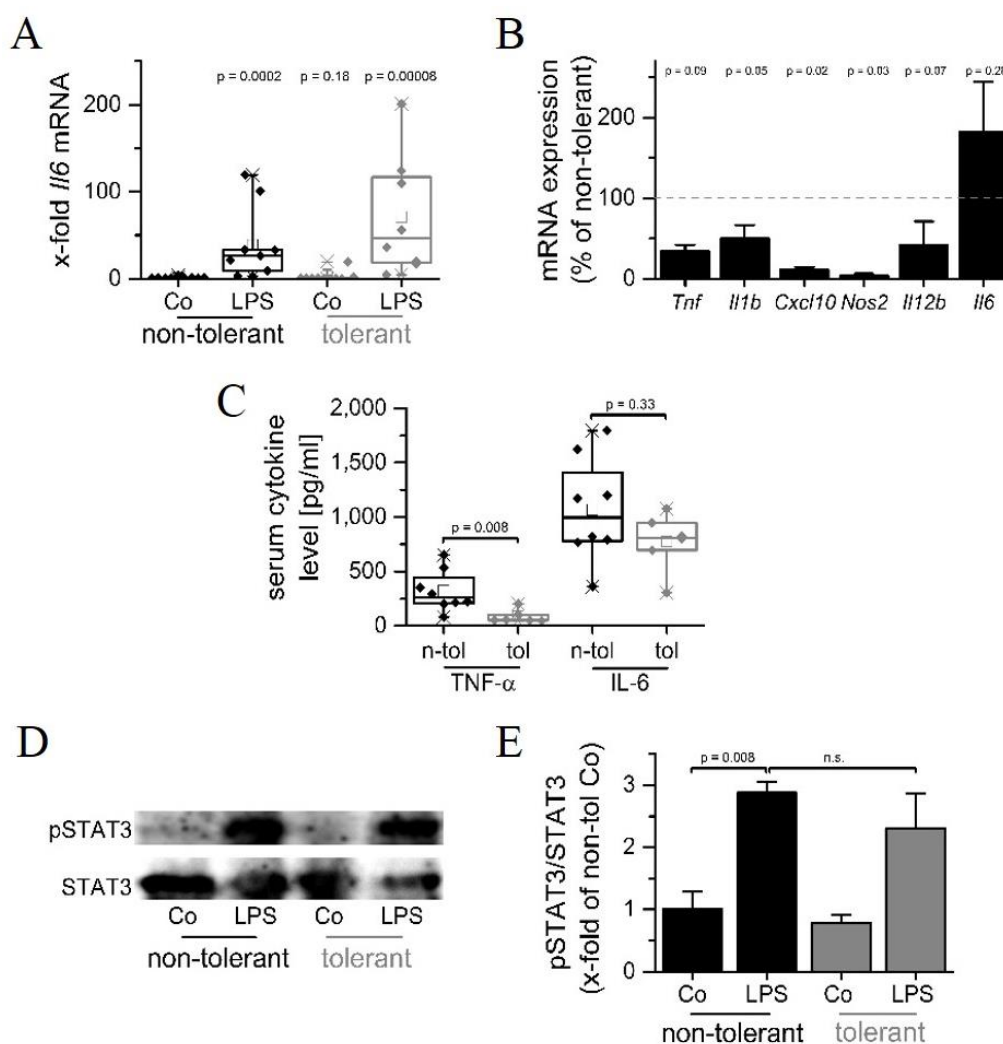


Figure 4-5: Hepatic inflammatory cytokine expression in the endotoxin tolerance model. **A, B:** Real-time RT-PCR analysis of liver tissue of non-tolerant or tolerant animals treated with high-dose LPS (LPS) or vehicle (Co) ($n = 10-12$). **A:** *Il6* mRNA expression shown as x-fold of non-tolerant Co. p-values were calculated in comparison with non-tolerant Co (Mann Whitney U test). **B:** *Tnf*, *Il1b*, *Cxcl10*, *Nos2*, *Il12b*, and *Il6* mRNA expression normalized to values for non-tolerant LPS-treated mice (set as 100%). *Il6* mRNA expression values are taken from data shown in Figure 4-4, *C. Tnf* and *Il1b* data were taken from (Hoppstädter et al., 2015). P-values were generated in comparison with non-tolerant LPS-treated mice (Mann Whitney U test). **C:** LPS-induced serum cytokine levels in non-tolerant and LPS-tolerant mice ($n = 6-8$) were determined by ELISA. P-values were generated by Mann Whitney U test. **D, E:** Western blot analysis of STAT3 phosphorylation in liver tissues of sham- and LPS-treated tolerant and non-tolerant mice. **D:** One representative result is shown. **E:** pSTAT3 signal intensities were quantified and normalized to values for total STAT3 (t-test). Data are presented as x-fold of non-tolerant Co ($n = 3$).

Treatment of HepG2 cells with MCM from LPS-treated tolerant as well as non-tolerant cells resulted in a significant STAT3 activation (fig. 4-6, D and E). This effect was blocked by preincubation of MCM with an anti-IL-6 antibody, showing that MCM-induced STAT3 activation in hepatocytes was dependent on macrophage-derived IL-6. To examine whether IL-6 indeed promotes lipogenesis, we incubated HepG2 cells with recombinant IL-6 and determined their lipid content. The lipogenic growth-factor IGF2 served as a positive control (supp. fig. 1) (Laggai *et*

al., 2014). The amount of triglycerides, cholesteryl esters, phosphatidylcholine, and phosphatidylethanolamine was indeed significantly increased upon IL-6 exposure, and cholesterol levels showed a similar tendency (fig. 4-6, F).

Taken together, these data suggest that lipogenic IL-6 is not affected by LPS tolerance and is therefore involved in the development of steatosis in the endotoxin tolerance model.

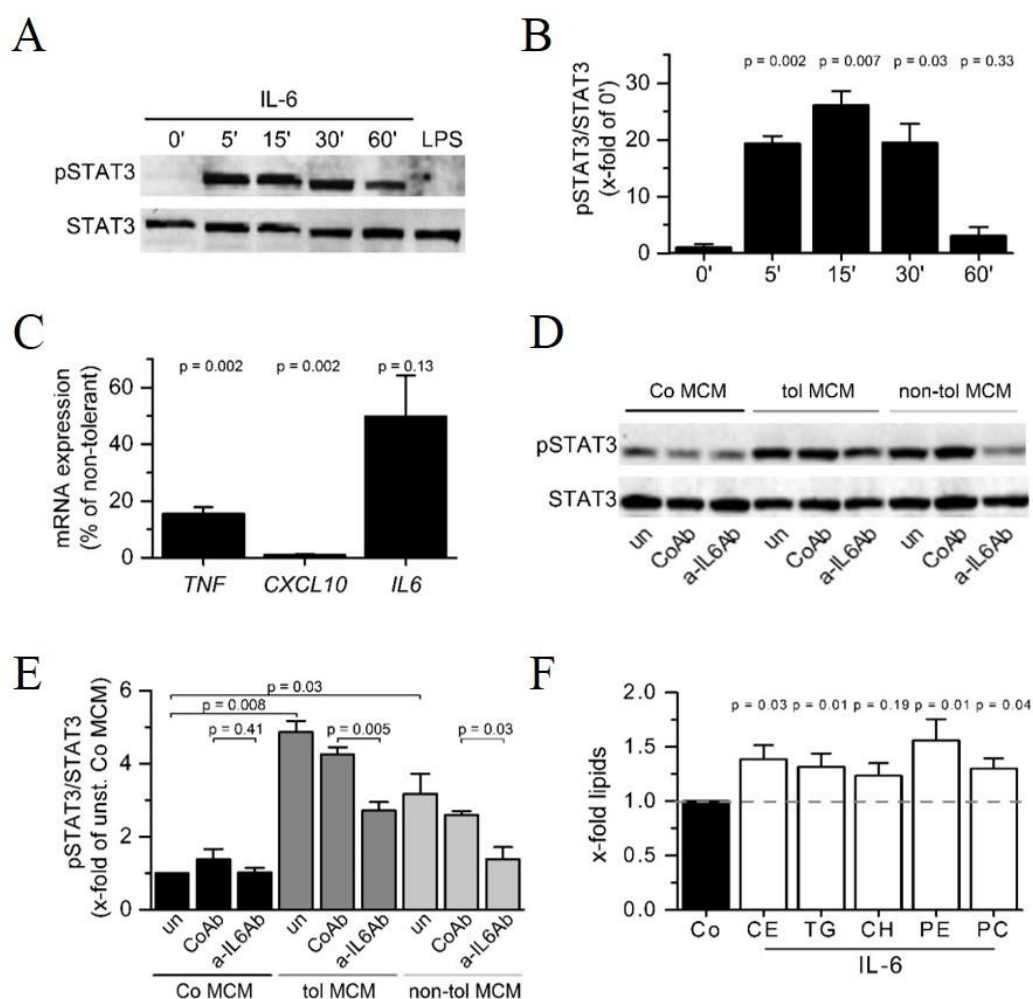


Figure 4-6: Hepatocyte activation by IL-6. **A, B:** HepG2 cells were treated with recombinant IL-6 (20 ng/ml) for up to 60 min or LPS (1 μ g/ml) for 30 min. The ratio of pSTAT3 to total STAT3 was analyzed by Western blot. **A:** One representative blot is shown. **B:** pSTAT3 signal intensities were quantified and normalized to total STAT3 expression. Data are presented as x-fold of 0 min values ($n = 3$, duplicates), and p-values were calculated in comparison with 0' (t-test). **C:** Real-time RT-PCR analysis for *TNF*, *CXCL10* and *IL6* mRNA expression in non-tolerant or LPS-tolerant human macrophages treated with high-dose LPS ($n = 3$, duplicates). Values for non-tolerant LPS-treated cells were set to 100%. P-values were calculated in comparison with non-tolerant LPS-treated macrophages (Mann Whitney U test). **D, E:** Macrophage-conditioned medium (MCM) of untreated (Co) and LPS-treated tolerant (tol) and non-tolerant (non-tol) macrophages were collected. MCM samples were either left untreated (un) or incubated for 30 min at 37°C with a control antibody (CoAb, 1 μ g/ml) or a neutralizing antibody against IL-6 (a-IL6Ab, 1 μ g/ml). Subsequently, MCM was added to HepG2 cells, and STAT3 activation was assessed by Western blot. **D:** One representative result is shown. **E:** Signal intensities were quantified, and the pSTAT3/total STAT3 ratio was expressed as x-fold of untreated Co MCM ($n = 2$, duplicates, t-test). **F:** HepG2 cells were treated with recombinant IL-6 (20 ng/ml, 72 h), and lipid class analysis by TLC was performed ($n = 6$, duplicates). Data are expressed as x-fold of untreated cells, and p-values were generated in comparison with untreated controls (Mann Whitney U test). CE: cholesteryl ester, TG: triglycerides, CH: cholesterol, PE: phosphatidylethanolamine, PC: phosphatidylcholine. Ceramides were below detection limit.

4.4 Discussion

Translocation of gut bacteria and bacterial components into the liver has been shown to promote chronic liver disease (Schnabl, 2013). In fact, increased levels of LPS in the portal or systemic circulation have been found in both ASH and NASH, probably due to an impaired gut epithelial integrity (Bode, Kugler and Bode, 1987; Nanji *et al.*, 1993; Enomoto *et al.*, 1998; Bode and Bode, 2003; Amar *et al.*, 2008).

Persistent innate immune activation by LPS usually suppresses pro-inflammatory innate immune responses, as observed in advanced sepsis or chronic infections (Biswas and Lopez-Collazo, 2009; Collins and Carmody, 2015). However, reports on the effect of LPS tolerance on IL-6 expression in macrophages and other myeloid cells are not consistent. These discrepancies might be related to the purity, type, and dose of LPS (Huber *et al.*, 2006; Rutledge *et al.*, 2012; Pupo *et al.*, 2013; Biedroń, Peruń and Józefowski, 2016). LPS lacking the O-antigen is called rough LPS (R-LPS), as opposed to O-antigen-containing smooth LPS (S-LPS). R- and S-LPS have been often indiscriminately used in the literature. However, recent reports have revealed that different LPS chemotypes might differ in their stimulatory potential, most likely as the result of differential receptor usage (Huber *et al.*, 2006; Pupo *et al.*, 2013; Biedroń, Peruń and Józefowski, 2016). It was recently shown that the dose–response of a natural LPS mixture obtained from *E. coli* O111 resembled the response to R-LPS fractions (Pupo *et al.*, 2013), which supports earlier findings that short-chain forms of LPS dominate the innate immune response of macrophages to LPS *in vitro* (Huber *et al.*, 2006). Therefore, we used R-LPS for all our studies.

Whereas IL-6 expression upon re-stimulation with LPS was abrogated in some *in vitro* settings in LPS-tolerized cells (Collins and Carmody, 2015), other studies suggested that LPS tolerance does not affect IL-6 induction, thereby supporting our findings obtained both *in vivo* and in primary human macrophages. Concordantly, primary rat Kupffer cells obtained from LPS-tolerant rats expressed high levels of IL-6 upon *in vitro* re-stimulation, whereas TNF- α production was repressed (Hafenrichter *et al.*, 1994). In addition, TNF- α , but not IL-6, was induced to a significantly lower degree after LPS treatment in liver and lung of endotoxin-tolerant rats when compared with non-tolerant controls (Flohé *et al.*, 1999). Another study reported that endotoxin tolerance reduced mortality caused by hemorrhagic shock, which was associated with decreased hepatic TNF- α production, but increased IL-6 levels (Ackermann *et al.*, 2001).

IL-6 represents a pleiotropic cytokine that can exert pro- as well as anti-inflammatory actions (Opal and DePalo, 2000). Pretreatment of murine bone marrow-derived macrophages with IL-6 led to attenuated LPS-induced expression of multiple pro-inflammatory genes, including *Tnf* and

Nos2 (Mauer *et al.*, 2014). In accordance, *in vivo* differentiated human macrophages showing rather regulatory properties express substantially higher levels of IL-6 than inflammatory macrophages (Hoppstädter *et al.*, 2010).

Inactivation of the IL-6 receptor in myeloid cells resulted in increased susceptibility to LPS-induced endotoxemia in an *in vivo* mouse model, suggesting that IL-6 may, in fact, limit innate pro-inflammatory responses (Mauer *et al.*, 2014). Of note, high fat diet-induced TNF- α production was reported to be higher in IL-6 knockout mice when compared with their wild-type counterparts (Vida *et al.*, 2015).

In general, plasma IL-6 levels correlate with obesity and the metabolic syndrome (Bastard *et al.*, 2000; Glund and Krook, 2008). IL-6 expression has also been reported to be markedly increased in the livers of NASH patients as compared with patients with simple steatosis or normal biopsies, suggesting that increased hepatic IL-6 production plays a significant role in NASH development (Wieckowska *et al.*, 2008).

Interestingly, subjecting NASH patients to a therapy including low-fat diet and exercise not only resulted in an improvement regarding liver enzymes, cholesterol, and plasma hyaluronic acid levels, but also in decreased IL-6 levels, whereas other cytokines that were chronically elevated in these patients, such as TNF- α , were not affected (Kugelmas *et al.*, 2003).

The low-grade inflammatory response induced by obesity may not only be involved in NASH progression, but also in tumor promotion. Enhanced expression of both IL-6 and TNF- α has been shown to contribute to obesity-promoted HCC development in a mouse model (Park *et al.*, 2010). The same study demonstrated that depletion of either IL-6 or the TNF receptor reduced fat accumulation in livers of high fat diet-fed mice. Our observations suggest that Kupffer cell-derived IL-6, rather than TNF- α , may be involved in hepatic lipid accumulation upon repeated LPS exposure, since, unlike TNF- α , neither IL-6 expression nor the hepatic lipid content was significantly affected by endotoxin tolerance. Both IL-6 receptor subunits, i.e. IL6-R and the signal transduction subunit gp130, are expressed on murine hepatocytes (Klein *et al.*, 2005), and studies with primary rat hepatocytes indeed suggested a direct involvement of IL-6, but not TNF- α , in hepatic lipid accumulation (Brass and Vetter, 1994, 1995). In our hands, IL-6 potently activated STAT3 and caused lipid accumulation in hepatocytes. STAT3 phosphorylation leads to its translocation into the nucleus and the transcription of respective target genes, including genes involved in lipogenesis (Kinoshita *et al.*, 2008; Vida *et al.*, 2015).

Sterol regulatory element-binding proteins (SREBPs) are key transcription factors that regulate genes involved in de novo lipid synthesis (Ruiz *et al.*, 2014). SREBP-1c (SREBF1) is the predominant SREBP isoform in murine livers, and its depletion has been shown to attenuate fatty liver development in obese mice (Yahagi *et al.*, 2002). Interestingly, treatment of HepG2 hepatoma cells with IL-6 has been shown to result in an activation of both SREBF-1 and -2, as indicated by increased binding to sterol responsive elements (SREs) (Gierens *et al.*, 2000). We observed that *Srebf1* was induced in livers of LPS-treated endotoxin-tolerant mice and tended to be upregulated in non-tolerant mice upon LPS challenge. The significant induction of the lipogenic SREBF-1 target gene *Elovl6* (Kumadaki *et al.*, 2008) in liver tissues of LPS-tolerized and sham-treated mice further confirmed an activation of SREBF1 upon LPS administration in our setting. ELOVL-6 itself catalyzes the elongation of C16 to C18 fatty acids (Matsuzaka *et al.*, 2007), is lipogenic (Laggai *et al.*, 2014), and has been shown to promote NASH development (Matsuzaka *et al.*, 2012; Muir *et al.*, 2013; Kessler *et al.*, 2014). Not only the amount of total hepatic fatty acids but also the C18/C16 ratio has been shown to be increased in a model of NASH, which was not observed in a model of simple steatosis. Depletion of Kupffer cells abrogated both quantitative and qualitative NASH-associated alterations in hepatic lipids (Kessler *et al.*, 2014), suggesting that Kupffer cell-derived mediators, such as IL-6, are involved in this process.

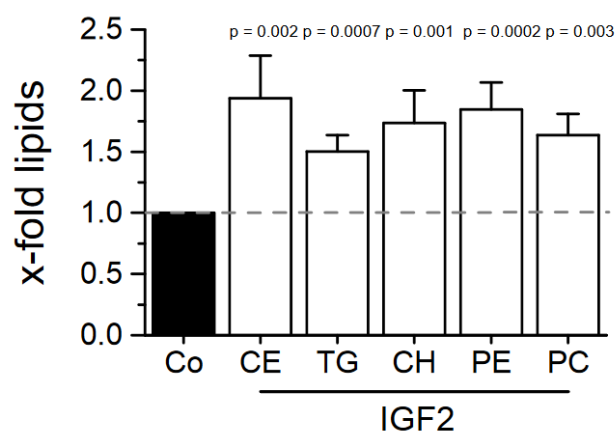
Furthermore, we observed that *Ppara* expression was reduced upon LPS-treatment, which was not affected by LPS-tolerance. Interestingly, this effect has previously been associated with hepatic IL-6 expression (Chew *et al.*, 2014). PPAR- α is a member of the nuclear hormone receptor family of transcription factors, which can be activated by unsaturated fatty acids and their derivatives. PPAR- α is expressed in the liver, heart, skeletal muscle, and brown adipose tissue, where it regulates genes that control mitochondrial and peroxisomal fatty acid oxidation, fatty acid transport, and hepatic glucose production (Pawlak, Lefebvre and Staels, 2015). Thus, PPAR- α downregulation may contribute to excess lipid deposition in the liver upon LPS exposure.

Lipid class analysis indicated that LPS enhanced the accumulation of a wide range of lipids, which have also been reported to be elevated in NAFLD, including triglycerides, cholesterol, and ceramides. As both cholesterol and ceramides exert cytotoxic effects (Arora *et al.*, 1997; Tabas, 2002), their abundance may aggravate liver damage and inflammatory responses. In addition, both phosphatidylcholine (PC) and phosphatidylethanolamine (PE) levels were increased in the livers of LPS-treated naïve and endotoxin-tolerant animals, as observed in other steatosis models (Kessler *et al.*, 2016), whereas the PC/PE ratio decreased. This effect was also observed in liver biopsies of NASH patients when compared with healthy subjects and has been suggested as a marker for the progression from steatosis to steatohepatitis (Li *et al.*, 2006).

In conclusion, our data indicate that endotoxin tolerance does not influence LPS-induced hepatic lipid accumulation, although the effect requires the presence of Kupffer cells. Our results furthermore suggest that Kupffer cell-derived IL-6 production is not abrogated by LPS tolerance and may drive hepatic lipid storage.

4.5 Supplement

The lipogenic growth-factor IGF2 served as a positive control for lipogenesis promotion (Supplemental Figure 1):



Supplemental Figure 1: Lipid levels in HepG2 cells after IGF2 treatment. HepG2 cells were treated with recombinant IGF2 (75 ng/ml, 72 h), and lipid class analysis by TLC was performed (n = 6, duplicates). Data are expressed as x-fold of untreated cells (Co), and p-values were generated in comparison with untreated controls (Mann Whitney U test). CE: cholesteryl ester, TG: triglycerides, CH: cholesterol, PE: phosphatidylethanolamine, PC: phosphatidylcholine.

5. Material and Methods

5.1 Material

5.1.1 General Material

Cell culture medium RPMI 1640, FCS, penicillin, streptomycin, glutamine, Trypsin-EDTA and Accutase[®] as well as the MMP activator 4-aminophenylmercuric acetate (APMA, # 9563) and dexamethasone (# D4902) were purchased from Sigma-Aldrich (now Merck, Darmstadt, Germany). QIAzol Lysis Reagent was obtained from Qiagen (# 79306, Hilden, Germany). LPS (LPS-EK ultrapure from *E. coli* K12, # t1rl-pek1ps) and Pam₃CSK₄ (# t1rl-pms) for *in vitro* studies, the neutralizing antibody against human IL-6 (# mabg-hil6-3, [3H3]) and the matching IgG1 control (# mabg1-ctrlm, [T8E5]) as well as the selective antibiotics Hygromycin B (#ant-hg-1) and Zeocin[™] (#ant-zn-1) were from InvivoGen (San Diego, USA). TE buffer and molecular water for RNA analysis were from AppliChem (Darmstadt, Germany). Recombinant human IL-6 was from Miltenyi Biotech (# 130-095-352, premium grade, Bergisch Gladbach, Germany). Other chemicals were purchased from either Sigma-Aldrich (now Merck, Darmstadt, Germany), Carl Roth (Karlsruhe, Germany) or VWR (Radnor, USA) unless otherwise noted.

5.1.2 General buffers

PBS: 137 mM NaCl, 2.7 mM KCl, 10.1 mM Na₂HPO₄, 1.8 mM KH₂PO₄; pH 7.4

RIPA: 150 mM NaCl, 50 mM Tris (pH 8.0), 1% NP-40, 0.1% SDS, 0.5% Na-Desoxycholate

5.2 Mice

Mice were housed in a 12/12 h light/dark cycle with food and water ad libitum under stable conditions regarding temperature and humidity. For tolerance experiments and Kupffer cell depletion, mice were treated as described previously (Hoppstädter et al. 2015; Kessler et al. 2014).

All animal procedures were performed in accordance with the local animal welfare committee (permission no. 34/2010 and 35/2013; Landesamt für Soziales, Gesundheit und Verbraucherschutz Saarland).

5.3 Human lung and lung-tumor tissue

Human non-tumor lung tissue or the autogenic tumor tissue has been obtained from patients undergoing lung resection (SHG Kliniken Völklingen, Germany). The use of human material was reviewed and approved by the local ethics committee (State Medical Board of Registration, Saarland, Germany; permission no. 213/06). The informed consent of all participating subjects was obtained. The following tissues were utilized for mRNA sequencing experiments (5.8):

Gender	Age (years)	Tumor stage
male	70	T2aN1
female	74	T1aN0
female	75	pT2apN0

5.4 Cell culture

All cells were cultivated at 37°C and 5% CO₂.

5.4.1 Human alveolar macrophages (AMs) and tumor-associated macrophages (TAMs)

AMs and TAMs were isolated from human lung tissue or the autogenic lung-tumor tissue obtained from patients undergoing lung resection (see chapter 5.3).

A schematic workflow for the isolation is shown in figure 5-1. For TAM isolation, tumor tissue was manually cut into small pieces. Pieces were enzymatically digested using a commercially available enzyme mix optimized for the digestion of human tumors (human tumor dissociation kit, # 130-095-929, Miltenyi Biotec, Bergisch Gladbach, Germany). Additionally, mechanical dissociation was performed before and during the digestion procedure in C Tubes (# 130-093-237, Miltenyi Biotec) using the gentleMACS Octo Dissociator (Miltenyi Biotec) according to the manufacturer's instructions. Cells were washed, resuspended in RPMI 1640 medium without any supplements and incubated for 0.5 h in a T175 flask. Adherent cells were thoroughly washed with PBS to remove non-adherent cells, such as fibroblasts or erythrocytes, and further cultivated in AM/TAM medium. On the next day, TAMs were detached with accutase, and cultivated at a density of 0.5×10^6 cells per well in a 12-well plate overnight before used for further experiments. Morphology was checked with an Axiovert40 CFL microscope (Carl Zeiss, Oberkochen, Germany) and pictures were taken with a Canon DS126151 camera.

AM isolation was performed according to a previously described method (Hoppstädter *et al.*, 2010, 2012) with minor modifications. After visible bronchi were removed, the lung tissue was

chopped and washed with 100–200 ml PBS. Washing buffer was collected and AMs were obtained by centrifugation. Remaining erythrocytes were lysed by quickly resuspending the pellet in autoclaved water, followed by immediate washing with PBS and centrifugation. The obtained cell pellet was mock-digested by treatment with the same enzyme mix and mechanical dissociation as used for the tumor tissue, and AM cells were seeded as described for TAMs.

AM/TAM medium: RPMI 1640, 5% FCS, 100 U/ml penicillin G, 100 µg/ml streptomycin, 2 mM glutamine

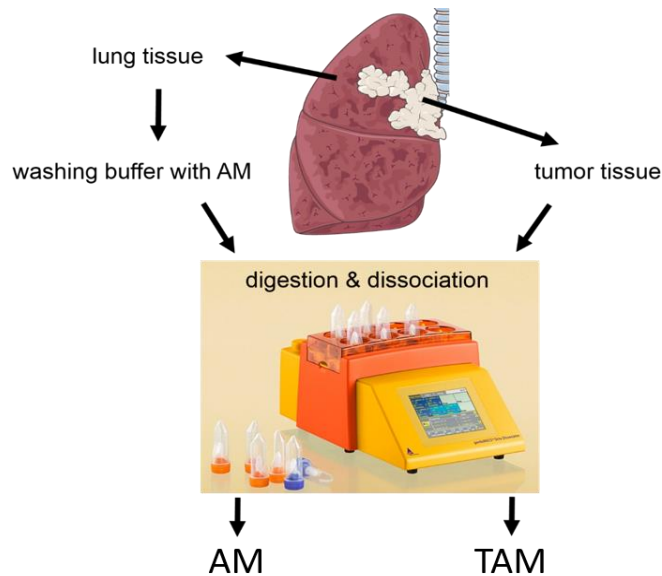


Figure 5-1: Schematic workflow for the isolation of AM and TAM single cell suspensions from human tissue. Lung illustration was obtained and modified from Servier Medical Art by Servier, <https://smart.servier.com/>, licensed under Creative Commons Attribution 3.0 Unported License, <http://creativecommons.org/licenses/by/3.0/>. Picture of MACS dissociator was obtained from the <https://www.miltenyibiotec.com/homepage>.

5.4.2 Human monocyte-derived macrophages (MDM)

Buffy coats were obtained from healthy adult blood donors (Blood Donation Center, Klinikum Saarbrücken, Germany). The use of human material for the isolation of primary cells was approved by the local ethics committee (permission no. 130/08).

Monocytes were isolated from buffy coats by density gradient centrifugation using Lymphocyte Separation Medium 1077 (# C-44010, PromoCell, Heidelberg, Germany) and LeucoSEP tubes (# 227290, Greiner Bio-One, Kremsmünster, Austria). In brief, 15 ml separation medium and 35 ml donor blood were given into one LeucoSEP tube and spun for 30 min at 300 x g without break to maintain the gradient, 4 tubes in total per donor. Upper plasma phase was discarded and the white peripheral blood mononuclear cell (PBMC) ring was transferred into a new falcon tube. After washing with PBS, monocytes were purified from the PBMC fraction by magnetic cell

sorting using anti-CD14 microbeads (# 130-050-201, Miltenyi Biotec, Bergisch Gladbach, Germany) and LS Columns (# 130-042-401, Miltenyi Biotec) according to the manufacturer's instructions, except that only 10% of the recommended bead amount was used (Stögbauer *et al.*, 2008). Monocyte purity was > 95% as assessed by CD14 expression (diploma thesis Daniela Oster, 2015). Finally, monocytes were seeded into a 12-well plate in a density of 0.5×10^6 cells/well. They were differentiated into macrophages in medium containing 20 ng/ml M-CSF (MDM medium) for 6-7 d with medium exchange every other day.

MDM medium: RPMI 1640 with 10% FCS, 100 U/ml penicillin G, 100 mg/ml streptomycin, 2 mM glutamine and 20 ng/ml M-CSF

For TAM-like model in chapter II:

Due to the limited number of primary TAMs, we established an *in vitro* TAM-like macrophage model on the basis of Edin et al. (2013). Differentiated MDMs were polarized for 24 h in MDM medium plus treatment as follows:

- 100 ng/ml LPS + 20 ng/ml IFN- γ → M1
- 20 ng/ml IL-4 → M2(IL4)
- 20 ng/ml IL-10 → M2(IL10)
- tumor cell conditioned medium (see 5.4.4) + 20 ng/ml M-CSF → TAM-like

All cytokines were obtained from Miltenyi Biotec (Bergisch Gladbach, Germany): Human M-CSF, premium grade (#130-096-489), Human IFN- γ 1b, premium grade (#130-096-481), Human IL-10, research grade (#130-093-947), Human IL-4, premium grade (#130-093-919).

For endotoxin tolerance in chapter III:

To induce endotoxin tolerance, MDM were treated with 100 ng/ml LPS or medium only. After 24 h, supernatant was removed and fresh medium with or without LPS (1 μ g/ml) was added for another 4 h. Subsequently, cells were harvested for qPCR analysis. Supernatants were pooled and stored at -80°C until further use.

5.4.3 Human umbilical vein endothelial cells (HUVECs)

HUVECs are primary cells obtained by isolation of human umbilical veins. The umbilical cords were provided by the Klinikum Saarbrücken (Saarbrücken, Germany; ethics committee permission no. 131/08). Preparation and cultivation of cells as previously described was performed by Theo Ranßweiler (Diesel *et al.*, 2012). For all experimental procedures HUVEC cell were used in passage three. Cells were detached by Trypsin-EDTA, seeded at a density of 1×10^5 cells per well in a 24-well plate and incubated overnight before further treatment.

HUVEC medium: Endothelial Cell Growth Medium (# C-22010, PromoCell, Heidelberg, Germany) with supplement mix (# C-39215, PromoCell), penicillin 100 U/ml, streptomycin 100 mg/ml, kanamycin 50 mg/ml, and 10% FCS.

5.4.4 Cell lines (THP-1, A549, HepG2, HEK-Dual™ hTLR2)

THP-1 is a human leukemic monocytic cell line that grows in suspension. After treatment with phorbol-12-myristat-13-acetat (PMA) cells differentiate into macrophage-like cells and adhere. Here, cells were differentiated with 100 nM PMA (# 524400, Calbiochem/Merck-Millipore, Darmstadt, Germany) for 48 h.

A549 is a human adenocarcinomic type II pulmonary epithelial cell line and therefore a common model for in vitro NSCLC studies. In this work, A549 cells were used to generate tumor cell conditioned medium (TCM) for the TAM-like macrophage model. In detail, 1×10^6 cells were seeded in a T75 culture flask for 3 d, until 90% confluency was reached. Supernatant was discarded and fresh medium was added to the cells. After 48 h medium was collected and sterile-filtered (0.2 μ m) and used immediately as TCM for macrophage polarization (5.4.2).

HepG2 is a human liver cancer cell line that has been derived from a well-differentiated hepatocellular carcinoma and is often used as an *in vitro* model for human hepatocytes.

HEK-Dual™ hTLR2 (NF/IL8) is a reporter cell line purchased from InvivoGen (# hkd-hltr2hi, San Diego, USA). According to the supplier, this cell line features a triple knockout of TLR3, TLR5 and the TNF receptor (TNFR), what enables the study of hTLR2 signaling without interference from other TLRs. Additionally, it expresses a luciferase under the control of the endogenous IL-8 promotor allowing a monitoring of TLR2 stimulation by expression of IL-8 dependent reporter using Quanti-Luc™.

THP-1, A549, and HepG2 medium: RPMI 1640, 10% FCS, 100 U/ml penicillin G, 100 μ g/ml streptomycin, 2 mM glutamine

HEK-Dual™ hTLR2 (NF/IL8) medium: DMEM, (4.5 g/l glucose), 10% heat inactivated FCS, 50 U/ml penicillin, 50 μ g/ml streptomycin, 100 μ g/ml Normocin™, 2 mM L-glutamine, 100 μ g/ml Hygromycin B and 50 μ g/ml Zeocin™

5.5 Extracellular vesicle (EV) isolation

EVs were purified from cell culture supernatant by sequential centrifugation as previously described (Théry, Clayton and Amigorena, 2006). The general isolation workflow is depicted in figure 5-2. THP-1 cells or AMs were cultured in medium without FCS, since FCS itself already contains a huge number of bovine EV (Théry, Clayton and Amigorena, 2006; Kornilov *et al.*, 2018).

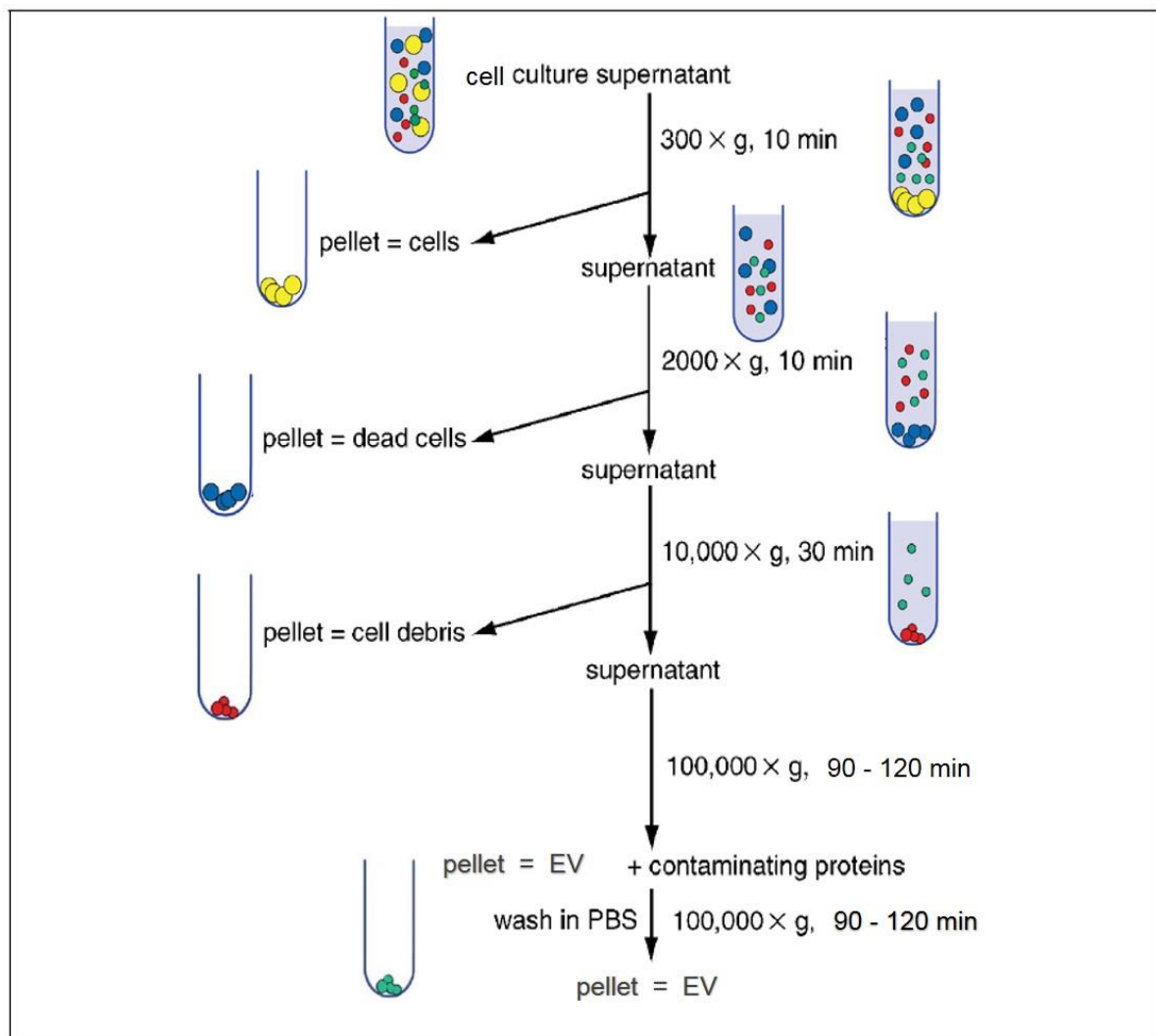


Figure 5-2: EV isolation workflow overview, modified after Théry *et al.* 2006; Momen-Heravi *et al.* 2013. See text for details.

After three days, cell culture supernatants were collected in a falcon tube prior to a first centrifugation step at 300 x g for 10 min to remove any cell contamination. To remove any dead cells and large cell debris, the supernatants were then spun at 2,000 x g for 10 min and at 10,000 x g for 30 min. Finally, supernatants were transferred into stable polycarbonate tubes (# 4416, Laborgeräte Beranek GmbH, Weinheim, Germany) and EVs were collected by spinning at 100,000 x g for 90 – 120 min in an L70 ultracentrifuge with 70Ti rotor (Beckman Coulter, Krefeld, Germany). EVs were washed with 25 ml sterile-filtered PBS (0.2 µm filter) and pelleted again by ultracentrifugation at the same high speed. EV pellet was then resuspended in 200 – 350 µl sterile-filtered PBS and stored in protein LoBind microcentrifuge tubes (# Z666505, Eppendorf AG, Hamburg, Germany) at -80°C. EV preparations were analyzed by NTA (5.5.1) and protein concentrations were determined by Pierce BCA protein assay (5.9).

5.5.1 Nanoparticle tracking analysis (NTA)

Fluorescence nanoparticle tracking analysis (NTA) is a method for direct, real-time visualization and analysis of nanoparticles in liquids to determine their size distribution and total concentration. NTA therefore relates the rate of Brownian motion to particle size by visualizing particles by light scattering using a conventional light microscope (Dragovic *et al.*, 2011).

All measurements were conducted at the Leibniz Institute for New Materials (INM) Saarbrücken, Germany, together with **Dr. Jana Fleddermann** with a NanoSight LM10 (NanoSight Ltd., Amesbury, United Kingdom).

EV suspensions were diluted 1:200 in sterile-filtered PBS prior to the measurement to obtain an optimal concentration range. 300-500 µl of the dilution were injected into the sample chamber. A video of 60 sec was recorded and analyzed by the NTA software Nanosight NTA 2.3 to calculate vesicle size and concentration.

5.6 RNA isolation and reverse transcription

RNA isolation for chapter I:

Total RNA from HUVEC was extracted using the High Pure RNA Isolation Kit (# 11828665001, Roche, Basel, Switzerland) according to the manufacturer's instructions.

RNA isolation for chapter II:

Total RNA from AM/TAM and polarized MDM was extracted using the Direct-zol™ RNA Miniprep Kit (# 2050, Zymo Research, Irvine, USA) according to the manufacturer's instructions. Prior to RNA isolation, cells were lysed with QIAzol Lysis Reagent.

RNA isolation for chapter III:

Total RNA from MDM cells and murine liver tissue was extracted using QIAzol Lysis Reagent according to the manufacturer's protocol. Residual genomic DNA was removed by treatment with Ambion DNase I (# AM2222, Thermo Fisher Scientific, Waltham, USA).

Efficiency of DNase I treatment was tested performing an Alu-PCR for human samples (primer: A1S 5'-TCATGTCGACGCGAGACTCCATCTCAAA-3') or a SINE-PCR for murine samples (primer: forward 5'-CTTCTGAGTGTTTGAAGAC-3'; reverse 5'-CTGGAACTCAC-TCTGAAGAC-3'). Primers were obtained from Eurofins MWG Operon.

The conditions for the PCR runs in a T100 thermal cycler (Bio-Rad Laboratories, München, Germany) were as follows:

Initial denaturation	15 min at 94°C	
Denaturation	1 min at 94°C	} 30 cycles
Annealing	1 min at 56°C (Alu)/59°C (SINE)	
Elongation	1 min at 72°C	
Final elongation	10 min at 72°C	

Reverse transcription:

Concentration and purity (260/280 ratio) of the isolated mRNA was measured at 260 nm using a NanoDrop™ Lite spectral photometer (Thermo Fisher Scientific, Waltham, USA).

500 ng of total RNA was reverse transcribed using the High-Capacity cDNA Reverse Transcription Kit (# 4368814, Applied Biosystems, Foster City, USA) as recommended by the supplier together with RNaseOut Recombinant Ribonuclease Inhibitor (# 10777019, Invitrogen, Carlsbad, USA).

Subsequently, the complementary DNA (cDNA) was diluted with TE buffer to a total volume of 100 µl prior to qPCR analysis.

5.7 Quantitative RT-PCR

Transcripts were detected using the 5 x HOT FIREPol® EvaGreen® qPCR Mix Plus (# 08-25-00020, Solis BioDyne, Tartu, Estonia) according to the manufacturer's instructions using a CFX96 Touch™ Real-Time PCR Detection System (Bio-Rad Laboratories, München, Germany) using the following conditions:

Initial denaturation	15 min at 95°C	} 40 cycles
Denaturation	20 sec at 95°C	
Annealing	20 sec at x °C (see table 6-1)	
Elongation	20 sec at 72°C	
Melt curve	5 sec 65-95°C	

Primer sequences and corresponding conditions are given in Table 5-1. All primer were obtained from Eurofins MWG Operon. For human IL-6, samples were analyzed with dual-labelled probes as described previously (Hoppstädter *et al.*, 2010). For absolute quantification, standards of the respective PCR product cloned into pGEMTeasy (Promega) were run alongside the samples to generate a standard curve as described (Hoppstädter *et al.*, 2010). Alternatively, the $\Delta\Delta CT$ calculation method was chosen for a relative quantification. All samples and standards were analyzed in triplicate. The relative gene expression was calculated by normalizing gene expression to an indicated housekeeping gene (*ACTB* or *Rn18s*).

Table 5-1: Primer sequences and corresponding conditions for qPCR reactions. Indicated are primer volumes (10 μ M stock), annealing temperature and whether an internal plasmid standard was used.

Gene	Forward Primer Sequence 5' – 3'	Reverse Primer Sequence 5' – 3'	Volume [μ l]	Annealing [°C]	standard
Human <i>ACTB</i>	TGCGTGACATTAAGGAGAAG	GTCAGGCAGCTCGTAGCTCT	0.5	60	yes
Human <i>CCL2</i>	TTGATGTTTTAAGTTTATCTTTCATGG	CAGGGGTAGAACTGTGGTTCA	1	60	no
Human <i>CXCL10</i>	GAGCCTACAGCAGAGGAACC	AAGGCAGCAAATCAGAATCG	0.5	60	yes
Human <i>DUSP1</i>	CAG CTG CTG CAG TTT GAG TC	AGG TAG CTC AGC GCA CTG TT	0.6	64	no
Human <i>ICAM</i>	GAAGTGCCCTCCATAGACA	TCAAGGGTTGGGGTCAGTAG	0.4	61	yes
Human <i>IL6</i>	AATAATAATGGAAAGTGGCTATGC	AATGCCATTTATTGGTATAAAAAAC	(probe) 1.25	57	yes
Human <i>SELE</i>	AGCCCAGAGCCTTCAGTGTA	CCCTGCATGTCACAGCTTTA	0.4	61	no
Human <i>TNF</i>	CTCCACCCATGTGCTCCTCA	CTCTGGCAGGGGCTCTTGAT	0.5	60	yes
Human <i>VCAM</i>	CGAGACCACCCAGAATCTA	CTGTGGTGCTGCAAGTCAAT	0.4	61	no
Murine <i>Arg1</i>	ACAAGACAGGGCTCCTTTCAG	GGCTTATGGTTACCTCCCG	0.5	60	yes
Murine <i>Cxcl10</i>	GAGAATGAGGGCCATAGGGA	CATCGTGGCAATGATCTCAAC	0.5	60	yes
Murine <i>Elov16</i>	ACAATGGACCTGTCAGCAAA	GTACCAGTGCAGGAAGATCAGT	0.2	60	yes
Murine <i>Emr1</i>	CTTTGGCTATGGGCTTCCAGTC	GCAAGGAGGACAGAGTTTATCGTG	0.5	60	yes
Murine <i>Il1β</i>	CCAAAAGATGAAGGGCTGCTT	GGAAGGTCACGGGAAAGAC	0.5	60	yes
Murine <i>Il6</i>	AAGAAATGATGGATGCTACCAAATG	GTAATCCAGAAGCCAGAGGAAATT	0.4	60	yes
Murine <i>Il10</i>	GCCCAGAAATCAAGGAGCAT	GAAATCGATGACAGCGCCT	0.5	60	yes
Murine <i>Il12b</i>	TGGAGCACTCCCCATTCCTA	GAGGAACGCACCTTTCTGGT	0.5	60	yes
Murine <i>Mxipl</i>	CTGGGGACCTAAACAGGAGC	GAAGCCACCTATAGCTCCC	0.5	60	yes
Murine <i>Nos2</i>	CTTCTGGACATTACGACCC	TACTCTGAGGGCTGACACAA	0.5	60	yes
Murine <i>Ppara</i>	CCTTCCCTGTGAACCTGACG	CCACAGAGCGCTAAGCTGT	0.5	60	yes
Murine <i>Srebf1</i>	GGCTCTGGAACAGACACTGG	GGCCCGGGAAGTCACTGT	0.5	61	yes
Murine <i>Tnf</i>	CCATTCTGAGTTCTGCAAAGG	AGGTAGGAAGGCTGAGATCTTATC	0.5	60	yes
Mu <i>Rn18s</i> / Hu <i>RN18S5</i>	AGGCTGTGATGCCCTTAGA	GAATGGGGTTCAACGGGTTA	0.5	61	yes

5.8 mRNA sequencing

For comprehensive transcriptome analysis of AMs/TAMs as well as “TAM-like model” cells, high throughput sequencing of cDNA using new generation sequencing (NGS) was performed. Libraries were prepared from 250 ng total RNA for “TAM-like model” and 500 ng for AM and TAM samples with an input of RNA integrity (RIN) > 9 according to Agilent2100 Bioanalyzer and Agilent RNA 6000 Pico Kit (# 5067-1513, Agilent Technologies, Santa Clara, USA). To gain pure mRNA, poly-A enrichment was performed on the input total RNA using the NEB Next Poly(A) mRNA Magnetic Isolation Module (NEB # E7490, New England Biolabs, Ipswich, USA) according to the manufacturer’s instructions. The cDNA library preparation was conducted with the NEBNext® Ultra™ Directional RNA Library Prep Kit for Illumina® (# E7420, New England Biolabs) as described in the instruction manual. In brief, first- and second-strand cDNA synthesis and chemical fragmentation were performed, followed by adapter ligation and PCR amplification of the final library (10 PCR cycles for AMs/TAMs and 12 cycles for TAM-like model samples). PCR cleanup was performed using Agencourt AMPure® XP beads (# A63881, Beckmann Coulter, Krefeld, Germany).

RNA libraries were **sequenced by Dr. Gilles Gasparoni** for 2×55 bp on an Illumina HiSeq2500 Sequencer using a V3 paired-end flow cell.

The obtained raw data were **processed by Dr. Karl Nordström**. Raw reads were subjected to quality control (QC) through FastQC version 0.11.2. Library adaptor removal and trimming was done using CutAdapt v.1.4.1 and TrimGalore! version 0.3.3, respectively. Trimmed reads were mapped with STAR v2.4.0f1 to the human reference genome (hs37d5).

Gene expression was **quantified by Natalie Wirth** using the Salmon software (Patro *et al.*, 2017) using Ensembl gene annotation (v88). Salmon computes TPM and read counts for each gene for each RNA-sequencing sample considering transcript annotation and modeling of RNA-Seq biases along transcripts. For computation of PCA plots gene expression values between samples have been normalized using the RUV approach (Risso *et al.*, 2014). All analyses have been conducted in the R programming language.

Raw TPM data are available in the appendix.

5.9 Determination of protein concentration

Total protein concentrations for ECV suspensions and cell lysates were determined by Pierce BCA protein assay kit (Thermo Fisher Scientific, Dreieich, Germany) using a GloMax[®] Discover Multimode Microplate Reader (Promega, Mannheim, Germany) according to the manufacturer's instructions.

5.10 Western Blot

Preparation of samples:

HepG2 lysates as well as murine liver tissue lysates were prepared in lysis buffer as described previously (Laggai et al. 2014; Hoppstädter et al. 2012). Samples were sonicated, centrifuged at 10,000 x g for 10 min at 4°C, and stored at -80°C until further use.

Cell culture supernatants were centrifuged for 25 min at 10,000 x g, to remove cell debris, and then supplemented with a 7 x protease inhibitor mixture (Complete[®], Roche Diagnostics, Basel, Switzerland). They were further concentrated 10 x by centrifugation at 15,000 x g for 8 min in Vivaspin[®]500 tubes with 10 kDa cut off (# VS0102, 10,000 MWCO, Sartorius, Göttingen, Germany). Concentrated supernatants as well as isolated ECVs were further diluted with a 4 x loading buffer (Roti[®]-load 1 for reducing and Roti[®]-load 2 for non-reducing conditions, # K929.1/# K930.1, Carl Roth, Karlsruhe, Germany). Before gel electrophoresis, all samples were denatured at 95°C for 5 min and subsequently kept on ice before gel loading.

Lysis buffer: 50 mM Tris-HCl, 1% SDS, 10% glycerol, 5% β-mercaptoethanol, 0.004% bromophenol blue. Buffer was supplemented with a 7 x protease inhibitor mixture (Complete[®], Roche Diagnostics, Basel, Switzerland) according to the manufacturer's instructions prior to use.

SDS-PAGE and immunodetection procedure:

SDS-polyacrylamide gel electrophoresis (PAGE) was carried out using polyacrylamide gels (4% stacking gel and 12% resolving gel) and the Mini-PROTEAN[®] system (Bio-Rad Laboratories, München, Germany). To estimate the molecular mass, a prestained protein ladder was used (# 26616, Thermo Fisher Scientific, Waltham, USA). Samples were transferred onto an Immobilon FL-PVDF membrane (# IPFL00010, Millipore-Merck, Darmstadt, Germany) using a Mini Trans-Blot[®]Cell (Bio-Rad). To saturate unspecific binding sites, the membrane was blocked for 2 - 4 h at room temperature in blocking buffer for near infrared fluorescent Western blotting (# MB-070, Rockland Immunochemicals, Pottstown, USA). Then the membrane was incubated

with primary antibody at 4°C overnight or for 48 h in the case of rabbit anti-TLR2. For antibody dilutions see table 5-2. After thorough washing with PBST (PBS + 0.1% Tween-20), membrane was stained with appropriate IRDye 680 or IRDye 800 conjugated secondary antibodies diluted in blocking buffer for 2 h at room temperature. Finally, the membrane was washed again and signals were detected and quantified using an Odyssey imager and software (LI-COR Biosciences, Lincoln, USA).

Table 5-2: Antibodies used for immunodetection and dedicated dilution in Rockland blocking buffer (RBB) or 5% milk powder in PBST (MP).

antibody	dilution	order no.	company
anti-TLR2 [EPNCIR133] rabbit mAb	1:1,000 in MP	ab108998	Abcam
anti- α -Tubulin [DM 1A] mouse mAb	1:1,000 in RBB	T9026	Sigma
IRDye® 680 Conjugated Goat Anti-Rabbit IgG	1:5,000 in RBB	P/N 926-68071	Licor
IRDye® 800CW Conjugated Goat Anti-Mouse IgG	1:10,000 in RBB	P/N 926-32210	Licor

5.11 Proteomic analysis of EV

Mass spectrometry analyses of EV and related sample preparation were **performed by Sandra Plant and Dr. Claudia Fecher-Trost** at the Institute of Experimental and Clinical Pharmacology and Toxicology (Saarland University). EVs from three independent preparations were analyzed.

To reduce the sample volume, 30 μ g EV protein were precipitated by trichloroacetic acid (TCA) precipitation, with an end concentration of 20% TCA. Samples were washed thrice with acetone with 10 min centrifugation steps in between (14,000 rpm at 4°C). After a final centrifugation of 15 min in a SeedVac Plus concentrator (Savant, Thermo Fisher, Waltham, USA), samples were resuspended in 2 x Lämmli buffer (4% SDS, 20% glycerol, 120 mM Tris-HCl (pH 6.8), 0.02% bromophenol blue in Millipore water) and denatured at 95°C for 5 min. Proteins were separated on NuPAGE® 10% gels and prepared for mass spectrometry as described previously (Fecher-Trost *et al.*, 2013). Three protein bands per sample were cut out of the gel and incubated with porcine trypsin for in-gel digestion at 37°C overnight. Resulting peptides were extracted two times by shaking the gel pieces in aqueous extraction buffer (2.5% formic acid, 50% acetonitrile). Extracted peptides were concentrated via vacuum centrifugation and resuspended in 0.1% formic acid. 6 μ l of each tryptic peptide extract were analyzed by online nanoflow LC-HR-MS/MS (Ultimate 3000 RSLC nano system equipped with an Ultimate3000 RS autosampler coupled to an

LTQ Orbitrap Velos Pro, all Thermo Fisher Scientific, Dreieich, Germany) as described previously (Fecher-Trost *et al.*, 2013). Peptides were analyzed at a flow rate of 200 $\mu\text{l}/\text{min}$ with buffer A (water and 0.1% formic acid) and B (90% acetonitrile and 0.1% formic acid) using the following gradient (figure 5-3):

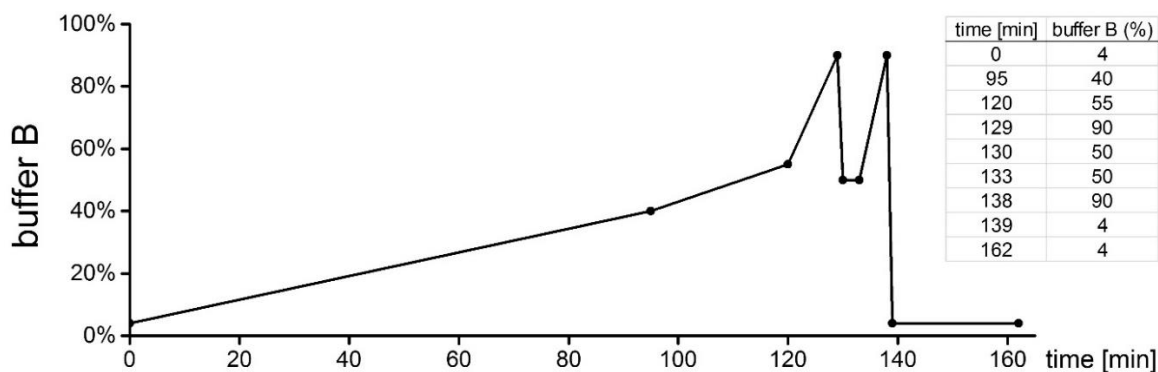


Figure 5-3: Gradient for nano-liquid chromatography with table giving the exact time points of buffer B concentration changes.

Fragmented peptides were identified using software Proteome Discoverer 1.4 (Thermo Fischer Scientific) and database SwissProt 2015_01 (species human). For further data evaluation, software Scaffold4 (version 4.8.3) was used. Raw data are accessible via the PRoteomics IDentifications (PRIDE) database (accession code assignment pending).

5.12 cryo-TEM

EV were visualized *via* cryo-transmission electron microscopy (TEM), as it allows the observation of samples in their native environment without any staining or fixation. The aqueous sample is frozen so rapidly that no ice crystals can form and the water remains in an amorphous transparent state. All cryo-TEM preparations and analyses were **performed by Dr. Marcus Koch** at the Leibniz Institute for New Materials (INM) Saarbrücken, Germany.

A 3 μl droplet of the aqueous EV solution was placed onto a holey carbon covered TEM grid (Plano, Wetzlar, Germany, type S147-4), plotted onto a thin liquid film for 2 sec and plunged into a bath of liquid ethane at -165°C using a Gatan CP3 cryoplunger (Pleasanton, CA, USA). The frozen sample was transferred under liquid nitrogen to a Gatan cryo-TEM sample holder (model 914) and investigated at -173°C by low-dose bright-field imaging Transmission Electron Microscopy (TEM, JEOL JEM-2100 LaB6, Akishima, Tokyo, Japan). A Gatan Orius SC1000 CMOS camera was used to acquire images of 1024 x 1024 pixels and 1 sec illumination time.

5.13 Flow cytometry

Flow cytometry represents a laser-based analytical technology mainly used to measure fluorescence intensity when combined with fluorochrome-conjugated antibodies or fluorescent particles.

The following general buffers were used for flow cytometric analysis:

FACSwash: PBS + 2.5 % FCS + 0.05 % sodium azide

SAP: FACS wash + 0.2 % saponin + 0.05 % sodium azide

SAPblock: PBS + 20% FCS + 0.2% saponin

PA: 1% (w/v) paraformaldehyde in PBS

5.13.1 EV analysis

For analysis of EV surface proteins by flow cytometry, vesicles were coupled to the surface of 4 µm aldehyde/sulfate latex beads (# A37304, Invitrogen, Carlsbad, USA). In detail, EV (20 µg protein) or 20 µg BSA in PBS (as negative control) were bound to 20 µl latex beads for 15 min at room temperature in a final volume of 100 µl of PBS. Volume was filled up to 500 µl PBS, followed by gentle shaking for 1 h. The reaction was stopped by adding 500 µl of glycine (to a final concentration of 100 mM glycine) for 30 min at room temperature to saturate any remaining free binding sites on the beads. EV- or BSA-coupled beads were washed three times with EVwash (PBS + 1% BSA), with centrifugation steps at 2,000 x g for 3 min in between. They were then stained with the TLR2 ligand Pam3CSK4 or as co-staining with antibodies directed against TLR2 together with the EV marker CD9 or CD63 on ice in the dark (table 5-3). After 30 min, samples were washed twice and analyzed on a BD LRS Fortessa (BD Biosciences, Franklin Lakes, USA) using BD FACSDiva 8.0. For graphical illustrations BD FACSuite (version 1.0) software was used.

Table 5-3: Antibodies and ligands used for EV flow cytometry.

antibody / ligand	amount per sample	order no.	supplier
FITC anti-human CD9, Mouse IgG1, kappa [HI9a 25]	0.5 µg	BLD-312103	Biozol
FITC anti-human CD63, Mouse IgG1, [H5C6]	1 µg	BLD-353005	Biozol
FITC Mouse IgG1, kappa Isotype Ctrl (FC) [MOPC-21]	1 µg	BLD-400109	Biozol
APC anti-human TLR2 (CD282) Mouse IgG2a [TL2.1]	2 µg	17-9922-41	Thermofisher
APC Mouse IgG2a kappa Isotype Control [eBM2a]	2 µg	17-4724-81	Thermofisher
Rhodamin-conjugatet Pam3CSK4	0.5 µg	tlrl-rpms	Invivogen

5.13.2 Nanoparticle uptake

For nanoparticle uptake analysis in AMs and TAMs, 0.5×10^6 cells/well were seeded into a 12-well plate. On the next day, cells were incubated for 1 h with fluorescent 25 nm silica nanoparticles (50 $\mu\text{g/ml}$). Particles are further described in Hoppstädter et al. (2015). Afterwards, macrophages were washed two times with PBS and detached from plates using PBS containing 5 mM EDTA. Cells were resuspended in FACSwash and examined on a FACSCalibur (BD Biosciences). Results were analyzed using FlowJo software and are presented as relative GMFI (geometric mean fluorescence intensity of particle-loaded cells related to geometric mean fluorescence intensity of untreated controls).

5.13.3 Expression of intracellular marker CD68

To detect intracellular CD68 in AMs and TAMs, the washed cells were fixed for 10 min in PA. After permeabilization in SAP for 10 min, unspecific binding sites were blocked with SAPblock for 30 min on ice. Cells were washed with FACSwash and then stained with anti-CD68 or the appropriate isotype control in SAP for 10 min at room temperature in the dark. After a final washing step, cells were resuspended in PA and immediately analyzed on a BD FACSCalibur (BD Biosciences, Franklin Lakes, USA). Results were evaluated as described for nanoparticle uptake (6.13.2).

Antibody: PE-labelled mouse anti-human CD68 [Y1/82A] (# 130-099-685, Miltenyi)

Isotype control: PE-labelled mouse anti-IgG2b (# 130-098-875, Miltenyi)

5.14 EV uptake experiments

5.14.1 EV uptake by primary HUVECs

EVs (5×10^9 in total) were pre-incubated with the TLR2 ligand Pam (1 $\mu\text{g/ml}$) for 30 min at 37°C in 250 μl of HUVEC medium. The EV-Pam mix was then used as treatment for HUVECs for a duration of 4 h. Alternatively, HUVECs were incubated with EV (5×10^9 in total) for 3 h prior to washing with PBS and 4 h treatment with Pam (1 $\mu\text{g/ml}$). Subsequently, cells were harvested for RNA isolation and Pam-induced gene expression was determined by qRT-PCR

5.14.2 EV uptake by HEK-Dual reporter cells

HEK-Dual™ hTLR2 reporter cells express TLR2, and a secretable luciferase reporter gene (Lucia luciferase) placed under the control of the endogenous IL-8 promoter.

Cells were seeded into 96-well plates (5×10^5 cells/well) and immediately treated with Pam3 only (1 ng/mL) or co-treated with Pam3 in the same concentration and the specified vesicles (5×10^9 EVs/ml) to monitor TLR2-dependent activation. The Pam3/vesicle mix was preincubated for 30 min at 37°C before it was added to the cells. After 24 h, supernatants were collected, and the activity of Lucia luciferase was determined using the QuantiLuc reagent (Invivogen, #rep-qlc1) according to the supplier's instructions and a GloMax® Discover Multimode Microplate Reader (Promega, Mannheim, Germany)

5.15 Lipid analysis

5.15.1 Lipidomic analysis in human tissue samples

To obtain a lipidomic profile of lung adenocarcinoma samples, 22 normal lung tissues and 29 tumor tissues from patients undergoing lung resection were analyzed and compared. The Patient data can be taken from the following table:

Gender	Age (years)	Tumor stage	Tissue	
			Lung	Tumor
female	57	T2aN0	x	x
male	54	T2bN1	x	x
male	64	T2aN1	x	x
female	85	T3N0	x	x
female	71	T3N0	x	x
female	74	T3N0	x	x
female	74	T2aN0	x	x
male	66	T4N1	x	x
male	73	T1aN0	x	x
female	65	T2aN2	x	x
male	69	T3N1	x	x
male	70	T2aN1	x	x
male	73	T3N1	x	x
male	64	T2aN2	x	x
female	75	T1aN0	x	x
female	53	T2bN2	x	x
female	76	pT2apN0	x	x
female	42	T3N0	x	x
male	68	T2bN0	x	x
male	63	T3N2	x	x
male	46	T3N2	x	x
male	71	T2aN0	x	x
female	66	T4N2	-	x
male	70	T2aN0	-	x
female	61	T2aN0	-	x
male	73	T4N0	-	x
female	62	T1bN0	-	x
female	77	T3N0	-	x
male	78	T2bN1	-	x

25 – 30 mg tissue was mixed with a 1:1 mixture of water and methanol (20 µl/mg tissue) in 2 ml tubes filled with 2.8 mm ceramic beads (Precellys Ceramic Kit 2.8 mm, # 10479394, Peqlab Biotechnologie, Erlangen, Germany). The samples were homogenized using a Precelly 24 (Peqlab) with the following program: 4 x 30 sec at 6000 rpm with 45 sec break in between. The further lipidomic analysis was **performed by Dr. Gerhard Liebisch** at Institute for Clinical Chemistry and Laboratory Medicine, University of Regensburg. In brief, lipid quantification of tissue homogenates was performed using electrospray-ionisation mass spectrometry with a hybrid quadrupole-orbitrap QExactive mass spectrometer (Thermo Fisher Scientific, Dreieich, Germany) and selected reaction monitoring (SRM). Detailed methods for phosphatidylethanolamine (PE), PE-based plasmalogens (PE P), phosphatidylcholine (PC), lyso-PC (LPC), PC ether (PC O), phosphatidylserine (PS), phosphatidylglycerol (PG) and phosphatidylinositol (PI), ceramide (Cer), hexosylceramide (HexCer) and sphingomyelin (SM) are described in Siguener et al. (2017).

For LPC ether (LPC O), PE ether (PE O), diacylglycerol (DG), triacylglycerol (TG), cholesteryl ester (CE) and free cholesterol (FC) Fourier Transform Mass Spectrometry (FTMS) was used.

5.15.2 Quantification of total lipids (SPV assay) and distinct lipid classes (TLC) in murine liver samples

Freeze-dried liver tissues were dispersed in hexane/2-propanol [3:2 (v/v)]. After centrifugation for 10 min at 4°C and 10,000 x g, the supernatant was dried under a nitrogen stream, and the samples were re-dissolved in chloroform/methanol [2:1 (v/v)]. Total lipid content was analyzed by the colorimetric sulfo-phospho-vanillin (SPV) assay according to Kessler et al. (2016). Distinct lipid classes were detected by thin layer chromatography (TLC) (**performed by Dr. Stephan Laggai**) as described previously (Laggai *et al.*, 2013; Kessler *et al.*, 2016). Signal intensities were quantified using ImageJ software.

5.16 Caspase-3-like activity assay

After treatment THP-1 or AM cells were washed with PBS, lysed with 300 µl ice-cold lysis buffer per million cells (25 mM HEPES, 5 M MgCl₂, 1 M EGTA, 0.1% Triton X-100) and stored at -80°C. After thawing on ice, cells were scratched off the culture plates, collected by centrifugation (14,000 rpm, 10 min, 4°C) and 10 µl of the supernatants (triplicates) were transferred to a black, flat-bottom 96well microtiter plate. Then, 90 µl substrate buffer (50 mM HEPES, 4 mM

DTT, 0.1% CHAPS, 1% sucrose, pH 7.5) were added per well, containing the Caspase-3 substrate Ac-DEVD-AFC (#ALX-260-032, Enzo Life Sciences, Lörrach, Germany). Generation of free AFC at 37°C was measured after 2 h by fluorescence measurement (excitation: 405 nm; emission filter: 495-505 nm) using a GloMax[®] Discover Multimode Microplate Reader (Promega, Mannheim, Germany). Caspase activity was normalized to total protein content per sample.

5.17 Histology

Immunohistochemical F4/80 staining was performed as previously reported (Kessler et al., 2014; Laggai et al., 2014). In brief, F4/80 was detected using the Vectastain Peroxidase Elite ABC kit/DAB with anti-F4/80 antibodies (MCA497G, AbD Serotec) 1:1,000 overnight at 4°C. Epitopes were demasked with 10 mM citrate buffer pH 6.0 for 10 min in a water bath at 95 °C. Images were captured using an Axio Star plus microscope coupled to an Axio Cam ICc 1 camera (Zeiss, Oberkochen, Germany). Histology was **performed by Dr. Yvette Simon.**

5.18 Enzyme-linked immunosorbent assay (ELISA)

The serum concentrations of TNF- α and IL-6 were determined by ELISA (#MTA00 and #M6000B, Cayman Chemicals, Ann Arbor, USA) as recommended by the supplier. ELISAs were **performed by Dr. Jessica Hoppstädter.**

5.19 TNF bioassay

This bioassay is based on quantification of cytotoxic TNF- α activity on L929 cells in the presence of actinomycin D and was **performed by Dr. Jessica Hoppstädter** as described previously (Kierner, Müller and Vollmar, 2002; Diesel *et al.*, 2013).

5.20 Statistics

Data are shown as means + SEM or box plots (with or without single values) with 25th/75th percentile boxes, geometric medians (line), means (square), and 10th/90th percentile as whiskers. P-Values were determined by ANOVA with post-hoc Tukey test for normally distributed data or Mann-Whitney U test or t-test where applicable. The applied test is each indicated in the figure legend. Outliers were determined using the Grubbs' test. The OriginPro 2015G software (OriginLab Corporation) was used for illustration and statistical analyses.

6. References

- Ackermann, M. *et al.* (2001) ‘Cytokine synthesis in the liver of endotoxin-tolerant and normal rats during hemorrhagic shock.’, *Journal of endotoxin research*, 7(2), pp. 105–12. doi: 10.1177/09680519010070020401.
- Adams, L. A. *et al.* (2009) ‘NAFLD as a risk factor for the development of diabetes and the metabolic syndrome: An eleven-year follow-up study’, *American Journal of Gastroenterology*, 104(4), pp. 861–867. doi: 10.1038/ajg.2009.67.
- Adams, L. A., Angulo, P. and Lindor, K. D. (2005) ‘NonAlcoholic Fatty Liver Disease’, *CMAJ*, 172(7), pp. 899–905. doi: 10.1503/cmaj.045232.
- Ahmad, A. and Gadgeel, S. M. (eds) (2016) *Lung Cancer and Personalized Medicine: Novel Therapies and Clinical Management*. Cham: Springer International Publishing (Advances in Experimental Medicine and Biology). doi: 10.1007/978-3-319-24932-2.
- Almatroodi, S. A. *et al.* (2016) ‘Characterization of M1/M2 Tumour-Associated Macrophages (TAMs) and Th1/Th2 Cytokine Profiles in Patients with NSCLC’, *Cancer Microenvironment*, 9(1). doi: 10.1007/s12307-015-0174-x.
- Almatroodi, S. A., McDonald, C. F. and Pouniotis, D. S. (2014) ‘Alveolar Macrophage Polarisation in Lung Cancer’, *Lung Cancer International*, 2014, pp. 1–9. doi: 10.1155/2014/721087.
- de Alwis, N. M. W. and Day, C. P. (2008) ‘Non-alcoholic fatty liver disease: The mist gradually clears’, *Journal of Hepatology*, 48(SUPPL. 1), pp. 104–112. doi: 10.1016/j.jhep.2008.01.009.
- Amar, J. *et al.* (2008) ‘Energy intake is associated with endotoxemia in apparently healthy men’, *American Journal of Clinical Nutrition*, 87(5), pp. 1219–1223. doi: 10.1093/ajcn/87.5.1219.
- Angulo, P. (2002) ‘Non-Alcoholic Fatty Liver Disease’, *New England Journal of Medicine*, 346(16), pp. 1221–1231. doi: 10.1055/s-0041-102787.
- Araujo, J. M. *et al.* (2016) ‘Repeated observation of immune gene sets enrichment in women with non-small cell lung cancer’, *Oncotarget*, 7(15). doi: 10.18632/oncotarget.7943.
- Arora, A. S. *et al.* (1997) ‘Ceramide induces hepatocyte cell death through disruption of mitochondrial function in the rat’, *Hepatology*, 25(4), pp. 958–963. doi: 10.1002/hep.510250428.
- Arora, H. *et al.* (2019) ‘The ATP-Binding Cassette Gene ABCF1 Functions as an E2 Ubiquitin-Conjugating Enzyme Controlling Macrophage Polarization to Dampen Lethal Septic Shock’, *Immunity*. Elsevier Inc., 50(2), p. 418–431.e6. doi: 10.1016/j.immuni.2019.01.014.
- Ascha, M. S. *et al.* (2010) ‘The incidence and risk factors of hepatocellular carcinoma in patients with nonalcoholic steatohepatitis’, *Hepatology*, 51(6), pp. 1972–1978. doi: 10.1002/hep.23527.

- Atri, C., Guerfali, F. Z. and Laouini, D. (2018) 'Role of human macrophage polarization in inflammation during infectious diseases', *International Journal of Molecular Sciences*, 19(6). doi: 10.3390/ijms19061801.
- Baenke, F. *et al.* (2013) 'Hooked on fat: the role of lipid synthesis in cancer metabolism and tumour development', *Disease Models & Mechanisms*, 6(6), pp. 1353–1363. doi: 10.1242/dmm.011338.
- Bastard, J. P. *et al.* (2000) 'Elevated levels of interleukin 6 are reduced in serum and subcutaneous adipose tissue of obese women after weight loss', *Journal of Clinical Endocrinology and Metabolism*, 85(9), pp. 3338–3342. doi: 10.1210/jc.85.9.3338.
- Bellentani, S. *et al.* (2010) 'Epidemiology of non-alcoholic fatty liver disease.', *Digestive Diseases*, 28(1), pp. 155–61. doi: 10.1159/000282080.
- Bender, E. (2014) 'Epidemiology: The dominant malignancy', *Nature*, 513(7517), pp. S2–S3. doi: 10.1038/513S2a.
- van Bergenhenegouwen, J. *et al.* (2013) 'TLR2 & Co: a critical analysis of the complex interactions between TLR2 and coreceptors', *Journal of Leukocyte Biology*, 94(5), pp. 885–902. doi: 10.1189/jlb.0113003.
- Biedroń, R., Peruń, A. and Józefowski, S. (2016) 'CD36 differently regulates macrophage responses to smooth and rough lipopolysaccharide', *PLoS ONE*, 11(4), pp. 2012–2017. doi: 10.1371/journal.pone.0153558.
- Biswas, S. K. *et al.* (2012) 'Macrophage polarization and plasticity in health and disease', *Immunologic Research*, 53(1–3), pp. 11–24. doi: 10.1007/s12026-012-8291-9.
- Biswas, S. K. and Lopez-Collazo, E. (2009) 'Endotoxin tolerance: new mechanisms, molecules and clinical significance', *Trends in Immunology*, 30(10), pp. 475–487. doi: 10.1016/j.it.2009.07.009.
- Biswas, S. K. and Mantovani, A. (2012) 'Orchestration of metabolism by macrophages', *Cell Metabolism*. Elsevier Inc., 15(4), pp. 432–437. doi: 10.1016/j.cmet.2011.11.013.
- Bode, C. and Bode, C. J. (2003) 'Effect of alcohol consumption on the gut', *Best Practice and Research Clinical Gastroenterology*, 17(4), pp. 575–592. doi: 10.1053/ybega.2003.392.
- Bode, C., Kugler, V. and Bode, J. C. (1987) 'Endotoxemia in patients with alcoholic and non-alcoholic cirrhosis and in subjects with no evidence of chronic liver disease following acute alcohol excess', *Journal of Hepatology*, 4(1), pp. 8–14. doi: 10.1016/S0168-8278(87)80003-X.
- Bohannon, J. K. *et al.* (2013) 'The immunobiology of toll-like receptor 4 agonists: From endotoxin tolerance to immunoadjuvants', *Shock*, 40(6), pp. 451–462. doi: 10.1097/SHK.0000000000000042.
- Bolli, E. *et al.* (2017) 'Novel insights in the regulation and function of macrophages in the tumor microenvironment', *Current Opinion in Oncology*, 29(1), pp. 55–61.

- Bouhleb, M. A. *et al.* (2007) 'PPAR γ Activation Primes Human Monocytes into Alternative M2 Macrophages with Anti-inflammatory Properties', *Cell Metabolism*, 6(2), pp. 137–143. doi: 10.1016/j.cmet.2007.06.010.
- Brass, E. P. and Vetter, W. H. (1994) 'Interleukin-6, but not tumour necrosis factor-alpha, increases lipogenesis in rat hepatocyte primary cultures.', *The Biochemical Journal*, 301 (Pt 1, pp. 193–197. doi: 10.1016/j.ijnurstu.2011.11.005.
- Brass, E. P. and Vetter, W. H. (1995) 'Stimulation of lipogenesis by interleukin-6 and misoprostol-free acid in isolated rat hepatocytes', *American Journal of Therapeutics*, 2, pp. 706–710.
- Bremnes, R. M. *et al.* (2011) 'The Role of Tumor-Infiltrating Immune Cells and Chronic Inflammation at the Tumor Site on Cancer Development , Progression , and Prognosis', *Journal of thoracic Oncology*, 6(4), pp. 824–833.
- Browning, J. D. *et al.* (2004) 'Prevalence of hepatic steatosis in an urban population in the United States: Impact of ethnicity', *Hepatology*, 40(6), pp. 1387–1395. doi: 10.1002/hep.20466.
- Burg, V. Der, Heusinkveld, M. and Burg, S. H. Van Der (2011) 'Identification and manipulation of tumor associated macrophages in human cancers Identification and manipulation of tumor associated macrophages in human cancers', *Journal of Translational Medicine*, 216(December 2011).
- Busillo, J. M. and Cidlowski, J. A. (2013) 'The five Rs of glucocorticoid action during inflammation: Ready, reinforce, repress, resolve, and restore', *Trends in Endocrinology and Metabolism*. Elsevier Ltd, 24(3), pp. 109–119. doi: 10.1016/j.tem.2012.11.005.
- Buzás, E. I. *et al.* (2018) 'Molecular interactions at the surface of extracellular vesicles', *Seminars in Immunopathology*. *Seminars in Immunopathology*, 40(5), pp. 453–464. doi: 10.1007/s00281-018-0682-0.
- Byrne, C. D. and Targher, G. (2015) 'NAFLD: A multisystem disease', *Journal of Hepatology*. European Association for the Study of the Liver, 62(S1), pp. S47–S64. doi: 10.1016/j.jhep.2014.12.012.
- Cain, D. W. and Cidlowski, J. A. (2017) 'Immune regulation by glucocorticoids', *Nature Reviews Immunology*. Nature Publishing Group, 17(4), pp. 233–247. doi: 10.1038/nri.2017.1.
- Cao, X. (2016) 'Self-regulation and cross-regulation of pattern-recognition receptor signalling in health and disease', *Nature Reviews Immunology*. Nature Publishing Group, 16(1), pp. 35–50. doi: 10.1038/nri.2015.8.
- Cavaillon, J. and Adib-Conquy, M. (2006) 'Bench-to-bedside review : Endotoxin tolerance as a model of leukocyte reprogramming in sepsis', 8, pp. 1–8. doi: 10.1186/cc5055.
- Cheng, T. *et al.* (2017) 'The International Epidemiology of Lung Cancer: Latest Trends, Disparities, and Tumor Characteristics', *Journal of Thoracic Oncology*, 11(10), pp. 1653–1671. doi: 10.1016/j.jtho.2016.05.021.The.

- Chew, G. S. *et al.* (2014) 'Interleukin-6 inhibition of peroxisome proliferator-activated receptor alpha expression is mediated by JAK2- and PI3K-induced STAT1/3 in HepG2 hepatocyte cells', *Molecular and Cellular Biochemistry*, 388(1–2), pp. 25–37. doi: 10.1007/s11010-013-1896-z.
- Chinenov, Y. and Rogatsky, I. (2007) 'Glucocorticoids and the innate immune system: Crosstalk with the Toll-like receptor signaling network', *Molecular and Cellular Endocrinology*, 275(1–2), pp. 30–42. doi: 10.1016/j.mce.2007.04.014.
- Chung, F.-T. *et al.* (2012) 'Tumor-associated macrophages correlate with response to epidermal growth factor receptor-tyrosine kinase inhibitors in advanced non-small cell lung cancer', *International Journal of Cancer*, 131(3), pp. E227–E235. doi: 10.1002/ijc.27403.
- Collins, P. E. and Carmody, R. J. (2015) 'The Regulation of Endotoxin Tolerance and its Impact on Macrophage Activation', *Critical Reviews in Immunology*, 35(4), pp. 293–323. doi: 10.1615/CritRevImmunol.2015015495.
- Colombo, M., Raposo, G. and Théry, C. (2014) 'Biogenesis, Secretion, and Intercellular Interactions of Exosomes and Other Extracellular Vesicles', *Annual Review of Cell and Developmental Biology*, 30(1), pp. 255–289. doi: 10.1146/annurev-cellbio-101512-122326.
- Conway, E. M. *et al.* (2016) 'Macrophages, Inflammation, and Lung Cancer', *American Journal of Respiratory and Critical Care Medicine*, 193(2), pp. 116–130. doi: 10.1164/rccm.201508-1545CI.
- Csak, T. *et al.* (2011) 'Fatty acid and endotoxin activate inflammasomes in mouse hepatocytes that release danger signals to stimulate immune cells', *Hepatology*, 54(1), pp. 133–144. doi: 10.1002/hep.24341.
- Day, C. P. (2010) 'Genetic and environmental susceptibility to non-alcoholic fatty liver disease', *Digestive Diseases*, 28(1), pp. 255–260. doi: 10.1159/000282098.
- Dembek, A. *et al.* (2017) 'Hepatic interleukin-6 production is maintained during endotoxin tolerance and facilitates lipid accumulation', *Immunobiology*. Elsevier GmbH., 222(6), pp. 786–796. doi: 10.1016/j.imbio.2017.01.003.
- Diesel, B. *et al.* (2012) 'Inflammation-induced up-regulation of TLR2 expression in human endothelial cells is independent of differential methylation in the TLR2 promoter CpG island', *Innate Immunity*, 18(1), pp. 112–123. doi: 10.1177/1753425910394888.
- Diesel, B. *et al.* (2013) 'Activation of Rac1 GTPase by nanoparticulate structures in human macrophages', *European Journal of Pharmaceutics and Biopharmaceutics*. Elsevier B.V., 84(2), pp. 315–324. doi: 10.1016/j.ejpb.2012.12.015.
- DiMarco, D. and Fernandez, M. (2015) 'The Regulation of Reverse Cholesterol Transport and Cellular Cholesterol Homeostasis by MicroRNAs', *Biology*, 4(3), pp. 494–511. doi: 10.3390/biology4030494.
- Dragovic, R. A. *et al.* (2011) 'Sizing and phenotyping of cellular vesicles using Nanoparticle Tracking Analysis', *Nanomedicine: Nanotechnology, Biology, and Medicine*. Elsevier Inc., 7(6), pp. 780–788. doi: 10.1016/j.nano.2011.04.003.

- Dulay, A. T. *et al.* (2009) 'Soluble TLR2 Is Present in Human Amniotic Fluid and Modulates the Intraamniotic Inflammatory Response to Infection', *The Journal of Immunology*, 182(11), pp. 7244–7253. doi: 10.4049/jimmunol.0803517.
- Durak-Kozica, M. *et al.* (2018) '3D visualization of extracellular vesicle uptake by endothelial cells', *Cellular and Molecular Biology Letters*, 23(1), pp. 1–9. doi: 10.1186/s11658-018-0123-z.
- Edin, S. *et al.* (2013) 'Phenotypic Skewing of Macrophages In Vitro by Secreted Factors from Colorectal Cancer Cells', *PLoS ONE*, 8(9). doi: 10.1371/journal.pone.0074982.
- Eggers, L. F. *et al.* (2017) 'Lipidomes of lung cancer and tumour-free lung tissues reveal distinct molecular signatures for cancer differentiation, age, inflammation, and pulmonary emphysema', *Scientific Reports*, 7(1), pp. 1–13. doi: 10.1038/s41598-017-11339-1.
- Enomoto, N. *et al.* (1998) 'Alcohol causes both tolerance and sensitization of rat Kupffer cells via mechanisms dependent on endotoxin', *Gastroenterology*, 115(2), pp. 443–451. doi: 10.1016/S0016-5085(98)70211-2.
- Epelman, S., Lavine, K. J. and Randolph, G. J. (2014) 'Origin and Functions of Tissue Macrophages', *Immuni*, 41(1), pp. 21–35. doi: 10.1016/j.immuni.2014.06.013.Origin.
- Erdbrügger, U. *et al.* (2014) 'Imaging flow cytometry elucidates limitations of microparticle analysis by conventional flow cytometry', *Cytometry Part A*, 85(9), pp. 756–770. doi: 10.1002/cyto.a.22494.
- Fabbrini, E., Sullivan, S. and Klein, S. (2010) 'Obesity and nonalcoholic fatty liver disease: Biochemical, metabolic, and clinical implications', *Hepatology*, 51(2), pp. 679–689. doi: 10.1002/hep.23280.
- Fan, J. *et al.* (2006) 'Hemorrhagic shock-activated neutrophils augment TLR4 signaling-induced TLR2 upregulation in alveolar macrophages: role in hemorrhage-primed lung inflammation.', *American journal of physiology. Lung cellular and molecular physiology*, 290(4), pp. L738–L746. doi: 10.1152/ajplung.00280.2005.
- Fan, J., Randall, S. and Asrar, M. (2003) 'TLR4 signaling induces TLR2 expression in endothelial cells via neutrophil NADPH oxidase', *Journal of Clinical Investigation*, 112(8), pp. 1234–1243. doi: 10.1172/JCI200318696.Introduction.
- Fecher-Trost, C. *et al.* (2013) 'The in vivo TRPV6 protein starts at a non-AUG triplet, decoded as methionine, upstream of canonical initiation at AUG', *Journal of Biological Chemistry*, 288(23), pp. 16629–16644. doi: 10.1074/jbc.M113.469726.
- Fisher, J. E. *et al.* (2013) 'Role of Kupffer cells and toll-like receptor 4 in acetaminophen-induced acute liver failure', *Journal of Surgical Research*. Elsevier Ltd, 180(1), pp. 147–155. doi: 10.1016/j.jss.2012.11.051.
- Flohé, S. *et al.* (1999) 'Endotoxin tolerance in rats: expression of TNF-alpha, IL-6, IL-10, VCAM-1 AND HSP 70 in lung and liver during endotoxin shock', *Cytokine*, 11(10), pp. 796–804. doi: 10.1006/cyto.1998.0490.

- Foey, A. D. (2012) 'Mucosal Macrophages: Phenotype and Functionality in Homeostasis and Pathology', *Handbook of Macrophages: Life Cycle, Functions and Diseases*, (March 2012), pp. 121–146.
- Franklin, R. A. and Li, M. O. (2016) 'Ontogeny of Tumor-Associated Macrophages and Its Implication in Cancer Regulation', *Trends in Cancer*. Elsevier Inc., 2(1), pp. 20–34. doi: 10.1016/j.trecan.2015.11.004.
- Fraternale, A., Brundu, S. and Magnani, M. (2015) 'Polarization and Repolarization of Macrophages', *Journal of Clinical and Cellular Immunology*, 06(02), pp. 1–10. doi: 10.4172/2155-9899.1000319.
- Fuhrmann, G. *et al.* (2015) 'Active loading into extracellular vesicles significantly improves the cellular uptake and photodynamic effect of porphyrins', *Journal of Controlled Release*. Elsevier B.V., 205, pp. 35–44. doi: 10.1016/j.jconrel.2014.11.029.
- Fuhrmann, G., Herrmann, I. K. and Stevens, M. M. (2015) 'Cell-derived vesicles for drug therapy and diagnostics: Opportunities and challenges', *Nano Today*. Elsevier Ltd, 10(3), pp. 397–409. doi: 10.1016/j.nantod.2015.04.004.
- Ganz, M. and Szabo, G. (2013) 'Immune and inflammatory pathways in NASH', *Hepatology International*, 7(2013), pp. S771–S781. doi: 10.1007/s12072-013-9468-6.
- Gautier, E. L. *et al.* (2012) 'Gene-expression profiles and transcriptional regulatory pathways that underlie the identity and diversity of mouse tissue macrophages', *Nature Immunology*, 13(11), pp. 1118–1128. doi: 10.1038/ni.2419.
- Geeraerts, X. *et al.* (2017) 'Macrophage metabolism as therapeutic target for cancer, atherosclerosis, and obesity', *Frontiers in Immunology*, 8(March). doi: 10.3389/fimmu.2017.00289.
- Gentles, A. J. *et al.* (2015) 'The prognostic landscape of genes and infiltrating immune cells across human cancers', *Nature Medicine*. Nature Publishing Group, 21(8), pp. 938–945. doi: 10.1038/nm.3909.
- Gierens, H. *et al.* (2000) 'Interleukin-6 Stimulates LDL Receptor Gene Expression via Activation of Sterol-Responsive and Sp1 Binding Elements', *Arteriosclerosis, Thrombosis, and Vascular Biology*, 20, pp. 1777–83.
- Ginhoux, F. *et al.* (2016) 'New insights into the multidimensional concept of macrophage ontogeny, activation and function', *Nature Immunology*, 17(1), pp. 34–40. doi: 10.1038/ni.3324.
- Ginhoux, F. and Guilliams, M. (2016) 'Tissue-Resident Macrophage Ontogeny and Homeostasis', *Immunity*. Elsevier Inc., 44(3), pp. 439–449. doi: 10.1016/j.immuni.2016.02.024.
- Glund, S. and Krook, A. (2008) 'Role of interleukin-6 signalling in glucose and lipid metabolism', *Acta Physiologica*, 192(1), pp. 37–48. doi: 10.1111/j.1748-1716.2007.01779.x.

- Goldstraw, P. *et al.* (2016) ‘The IASLC Lung Cancer Staging Project: Proposals for Revision of the TNM Stage Groupings in the Forthcoming (Eighth) Edition of the TNM Classification for Lung Cancer’, *Journal of Thoracic Oncology*, 11(1), pp. 39–51. doi: 10.1016/j.jtho.2015.09.009.
- Gordon, S. and Plüddemann, A. (2017) ‘Tissue macrophages: Heterogeneity and functions’, *BMC Biology*. BMC Biology, pp. 1–18. doi: 10.1186/s12915-017-0392-4.
- Gordon, S., Plüddemann, A. and Martinez Estrada, F. (2014) ‘Macrophage heterogeneity in tissues: Phenotypic diversity and functions’, *Immunological Reviews*, 262(1), pp. 36–55. doi: 10.1111/imr.12223.
- Guilliams, M. *et al.* (2013) ‘Alveolar macrophages develop from fetal monocytes that differentiate into long-lived cells in the first week of life via GM-CSF’, *The Journal of Experimental Medicine*, 210(10), pp. 1977–1992. doi: 10.1084/jem.20131199.
- Guo, C. *et al.* (2018) ‘Cholesterol Homeostatic Regulator SCAP-SREBP2 Integrates NLRP3 Inflammasome Activation and Cholesterol Biosynthetic Signaling in Macrophages’, *Immunity*. Elsevier Inc., 49(5), p. 842–856.e7. doi: 10.1016/j.immuni.2018.08.021.
- Hafenrichter, D. G. *et al.* (1994) ‘The Kupffer cell in endotoxin tolerance: mechanisms of protection against lethal endotoxemia’, *Shock*, 2(4), pp. 251–256.
- Hanahan, D. and Weinberg, R. A. (2011) ‘Review Hallmarks of Cancer : The Next Generation’, *Cell*. Elsevier Inc., 144(5), pp. 646–674. doi: 10.1016/j.cell.2011.02.013.
- Hanayama, R. *et al.* (2002) ‘Identification of a factor that links apoptotic cells to phagocytes’, *Nature*, 417(6885), pp. 182–187. doi: 10.1038/417182a.
- Hashimoto, D. *et al.* (2013) ‘Tissue-resident macrophages self-maintain locally throughout adult life with minimal contribution from circulating monocytes’, *Immunity*, 38(4), pp. 792–804. doi: 10.1016/j.immuni.2013.04.004.
- He, Y., Lawlor, N. T. and Newburg, D. S. (2016) ‘Human Milk Components Modulate Toll-Like Receptor-Mediated Inflammation’, *Adv Nutr*, 7, pp. 102–11. doi: 10.3945/an.115.010090.communities.
- Henrick, B. M. *et al.* (2012) ‘Milk matters: Soluble toll-like receptor 2 (sTLR2) in breast milk significantly inhibits HIV-1 infection and inflammation’, *PLoS ONE*, 7(7). doi: 10.1371/journal.pone.0040138.
- Henrick, B. M. *et al.* (2016) ‘Insights into soluble Toll-like receptor 2 as a downregulator of virally induced inflammation’, *Frontiers in Immunology*, 7(AUG). doi: 10.3389/fimmu.2016.00291.
- Hermoso, M. A. *et al.* (2004) ‘Glucocorticoids and Tumor Necrosis Factor Alpha Cooperatively Regulate Toll-Like Receptor 2 Gene Expression’, *Molecular and Cellular Biology*, 24(11), pp. 4743–4756. doi: 10.1128/mcb.24.11.4743-4756.2004.
- Homma, T. *et al.* (2004) ‘Corticosteroid and Cytokines Synergistically Enhance Toll-Like Receptor 2 Expression in Respiratory Epithelial Cells’, *American Journal of Respiratory Cell and Molecular Biology*, 31(4), pp. 463–469. doi: 10.1165/rcmb.2004-0161OC.

- Hoppstädter, J. *et al.* (2010) ‘Differential cell reaction upon Toll-like receptor 4 and 9 activation in human alveolar and lung interstitial macrophages’, *Respiratory Research*, 11, pp. 1–15. doi: 10.1186/1465-9921-11-124.
- Hoppstädter, J. *et al.* (2012) ‘Glucocorticoid-induced leucine zipper is downregulated in human alveolar macrophages upon Toll-like receptor activation’, *European Journal of Immunology*, 42(5), pp. 1282–1293. doi: 10.1002/eji.201142081.
- Hoppstädter, J., Kessler, S. M., *et al.* (2015) ‘Glucocorticoid-Induced Leucine Zipper: A Critical Factor in Macrophage Endotoxin Tolerance’, *The Journal of Immunology*, 194(12), pp. 6057–6067. doi: 10.4049/jimmunol.1403207.
- Hoppstädter, J., Seif, M., *et al.* (2015) ‘M2 polarization enhances silica nanoparticle uptake by macrophages’, *Frontiers in Pharmacology*, 6(MAR), pp. 1–12. doi: 10.3389/fphar.2015.00055.
- Hoppstädter, J. and Kiemer, A. K. (2015) ‘Glucocorticoid-induced leucine zipper (GILZ) in immuno suppression: master regulator or bystander?’, *Oncotarget*, 6(36), pp. 38446–38457. doi: 10.18632/oncotarget.6197.
- Hotamisligil, G. S. (2006) ‘Inflammation and metabolic disorders’, *Nature*, 444(December), pp. 860–867. doi: 10.1038/nature05485.
- Hotchkiss, R. S., Monneret, G. and Payen, D. (2013) ‘Sepsis-induced immunosuppression: From cellular dysfunctions to immunotherapy’, *Nature Reviews Immunology*. Nature Publishing Group, 13(12), pp. 862–874. doi: 10.1038/nri3552.
- Huber, M. *et al.* (2006) ‘R-form LPS, the master key to the activation of TLR4/MD-2-positive cells’, *European Journal of Immunology*, 36(3), pp. 701–711. doi: 10.1002/eji.200535593.
- Hume, D. A., Irvine, K. M. and Pridans, C. (2018) ‘The Mononuclear Phagocyte System: The Relationship between Monocytes and Macrophages’, *Trends in Immunology*. Elsevier Ltd, 0(0), pp. 1–15. doi: 10.1016/j.it.2018.11.007.
- Hussell, T. and Bell, T. J. (2014) ‘Alveolar macrophages: Plasticity in a tissue-specific context’, *Nature Reviews Immunology*. Nature Publishing Group, 14(2), pp. 81–93. doi: 10.1038/nri3600.
- Italiani, P. *et al.* (2014) ‘Transcriptomic profiling of the development of the inflammatory response in human monocytes in vitro e87680’, *PLoS ONE*, 9(2). doi: 10.1371/journal.pone.0087680.
- Italiani, P. and Boraschi, D. (2014) ‘From monocytes to M1/M2 macrophages: Phenotypical vs. functional differentiation’, *Frontiers in Immunology*, 5(OCT), pp. 1–22. doi: 10.3389/fimmu.2014.00514.
- Jackaman, C. *et al.* (2017) ‘Aging and cancer: The role of macrophages and neutrophils’, *Ageing Research Reviews*. Elsevier B.V., 36, pp. 105–116. doi: 10.1016/j.arr.2017.03.008.
- Jansen, F. *et al.* (2017) ‘Endothelial- and Immune Cell-Derived Extracellular Vesicles in the Regulation of Cardiovascular Health and Disease’, *JACC: Basic to Translational Science*, 2(6), pp. 790–807. doi: 10.1016/j.jacbts.2017.08.004.

- Joshi, N., Walter, J. M. and Misharin, A. V. (2018) 'Alveolar Macrophages', *Cellular Immunology*. Elsevier, 330(December 2017), pp. 86–90. doi: 10.1016/j.cellimm.2018.01.005.
- Kalra, H., Drummen, G. P. C. and Mathivanan, S. (2016) 'Focus on extracellular vesicles: Introducing the next small big thing', *International Journal of Molecular Sciences*, 17(2). doi: 10.3390/ijms17020170.
- Kawasaki, T. and Kawai, T. (2014) 'Toll-Like Receptor Signaling Pathways', *Frontiers in Immunology*, 5(5625), pp. 1524–1525. doi: 10.3389/fimmu.2014.00461.
- Kessler, S. M. *et al.* (2014) 'Fatty acid elongation in non-alcoholic steatohepatitis and hepatocellular carcinoma', *International Journal of Molecular Sciences*, 15(4), pp. 5762–5773. doi: 10.3390/ijms15045762.
- Kessler, S. M. *et al.* (2016) 'Transient hepatic overexpression of insulin-like growth factor 2 induces free cholesterol and lipid droplet formation', *Frontiers in Physiology*, 7(APR), pp. 1–11. doi: 10.3389/fphys.2016.00147.
- Kiemer, A. K., Müller, C. and Vollmar, A. M. (2002) 'Inhibition of LPS-induced nitric oxide and TNF- α production by α -lipoic acid in rat Kupffer cells and in RAW 264.7 murine macrophages', *Immunology and Cell Biology*, 80(6), pp. 550–557. doi: 10.1046/j.1440-1711.2002.01124.x.
- Kinoshita, S. *et al.* (2008) 'Role of Hepatic STAT3 in the Regulation of Lipid Metabolism', *Kobe Journal of Medical Science*, 54(4), pp. 200–208.
- Klein, C. *et al.* (2005) 'The IL-6–gp130–STAT3 pathway in hepatocytes triggers liver protection in T cell–mediated liver injury', *The Journal of Clinical Investigation*, 115(4), pp. 860–869. doi: 10.1172/JCI200523640.860.
- Kopf, M., Schneider, C. and Nobs, S. P. (2015) 'The development and function of lung-resident macrophages and dendritic cells', *Nature Immunology*, 16(1), pp. 36–44. doi: 10.1038/ni.3052.
- Kornilov, R. *et al.* (2018) 'Efficient ultrafiltration-based protocol to deplete extracellular vesicles from fetal bovine serum', *Journal of Extracellular Vesicles*. Taylor & Francis, 7(1). doi: 10.1080/20013078.2017.1422674.
- Kugelmas, M. *et al.* (2003) 'Cytokines and NASH: A pilot study of the effects of lifestyle modification and vitamin E', *Hepatology*, 38(2), pp. 413–419. doi: 10.1053/jhep.2003.50316.
- Kumadaki, S. *et al.* (2008) 'Mouse Elovl-6 promoter is an SREBP target', *Biochemical and Biophysical Research Communications*, 368(2), pp. 261–266. doi: 10.1016/j.bbrc.2008.01.075.
- Kuroishi, T. *et al.* (2007) 'Human parotid saliva contains soluble toll-like receptor (TLR) 2 and modulates TLR2-mediated interleukin-8 production by monocytic cells', *Molecular Immunology*, 44(8), pp. 1969–1976. doi: 10.1016/j.molimm.2006.09.028.

- van de Laar, L. *et al.* (2016) 'Yolk Sac Macrophages, Fetal Liver, and Adult Monocytes Can Colonize an Empty Niche and Develop into Functional Tissue-Resident Macrophages', *Immunity*. Elsevier Inc., 44(4), pp. 755–768. doi: 10.1016/j.immuni.2016.02.017.
- Laggai, S. *et al.* (2013) 'Rapid chromatographic method to decipher distinct alterations in lipid classes in NAFLD/NASH', *World Journal of Hepatology*, 5(10), pp. 558–567. doi: 10.4254/wjh.v5.i10.558.
- Laggai, S. *et al.* (2014) 'The *IGF2* mRNA binding protein p62/IGF2BP2-2 induces fatty acid elongation as a critical feature of steatosis', *Journal of Lipid Research*, 55(6), pp. 1087–1097. doi: 10.1194/jlr.M045500.
- Lahmar, Q. *et al.* (2016) 'Tissue-resident versus monocyte-derived macrophages in the tumor microenvironment', *Biochimica et Biophysica Acta - Reviews on Cancer*. Elsevier B.V., 1865(1), pp. 23–34. doi: 10.1016/j.bbcan.2015.06.009.
- Lang, R. *et al.* (2002) 'Shaping Gene Expression in Activated and Resting Primary Macrophages by IL-10', *The Journal of Immunology*, 169(5), pp. 2253–2263. doi: 10.4049/jimmunol.169.5.2253.
- Langjahr, P. *et al.* (2014) 'Metalloproteinase-dependent TLR2 ectodomain shedding is involved in soluble toll-like receptor 2 (sTLR2) production', *PLoS ONE*, 9(12), pp. 1–20. doi: 10.1371/journal.pone.0104624.
- Lavin, Y. *et al.* (2014) 'Tissue-resident macrophage enhancer landscapes are shaped by the local microenvironment', *Cell*. Elsevier Inc., 159(6), pp. 1312–1326. doi: 10.1016/j.cell.2014.11.018.
- Lavin, Y. *et al.* (2017) 'Innate Immune Landscape in Early Lung Adenocarcinoma by Paired Single-Cell Analyses', *Cell*. Elsevier Inc., 169(4), p. 750–765.e17. doi: 10.1016/j.cell.2017.04.014.
- LeBouder, E. *et al.* (2003) 'Soluble Forms of Toll-Like Receptor (TLR)2 Capable of Modulating TLR2 Signaling Are Present in Human Plasma and Breast Milk', *The Journal of Immunology*, 171(12), pp. 6680–6689. doi: 10.4049/jimmunol.171.12.6680.
- Lee, H. *et al.* (2018) 'Extracellular vesicle: An emerging mediator of intercellular crosstalk in lung inflammation and injury', *Frontiers in Immunology*, 9(APR). doi: 10.3389/fimmu.2018.00924.
- Lefebvre, P. *et al.* (2006) 'Sorting out the roles of PPAR in energy metabolism and vascular homeostasis', *Journal of Clinical Investigation*, 116(3), pp. 571–580. doi: 10.1172/JCI27989.
- Li, L. *et al.* (2011) 'Nuclear factor high-mobility group box1 mediating the activation of toll-like receptor 4 signaling in hepatocytes in the early stage of nonalcoholic fatty liver disease in mice', *Hepatology*, 54(5), pp. 1620–1630. doi: 10.1002/hep.24552.
- Li, L. *et al.* (2018) 'Activation of endothelial cells by extracellular vesicles derived from Mycobacterium tuberculosis infected macrophages or mice', *PLoS ONE*, 13(5), pp. 1–19. doi: 10.1371/journal.pone.0198337.

- Li, Z. *et al.* (2006) 'The ratio of phosphatidylcholine to phosphatidylethanolamine influences membrane integrity and steatohepatitis', *Cell Metabolism*, 3(5), pp. 321–331. doi: 10.1016/j.cmet.2006.03.007.
- Liew, F. Y. *et al.* (2005) 'Negative regulation of toll-like receptor-mediated immune responses', *Nature Reviews Immunology*, 5(6), pp. 446–458. doi: 10.1038/nri1630.
- Lin, Y. *et al.* (2000) 'The lipopolysaccharide-activated Toll-like receptor (TLR)-4 induces synthesis of the closely related receptor TLR-2 in adipocytes', *Journal of Biological Chemistry*, 275(32), pp. 24255–24263. doi: 10.1074/jbc.M002137200.
- Ma, J. *et al.* (2010) 'The M1 form of tumor-associated macrophages in non-small cell lung cancer is positively associated with survival time', *BMC Cancer*, 10, p. 112. Available at: <http://dx.doi.org/10.1186/1471-2407-10-112>.
- Mantovani, A. *et al.* (2002) 'Macrophase polarization: tumor-associated macrophages as a paradigm for polarized M2 mononuclear phagocytes', *TRENDS in Immunology*, 23(11), pp. 549–555. Available at: <http://immunology.trends.com>.
- Mantovani, A. *et al.* (2004) 'The chemokine system in diverse forms of macrophage activation and polarization', *Trends in Immunology*, 25(12), pp. 677–686. doi: 10.1016/j.it.2004.09.015.
- Mantovani, A. *et al.* (2017) 'Tumour-associated macrophages as treatment targets in oncology', *Nature Reviews Clinical Oncology*. Nature Publishing Group, 14(7), pp. 399–416. doi: 10.1038/nrclinonc.2016.217.
- Mantovani, A. and Sica, A. (2010) 'Macrophages, innate immunity and cancer: balance, tolerance, and diversity', *Current Opinion in Immunology*. Elsevier Ltd, 22(2), pp. 231–237. doi: 10.1016/j.coi.2010.01.009.
- Marien, E. *et al.* (2015) 'Non-small cell lung cancer is characterized by dramatic changes in phospholipid profiles', *International Journal of Cancer*, 137(7), pp. 1539–1548. doi: 10.1002/ijc.29517.
- Markowska, A. *et al.* (2017) 'A novel method for the isolation of extracellular vesicles and RNA from urine', *Journal of Circulating Biomarkers*, 6, pp. 1–7. doi: 10.1177/1849454417712666.
- Martinez, F. O. *et al.* (2008) 'Macrophage activation and polarization', *Frontiers in Bioscience*, 13(13), p. 453. doi: 10.2741/2692.
- Martinez, F. O. and Gordon, S. (2014) 'The M1 and M2 paradigm of macrophage activation: time for reassessment', *F1000Prime Reports*, 6(March), pp. 1–13. doi: 10.12703/P6-13.
- Matsuguchi, T. *et al.* (2000) 'Gene Expressions of Toll-Like Receptor 2, But Not Toll-Like Receptor 4, Is Induced by LPS and Inflammatory Cytokines in Mouse Macrophages', *The Journal of Immunology*, 165(10), pp. 5767–5772. doi: 10.4049/jimmunol.165.10.5767.
- Matsuzaka, T. *et al.* (2007) 'Crucial role of a long-chain fatty acid elongase, Elovl6, in obesity-induced insulin resistance', *Nature Medicine*, 13(10), pp. 1193–1202. doi: 10.1038/nm1662.

- Matsuzaka, T. *et al.* (2012) 'Elov16 promotes nonalcoholic steatohepatitis', *Hepatology*, 56(6), pp. 2199–2208. doi: 10.1002/hep.25932.
- Mauer, J. *et al.* (2014) 'Signaling by IL-6 promotes alternative activation of macrophages to limit endotoxemia and obesity-associated resistance to insulin', *Nature Immunology*, 15(5), pp. 423–430. doi: 10.1038/ni.2865.
- Maus, U. A. *et al.* (2006) 'Resident Alveolar Macrophages Are Replaced by Recruited Monocytes in Response to Endotoxin-Induced Lung Inflammation', *American Journal of Respiratory Cell and Molecular Biology*, 35(2), pp. 227–235. doi: 10.1165/rcmb.2005-0241OC.
- Medzhitov, R. (2001) 'Toll-like receptors and innate immunity', *Nature Reviews Immunology*, 1(2), pp. 135–145. doi: 10.1038/35100529.
- Mills, C. D., Lenz, L. L. and Harris, R. A. (2016) 'A breakthrough: Macrophage-directed cancer immunotherapy', *Cancer Research*. doi: 10.1158/0008-5472.CAN-15-1737.
- Misharin, A. V. *et al.* (2017) 'Monocyte-derived alveolar macrophages drive lung fibrosis and persist in the lung over the life span', *The Journal of Experimental Medicine*, 214(8), pp. 2387–2404. doi: 10.1084/jem.20162152.
- Miura, K. *et al.* (2016) 'Toll-like receptor 4 on macrophage promotes the development of steatohepatitis-related hepatocellular carcinoma in mice', *Journal of Biological Chemistry*, 291(22), pp. 11504–11517. doi: 10.1074/jbc.M115.709048.
- Molina, J. R. *et al.* (2008) 'Non-Small Cell Lung Cancer: Epidemiology, Risk Factors, Treatment, and Survivorship', *Mayo Clinic Proceedings*, 83(5), pp. 584–594. doi: 10.4065/83.5.584.
- Momen-Heravi, F. *et al.* (2013) 'Current methods for the isolation of extracellular vesicles', *Journal of Biological Chemistry*, 394(10), pp. 1253–1262. doi: 10.1515/hsz-2013-0141.
- Muir, K. *et al.* (2013) 'Proteomic and lipidomic signatures of lipid metabolism in NASH-associated Hepatocellular carcinoma', *Cancer Research*, 73(15), pp. 4722–4731. doi: 10.1158/0008-5472.CAN-12-3797.
- Murray, P. J. *et al.* (2014) 'Macrophage Activation and Polarization: Nomenclature and Experimental Guidelines', *Immunity*. Elsevier, 41(1), pp. 14–20. doi: 10.1016/j.immuni.2014.06.008.
- Murray, P. J. (2017) 'Macrophage Polarization', *Annual Review of Physiology*, 79(1), pp. 541–566. doi: 10.1146/annurev-physiol-022516-034339.
- Musso, G., Gambino, R. and Cassader, M. (2009) 'Recent insights into hepatic lipid metabolism in non-alcoholic fatty liver disease (NAFLD)', *Progress in Lipid Research*. Elsevier Ltd, 48(1), pp. 1–26. doi: 10.1016/j.plipres.2008.08.001.
- Nanji, A. A. *et al.* (1993) 'Severity of Liver Injury in Experimental Alcoholic Liver Disease. Correlation with Plasma Endotoxin, Prostaglandin E2, Leukotriene B4, and Thromboxane B2', *American Journal of Pathology*, 142(2), pp. 367–373.

- Netea, M. G. and van der Meer, J. W. M. (2011) ‘Immunodeficiency and Genetic Defects of Pattern-Recognition Receptors’, *New England Journal of Medicine*. Edited by R. S. Schwartz, 364(1), pp. 60–70. doi: 10.1056/NEJMra1001976.
- van Niel, G., D’Angelo, G. and Raposo, G. (2018) ‘Shedding light on the cell biology of extracellular vesicles’, *Nature Reviews Molecular Cell Biology*. Nature Publishing Group, 19(4), pp. 213–228. doi: 10.1038/nrm.2017.125.
- Noy, R. and Pollard, J. W. (2015) ‘Tumor-associated macrophages: from mechanisms to therapy’, *Immunity*, 41(1), pp. 49–61. doi: 10.1016/j.immuni.2014.06.010.Tumor-associated.
- Odegaard, J. I. *et al.* (2007) ‘Macrophage-specific PPAR γ controls alternative activation and improves insulin resistance’, *Nature*, 447(7148), pp. 1116–1120. doi: 10.1038/nature05894.
- Ohno, S. I., Drummen, G. P. C. and Kuroda, M. (2016) ‘Focus on extracellular vesicles: Development of extracellular vesicle-based therapeutic systems’, *International Journal of Molecular Sciences*, 17(2). doi: 10.3390/ijms17020172.
- Ohri, C. M. *et al.* (2009) ‘Macrophages within NSCLC tumour islets are predominantly of a cytotoxic M1 phenotype associated with extended survival’, *European Respiratory Journal*, 33(1), pp. 118–126. doi: 10.1183/09031936.00065708.
- Ohtaki, Y. *et al.* (2010) ‘Stromal Macrophage Expressing CD204 is Associated with Tumor Aggressiveness in Lung Adenocarcinoma’, *Journal of Thoracic Oncology*, 5(10), pp. 1507–1515.
- Okabe, Y. and Medzhitov, R. (2016) ‘Tissue biology perspective on macrophages’, *Nature Immunology*. Nature Publishing Group, 17(1), pp. 9–17. doi: 10.1038/ni.3320.
- Oliveros, J. C. (2007) ‘VENNY. an interactive tool for comparing lists with venn diagrams’. Available at: <http://bioinfogp.cnb.csic.es/tools/venny/index.html>.
- Opal, S. M. and DePalo, V. A. (2000) ‘Anti-inflammatory cytokines’, *Chest*. The American College of Chest Physicians, 117(4), pp. 1162–1172. doi: 10.1378/chest.117.4.1162.
- Ozinsky, A. *et al.* (2000) ‘The repertoire for pattern recognition of pathogens by the innate immune system is defined by cooperation between Toll-like receptors’, *Proceedings of the National Academy of Sciences*, 97(25), pp. 13766–13771. doi: 10.1073/pnas.250476497.
- Parayath, N. N., Parikh, A. and Amiji, M. M. (2018) ‘Repolarization of Tumor-Associated Macrophages in a Genetically Engineered Nonsmall Cell Lung Cancer Model by Intraperitoneal Administration of Hyaluronic Acid-Based Nanoparticles Encapsulating MicroRNA-125b’, *Nano Letters*. American Chemical Society, 18(6), pp. 3571–3579. doi: 10.1021/acs.nanolett.8b00689.
- Park, E. J. *et al.* (2010) ‘Dietary and Genetic Obesity Promote Liver Inflammation and Tumorigenesis by Enhancing IL-6 and TNF Expression’, *Cell*, 140(2), pp. 197–208. doi: 10.1016/j.cell.2009.12.052.

- Patro, R. *et al.* (2017) 'Salmon provides fast and bias-aware quantification of transcript expression', *Nature Methods*. Nature Publishing Group, 14(4), pp. 417–419. doi: 10.1038/nmeth.4197.
- Pawlak, M., Lefebvre, P. and Staels, B. (2015) 'Molecular mechanism of PPAR α action and its impact on lipid metabolism, inflammation and fibrosis in non-alcoholic fatty liver disease', *Journal of Hepatology*. European Association for the Study of the Liver, 62(3), pp. 720–733. doi: 10.1016/j.jhep.2014.10.039.
- Pena, O. M. *et al.* (2011) 'Endotoxin Tolerance Represents a Distinctive State of Alternative Polarization (M2) in Human Mononuclear Cells', *The Journal of Immunology*, 186(12), pp. 7243–7254. doi: 10.4049/jimmunol.1001952.
- Pinto, J. A. *et al.* (2018) 'Gender and outcomes in non-small cell lung cancer: an old prognostic variable comes back for targeted therapy and immunotherapy?', *ESMO Open*, 3(3), p. e000344. doi: 10.1136/esmoopen-2018-000344.
- Poczobutt, J. M. *et al.* (2016) 'Expression Profiling of Macrophages Reveals Multiple Populations with Distinct Biological Roles in an Immunocompetent Orthotopic Model of Lung Cancer', *The Journal of Immunology*, 196(6), pp. 2847–2859. doi: 10.4049/jimmunol.1502364.
- Van Der Pol, E. *et al.* (2010) 'Optical and non-optical methods for detection and characterization of microparticles and exosomes', *Journal of Thrombosis and Haemostasis*, 8(12), pp. 2596–2607. doi: 10.1111/j.1538-7836.2010.04074.x.
- Pupo, E. *et al.* (2013) 'Intact rough- and smooth-form lipopolysaccharides from *Escherichia coli* separated by preparative gel electrophoresis exhibit differential biologic activity in human macrophages', *FEBS Journal*, 280(4), pp. 1095–1111. doi: 10.1111/febs.12104.
- Qian, B.-Z. and Pollard, J. W. (2010) 'Macrophage Diversity Enhances Tumor Progression and Metastasis', *Cell*, 141(1), pp. 39–51. doi: 10.1016/j.cell.2010.03.014.
- Qin, Y., Li, H. and Qiao, J. (2016) 'TLR2/MyD88/NF- κ B signalling pathway regulates IL-8 production in porcine alveolar macrophages infected with porcine circovirus 2', *Journal of General Virology*, 97(2), pp. 445–452. doi: 10.1099/jgv.0.000345.
- Qiu, D. H. *et al.* (2011) 'In vitro inhibition of bacterial growth by iron chelators', *FEMS Microbiology Letters*, 314(2), pp. 107–111. doi: 10.1111/j.1574-6968.2010.02153.x.
- Quail, D. F. and Joyce, J. A. (2013) 'Microenvironmental regulation of tumor progression and metastasis', *Nature Medicine*, 19(11), pp. 1423–1437. doi: 10.1038/nm.3394.
- Quatromoni, J. G. and Eruslanov, E. (2012) 'Tumor-associated macrophages: function, phenotype, and link to prognosis in human lung cancer.', *American journal of translational research*, 4(4), pp. 376–89. doi: 2012;4(4):376-389.
- Raby, A.-C. *et al.* (2009) 'Soluble TLR2 reduces inflammation without compromising bacterial clearance by disrupting TLR2 triggering.', *Journal of immunology (Baltimore, Md. : 1950)*, 183(1), pp. 506–17. doi: 10.4049/jimmunol.0802909.

- Raymond, A., Ensslin, M. A. and Shur, B. D. (2009) 'SED1/MFG-E8: A Bi-motif protein that orchestrates diverse cellular interactions', *Journal of Cellular Biochemistry*, 106(6), pp. 957–966. doi: 10.1002/jcb.22076.
- Remmerie, A. and Scott, C. L. (2018) 'Macrophages and lipid metabolism', *Cellular Immunology*. Elsevier, 330(1), pp. 27–42. doi: 10.1016/j.cellimm.2018.01.020.
- Risso, D. *et al.* (2014) 'Normalization of RNA-seq data using factor analysis of control genes or samples', *Nature Biotechnology*, 32(9), pp. 896–902. doi: 10.1038/nbt.2931.
- Rivas-Fuentes, S. *et al.* (2015) 'Role of chemokines in non-small cell lung cancer: Angiogenesis and inflammation', *Journal of Cancer*, 6(10), pp. 938–952. doi: 10.7150/jca.12286.
- Rivera, C. A. *et al.* (2007) 'Toll-like receptor-4 signaling and Kupffer cells play pivotal roles in the pathogenesis of non-alcoholic steatohepatitis', *Journal of Hepatology*, 47(4), pp. 571–579. doi: 10.1016/j.jhep.2007.04.019.
- Robertson, K. A. *et al.* (2016) 'An Interferon Regulated MicroRNA Provides Broad Cell-Intrinsic Antiviral Immunity through Multihit Host-Directed Targeting of the Sterol Pathway', *PLoS Biology*, 14(3). doi: 10.1371/journal.pbio.1002364.
- Roebuck, K. A. (1999) 'Regulation of Interleukin-8 Gene Expression', *Journal of Interferon and Cytokine Research*, 19, pp. 429–438. doi: 10.1016/B978-012095440-7/50028-7.
- Van Rooijen, N. and Sanders, A. (1996) 'Kupffer cell depletion by liposome-delivered drugs: Comparative activity of intracellular clodronate, propamidine, and ethylenediaminetetraacetic acid', *Hepatology*, 23(5), pp. 1239–1243. doi: 10.1053/jhep.1996.v23.pm0008621159.
- Rozkova, D. *et al.* (2006) 'Glucocorticoids severely impair differentiation and antigen presenting function of dendritic cells despite upregulation of Toll-like receptors', *Clinical Immunology*, 120(3), pp. 260–271. doi: 10.1016/j.clim.2006.04.567.
- Ruiz, R. *et al.* (2014) 'Sterol regulatory element-binding protein-1 (SREBP-1) is required to regulate glycogen synthesis and gluconeogenic gene expression in mouse liver', *Journal of Biological Chemistry*, 289(9), pp. 5510–5517. doi: 10.1074/jbc.M113.541110.
- Rutledge, H. R. *et al.* (2012) 'Gene expression profiles of RAW264.7 macrophages stimulated with preparations of LPS differing in isolation and purity', *Innate Immunity*, 18(1), pp. 80–88. doi: 10.1177/1753425910393540.
- Sayiner, M. *et al.* (2016) 'Epidemiology of Nonalcoholic Fatty Liver Disease and Nonalcoholic Steatohepatitis in the United States and the Rest of the World', *Clinics in Liver Disease*, 20(2), pp. 205–214. doi: 10.1016/j.cld.2015.10.001.
- Schnabl, B. (2013) 'Linking intestinal homeostasis and liver disease', *Current Opinions in Gastroenterology*, 29(3), pp. 264–270. doi: 10.1002/bmb.20244.DNA.
- Schneider, C. *et al.* (2014) 'Induction of the nuclear receptor PPAR- γ by the cytokine GM-CSF is critical for the differentiation of fetal monocytes into alveolar macrophages', *Nature Immunology*, 15(11), pp. 1026–1037. doi: 10.1038/ni.3005.

- Scott, C. L. *et al.* (2016) ‘Bone marrow-derived monocytes give rise to self-renewing and fully differentiated Kupffer cells’, *Nature Communications*, 7, pp. 1–10. doi: 10.1038/ncomms10321.
- Shao, H. *et al.* (2018) ‘New Technologies for Analysis of Extracellular Vesicles’, *Chemical Reviews*, 118(4), pp. 1917–1950. doi: 10.1021/acs.chemrev.7b00534.
- Shapouri-Moghaddam, A. *et al.* (2018) ‘Macrophage plasticity, polarization, and function in health and disease’, *Journal of Cellular Physiology*, 233(9), pp. 6425–6440. doi: 10.1002/jcp.26429.
- Sheng, J., Ruedl, C. and Karjalainen, K. (2015) ‘Most Tissue-Resident Macrophages Except Microglia Are Derived from Fetal Hematopoietic Stem Cells’, *Immunity*. Elsevier Inc., 43(2), pp. 382–393. doi: 10.1016/j.immuni.2015.07.016.
- Shuto, T. *et al.* (2002) ‘Glucocorticoids synergistically enhance nontypeable Haemophilus influenzae-induced toll-like receptor 2 expression via a negative cross-talk with p38 MAP kinase’, *Journal of Biological Chemistry*, 277(19), pp. 17263–17270. doi: 10.1074/jbc.M112190200.
- Sica, A. *et al.* (2015) ‘Macrophage polarization in pathology’, *Cellular and Molecular Life Sciences*. Springer Basel, 72(21), pp. 4111–4126. doi: 10.1007/s00018-015-1995-y.
- Sica, A. and Mantovani, A. (2012) ‘Macrophage plasticity and polarization: in vivo veritas’, *Journal of Clinical Investigation*, 122(3), pp. 787–795. doi: 10.1172/JCI59643DS1.
- Siguener, A. *et al.* (2017) ‘Lipidomic and metabolic changes in the P4-type ATPase ATP10D deficient C57BL/6J wild type mice upon rescue of ATP10D function’, *PLoS ONE*, 12(5), pp. 1–17. doi: 10.1371/journal.pone.0178368.
- Smith, J. a *et al.* (2015) ‘Extracellular Vesicles: Commercial Potential As Byproducts of Cell Manufacturing for Research and Therapeutic Use’, *Bioprocess International*, 13(4), pp. 1–13.
- Solinas, G. *et al.* (2009) ‘Tumor-associated macrophages (TAM) as major players of the cancer-related inflammation’, *Journal of Leukocyte Biology*, 86(5), pp. 1065–1073. doi: 10.1189/jlb.0609385.
- Spann, N. J. *et al.* (2012) ‘Regulated accumulation of desmosterol integrates macrophage lipid metabolism and inflammatory responses’, *Cell*. Elsevier Inc., 151(1), pp. 138–152. doi: 10.1016/j.cell.2012.06.054.
- Stögbauer, F. *et al.* (2008) ‘Highly efficient and low-cost method to isolate human blood monocytes with high purity’, *Journal of Immunological Methods*, 337(1), pp. 78–80. doi: 10.1016/j.jim.2008.05.008.
- Suzuki, Y. *et al.* (2018) ‘Macrophage mannose receptor, CD206, predict prognosis in patients with pulmonary tuberculosis’, *Scientific Reports*, 8(1), pp. 1–9. doi: 10.1038/s41598-018-31565-5.
- Swinburn, B. A. *et al.* (2011) ‘The global obesity pandemic: Shaped by global drivers and local environments’, *The Lancet*. Elsevier Ltd, 378(9793), pp. 804–814. doi: 10.1016/S0140-6736(11)60813-1.

- Tabas, I. (2002) 'Consequences of cellular cholesterol accumulation: Basic concepts and physiological implications', *Journal of Clinical Investigation*, 110(7), pp. 905–911. doi: 10.1172/JCI200216452.The.
- Takeya, M. and Komohara, Y. (2016) 'Role of tumor-associated macrophages in human malignancies: friend or foe?', *Pathology International*, 66(9), pp. 491–505. doi: 10.1111/pin.12440.
- Théry, C., Clayton, A. and Amigorena, S. (2006) 'Isolation and Characterization of Exosomes from Cell Culture Supernatants', *Current Protocols in Cell Biology*, pp. 1–29.
- Tilg, H., Moschen, A. R. and Szabo, G. (2016) 'Interleukin-1 and inflammasomes in alcoholic liver disease/acute alcoholic hepatitis and nonalcoholic fatty liver disease/nonalcoholic steatohepatitis', *Hepatology*, 64(3), pp. 955–965. doi: 10.1002/hep.28456.
- Travis, W. D. *et al.* (2004) 'World Health Organization classification tumours of the lung, pleura, thymus and heart. Fourth edition', *International Agency for Research on Cancer (IARC) Press, Lyon*.
- Travis, W. D. (2011) 'Pathology of lung cancer', *Clinics in Chest Medicine*, 32, pp. 669–692. doi: 10.1017/CBO9780511545351.004.
- Travis, W. D. *et al.* (2015) 'The 2015 World Health Organization Classification of Lung Tumors: Impact of Genetic, Clinical and Radiologic Advances since the 2004 Classification', *Journal of Thoracic Oncology*. International Association for the Study of Lung Cancer, 10(9), pp. 1243–1260. doi: 10.1097/JTO.0000000000000630.
- Uesugi, T. *et al.* (2001) 'Toll-like receptor 4 is involved in the mechanism of early alcohol-induced liver injury in mice', *Hepatology*, 34(1), pp. 101–108. doi: 10.1053/jhep.2001.25350.
- Viaud, M. *et al.* (2018) 'Lysosomal cholesterol hydrolysis couples efferocytosis to anti-inflammatory oxysterol production', *Circulation Research*, 122(10), pp. 1369–1384. doi: 10.1161/CIRCRESAHA.117.312333.
- Vida, M. *et al.* (2015) 'Chronic administration of recombinant IL-6 upregulates lipogenic enzyme expression and aggravates high-fat-diet-induced steatosis in IL-6-deficient mice', *Disease Models & Mechanisms*, 8(7), pp. 721–731. doi: 10.1242/dmm.019166.
- Wang, N., Liang, H. and Zen, K. (2014) 'Molecular mechanisms that influence the macrophage M1-M2 polarization balance', *Frontiers in Immunology*, 5(NOV), pp. 1–9. doi: 10.3389/fimmu.2014.00614.
- Wang, R. *et al.* (2011) 'Tumor-associated macrophages provide a suitable microenvironment for non-small lung cancer invasion and progression', *Lung Cancer*. Elsevier Ireland Ltd, 74(2), pp. 188–196. doi: 10.1016/j.lungcan.2011.04.009.
- Wieckowska, A. *et al.* (2008) 'Increased hepatic and circulating interleukin-6 levels in human nonalcoholic steatohepatitis', *American Journal of Gastroenterology*, 103(6), pp. 1372–1379. doi: 10.1111/j.1572-0241.2007.01774.x.
- Wynn, T. A. and Vannella, K. M. (2016) 'Macrophages in Tissue Repair, Regeneration, and Fibrosis', *Immunity*. Elsevier Inc., 44(3), pp. 450–462. doi: 10.1016/j.immuni.2016.02.015.

- Yahagi, N. *et al.* (2002) 'Absence of sterol regulatory element-binding protein-1 (SREBP-1) ameliorates fatty livers but not obesity or insulin resistance in Lepob/Lepob mice', *Journal of Biological Chemistry*, 277(22), pp. 19353–19357. doi: 10.1074/jbc.M201584200.
- Yáñez-Mó, M. *et al.* (2015) 'Biological properties of extracellular vesicles and their physiological functions', *Journal of Extracellular Vesicles*, 4, p. 27066.
- Yuan, A. *et al.* (2015) 'Opposite Effects of M1 and M2 Macrophage Subtypes on Lung Cancer Progression', *Scientific Reports*. Nature Publishing Group, 5, pp. 1–12. doi: 10.1038/srep14273.
- Zeni, E. *et al.* (2007) 'Macrophage expression of interleukin-10 is a prognostic factor in nonsmall cell lung cancer', *European Respiratory Journal*, 30(4), pp. 627–632. doi: 10.1183/09031936.00129306.
- Zhang, B. *et al.* (2011) 'M2-Polarized tumor-associated macrophages are associated with poor prognoses resulting from accelerated lymphangiogenesis in lung adenocarcinoma', *Clinical Science*, 66(11), pp. 1879–1886. doi: 10.1590/S1807-59322011001100006.
- Zhang, X. *et al.* (2015) 'Exosomes in cancer: Small particle, big player', *Journal of Hematology and Oncology*. Journal of Hematology & Oncology, 8(1), pp. 1–13. doi: 10.1186/s13045-015-0181-x.
- Zheng, X. *et al.* (2017) 'Redirecting tumor-associated macrophages to become tumoricidal effectors as a novel strategy for cancer therapy', *Oncotarget*, 8(29), pp. 48436–48452. doi: 10.18632/oncotarget.17061.

Appendix

D) Table of selected **upregulated** DEGs (with transcripts of million kilobases, TPM)

Ensembl ID	Gene Symbol	Log Fold Change	Adjusted p-value	TAM TPM average	AM TPM average
ENSG00000164171	ITGA2	4,065663608	5,75E-49	1,77065125	0,094854113
ENSG00000092969	TGFB2	4,045727957	1,96E-48	4,86172125	0,235363125
ENSG00000039068	CDH1	3,586644734	1,17E-33	6,08033375	0,314004
ENSG00000087245	MMP2	2,659206781	3,03E-24	44,2640375	6,36305
ENSG00000156234	CXCL13	7,469881698	1,83E-21	5,196640125	0,02306015
ENSG00000137265	IRF4	2,984664066	1,18E-20	2,00556	0,189049
ENSG00000181374	CCL13	6,986005101	1,54E-20	52,96424375	0,374224125
ENSG00000170989	S1PR1	4,203447184	1,68E-18	6,55541375	0,23840175
ENSG00000151651	ADAM8	3,040901052	1,10E-16	70,779725	7,7767175
ENSG00000163235	TGFA	2,043086982	7,81E-13	6,2815975	1,42477875
ENSG00000189377	CXCL17	6,353378817	8,37E-12	0,417702875	0
ENSG00000163739	CXCL1	2,752135379	1,11E-11	29,90098	2,0944825
ENSG00000008516	MMP25	2,974338295	8,09E-11	8,18898	0,9807515
ENSG00000196611	MMP1	3,771496382	2,46E-10	5,0611825	0,2720334
ENSG00000062038	CDH3	2,081228982	7,35E-10	3,39386	0,72884625
ENSG00000118113	MMP8	4,491811412	8,34E-10	3,949052125	0,13627115
ENSG00000081181	ARG2	1,283134621	5,66E-09	9,35414	3,39749375
ENSG00000160712	IL6R	0,667863092	5,69E-09	33,4311875	20,6491
ENSG00000126353	CCR7	4,102545406	1,50E-08	14,6844025	0,7243921
ENSG00000138316	ADAMTS14	5,063523094	2,84E-08	2,292101775	0,051132338
ENSG00000107562	CXCL12	4,935314679	5,67E-08	6,933586375	0,107686988
ENSG00000108700	CCL8	4,783302976	5,99E-08	6,909124625	0,1789975
ENSG00000112715	VEGFA	2,732315291	1,03E-07	24,4147025	3,2229825
ENSG00000100644	HIF1A	2,030122105	1,26E-07	268,029625	58,9045875
ENSG00000136634	IL10	1,728316677	2,60E-07	15,26627375	4,98266625
ENSG00000177675	CD163L1	2,284682051	2,94E-07	17,71246625	2,59100225
ENSG00000169429	CXCL8	2,871861455	3,66E-07	308,5277	38,2088875
ENSG00000108691	CCL2	3,182908849	7,57E-07	172,0528	18,68006
ENSG00000079385	CEACAM1	1,451352385	8,66E-07	0,87113025	0,2355385
ENSG00000138685	FGF2	2,671809738	9,41E-06	0,199760263	0,036988595
ENSG00000168615	ADAM9	0,527427301	1,31E-05	172,4575	119,9549125
ENSG00000115590	IL1R2	1,713577465	1,51E-05	1,27956	0,30699075
ENSG00000137462	TLR2	1,541087614	1,53E-05	45,679575	14,43885
ENSG00000162892	IL24	1,951918069	4,05E-05	4,93255	1,170364375
ENSG00000179776	CDH5	3,382675582	4,92E-05	0,09422365	0,0087152
ENSG00000170458	CD14	1,756636699	8,81E-05	514,588625	140,519925
ENSG00000102970	CCL17	3,684616724	9,44E-05	2,8043025	0,201271588
ENSG00000017427	IGF1	2,585818995	0,00011881	1,200178375	0,129853213
ENSG00000115594	IL1R1	0,942894128	0,000127174	13,9470375	6,6761075
ENSG00000100985	MMP9	2,349195907	0,000156789	2836,125	555,9325
ENSG00000138378	STAT4	2,49266686	0,000185601	10,4193825	0,6558335
ENSG00000137496	IL18BP	1,364695473	0,000872805	53,6972125	21,284825
ENSG00000066056	TIE1	2,050514384	0,001438782	18,7285375	4,457004125
ENSG00000106178	CCL24	1,772778924	0,00189097	86,08205	22,90742875
ENSG00000008517	IL32	3,054326897	0,002821003	105,1891625	10,82108125
ENSG00000275302	CCL4	2,221081428	0,004475278	4,43141875	0,81177125
ENSG00000115604	IL18R1	1,708664235	0,008717038	0,449903625	0,121265688
ENSG00000124875	CXCL6	2,130981691	0,01305941	0,342237025	0,052936263
ENSG00000186951	PPARA	0,259663123	0,01518697	12,4493175	10,15714375
ENSG00000136244	IL6	2,552843585	0,01727736	1,205659875	0,163103263
ENSG00000143321	HDGF	0,385146106	0,02092805	125,951925	97,1694875
ENSG00000115009	CCL20	1,35702697	0,02539338	3,853828875	1,45792275
ENSG00000117595	IRF6	1,001037135	0,02585496	1,257113375	0,571566375
ENSG00000089250	NOS1	1,233848919	0,02625713	0,084933775	0,047199238
ENSG00000115232	ITGA4	0,797405124	0,02631496	13,1721625	7,64211875
ENSG00000111640	GAPDH	0,338345145	0,02988889	1160,123375	927,47875
ENSG00000275528	CCL15	2,01117022	0,03072093	2,892339625	0,6019315
ENSG00000163734	CXCL3	1,714997491	0,03534251	79,176525	21,7934
ENSG00000274233	CCL5	2,345640983	0,03603746	35,50282125	5,839600375
ENSG00000234487	HLA-F	0,877867398	0,03950396	277,655	127,55955
ENSG00000135074	ADAM19	2,548199327	0,04327102	1,805760625	0,277242288
ENSG00000230254	HLA-E	0,505686394	0,04547196	154,8837375	106,787575
ENSG00000143514	TP53BP2	0,277179907	0,04790066	23,37165	18,1791875

II) Table of selected **downregulated** DEGs (with transcripts of million kilobases, TPM)

Ensembl ID	Gene Symbol	Log Fold Change	Adjusted p-value	TAM TPM average	AM TPM average
ENSG00000052802	MSMO1	-2,830737335	2,46E-69	11,038065	77,678625
ENSG00000113161	HMGCR	-1,418124488	4,55E-62	14,147925	36,942775
ENSG00000186480	INSIG1	-1,748221636	8,18E-52	20,33209875	67,7221375
ENSG00000110921	MVK	-1,280828636	3,12E-51	5,65544625	13,7648625
ENSG00000130164	LDLR	-2,166151002	5,52E-48	3,3701275	14,5719875
ENSG00000198911	SREBF2	-1,340934067	9,48E-41	21,5359375	54,351925
ENSG00000104549	SQLE	-2,093308396	1,06E-35	4,861885	20,1190375
ENSG00000112972	HMGCS1	-1,090113892	4,01E-28	11,93374125	25,1581625
ENSG00000102349	KLF8	-2,059522108	6,75E-15	2,85501125	12,578955
ENSG00000001630	CYP51A1	-2,074441785	6,01E-14	17,45581625	73,4588
ENSG00000160752	FDPS	-0,706885456	1,39E-11	47,97215	76,3757
ENSG00000172893	DHCR7	-2,095016448	1,45E-11	2,54135125	9,684265
ENSG00000204228	HSD17B8	-1,104389307	6,12E-09	0,57821525	1,45303
ENSG00000136826	KLF4	-1,706719029	1,62E-08	6,89442625	22,2342625
ENSG00000038945	MSR1	-1,187816955	4,94E-07	452,891625	1041,927875
ENSG00000067064	IDI1	-1,214607677	6,84E-06	30,120425	70,2262
ENSG00000147155	EBP	-0,925308408	9,48E-06	37,5120875	71,83205
ENSG00000132196	HSD17B7	-0,70447233	2,56E-05	8,10497375	12,38473375
ENSG00000147383	NSDHL	-0,430542036	4,11E-05	10,72608625	14,67515
ENSG00000127528	KLF2	-1,135754658	0,001272426	2,4731675	5,65799875
ENSG00000172059	KLF11	-0,51239333	0,001484075	15,8614725	22,157675
ENSG00000172349	IL16	-0,478983616	0,00200492	21,9038375	30,5397375
ENSG00000067082	KLF6	-0,392424678	0,006405395	84,851325	112,848525
ENSG00000132170	PPARG	-1,047773249	0,008919781	57,6082125	117,875125
ENSG00000118922	KLF12	-0,585589431	0,008922304	0,3192135	0,4468535
ENSG00000177575	CD163	-0,584519667	0,009976858	200,662	296,47875
ENSG00000135929	CYP27A1	-0,508267106	0,01073156	559,639375	809,59875
ENSG00000173409	ARV1	-0,41781779	0,01269532	16,1085625	21,1689375
ENSG00000116133	DHCR24	-1,119426683	0,01269532	30,344475	67,7615375

Acknowledgement / Danksagung

Zuallererst danke ich Frau Prof. Kiemer für die Möglichkeit meine Dissertation in Ihrem Institut anfertigen zu können, die Bereitstellung des Arbeitsplatzes, der erforderlichen Mittel, des Themas dieser Arbeit und jegliche weitere Unterstützung.

Ich danke Herrn Prof. Schneider für das Übernehmen des Zweitgutachtens und auch für die vielseitige konstruktive Kritik als wissenschaftlicher Begleiter bei meinen Jahresberichten.

Jessica Hoppstädter danke ich sehr für die gute Betreuung während der letzten Jahre sowie das Teilen ihres immensen Wissens mit mir über Makrophagen, das FACSen, Origin, uvm.

Aus dem Arbeitskreis danke ich vor allem Beate, Vanessa, Charlotte, Rebecca und Tarek dafür, dass sie die Arbeitszeit so oft mit Spaß, guter Laune und Disneymagie, aber ebenso mit angeregtem fachlichem Austausch erfüllt haben. Ohne euch wären die letzten Jahre nicht dieselben gewesen! Außerdem geht ein riesiges Dankeschön an Tiffany und Theo, den guten Geistern im Hintergrund, für die Unterstützung im Labor bzw. Mausstall und zahlreich herzliche Gespräche.

Meiner ehemaligen Diplomandin Daniela danke ich für ambitionierte Etablierung des TAM-like Modells sowie die tolle gemeinsame Zeit im Labor und den bis heute bestehenden Kontakt.

Miriam Cheaib danke ich für die herzliche, geduldige und präzise Einführung in die Welt der Library-Präps und RNA-Sequenzierung. Martin Simon danke ich für jegliche Hilfe rund um die RNA-Seq sowie seine motivierende Art und stets offene Bürotür.

Des Weiteren danke ich aus dem BION-Team Gregor Fuhrmann für seine tollen und so wichtigen fachlichen Ratschläge und die Einführung in die Welt der Vesikel sowie Eilien Schulz für den freundschaftlichen Austausch nicht nur über Vesikel.

Außerdem danke all den lieben Menschen am INM, die mich auch bei den Vesikel-Versuchen unterstützt haben: Dr. Annette Kraegeloh für ihre hilfreichen fachlichen Ratschläge, Dr. Marcus Koch für die tollen cryo-TEM-Aufnahmen, Jana Fleddermann für ihre Zeit und Hilfe am Nano-sight sowie und vor allem Silke Kiefer für das niemals langweilige „betreute Zentrifugieren“ und ihren engagierten Einsatz bei kaputten Pumpen oder belegten Zentrifugenzeiten.

Claudia Fecher-Trost und Sandra Plant danke ich für die gute Zusammenarbeit bei den Proteomics. Toll, dass sich unsere Laborwege noch einmal gekreuzt haben.

Der Lungen-Fee Jana Westhues danke ich herzlich für ihre flexible Bereitstellung der Gewebe und noch mehr für unsere tollen gemeinsamen Autofahrten.

Meinem ehemaligen Biologielehrer Herrn Dr. Schuster danke ich herzlich dafür, dass der mich durch seine BioAG erst an die Naturwissenschaft herangeführt hat.

Meinen Mädels danke ich für den wichtigen Ausgleich zur Arbeit an unzähligen Abenden bei Trash-TV und immer wieder doch Gesprächen über die Arbeit.

Mehr als Dank gilt Sandra und Tim, für ihre wertvolle Freundschaft über die letzten 15 Jahre.

Mein größter Dank geht an meine Eltern, meine Brüder Dawid und Thomas und meinen Freund Sebastian für ihre unendliche Unterstützung und Liebe.